PHASE [illegible] REPORT

POSITIVE DEPLOYABLE SOLAR ARRAY DEVELOPMENT PROGRAM

FACILITY FORM 602

N67 14819
(ACCESSION NUMBER)

91
(PAGES)

CR-80917
(NASA CR OR TMX OR AD NUMBER)

(THRU)

0
(CODE)

03
(CATEGORY)

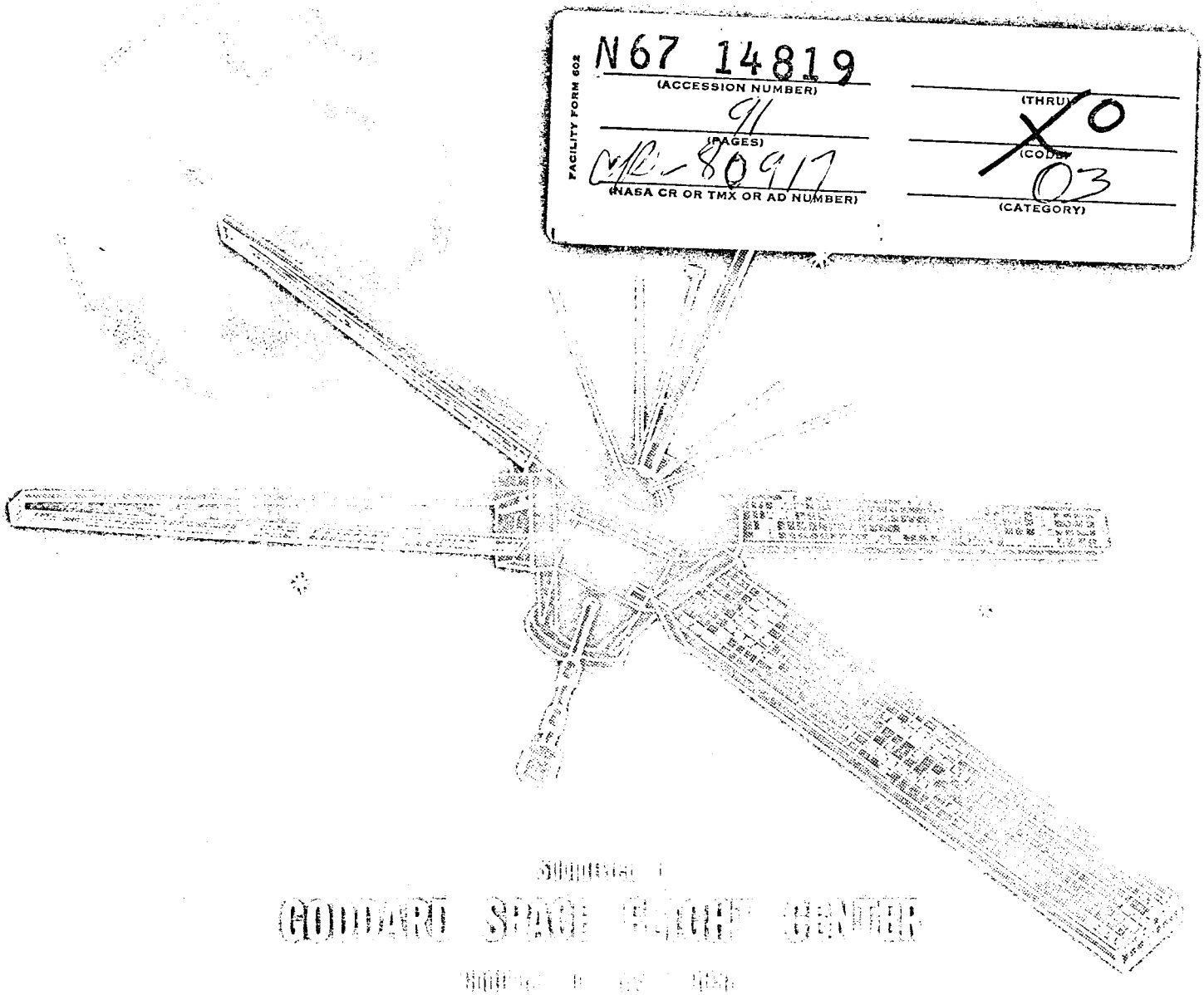

SUBMITTED TO

GODDARD SPACE FLIGHT CENTER

[illegible]

PREPARED BY

[illegible]

SSD 52.5

PHASE I REPORT

POSITIVE DEPLOYABLE SOLAR ARRAY DEVELOPMENT PROGRAM

JUNE 1966

Contract No. NAS 5-9658

Submitted To

GODDARD SPACE FLIGHT CENTER

Greenbelt, Maryland

Prepared By

FAIRCHILD HILLER
SPACE SYSTEMS DIVISION
14[illegible] RESEARCH [illegible] • ROCKVILLE, MARYLAND

TAPLE OF CONTENTS

		Page
1.0	Introduction	1-1
2.0	Design	2-1
2.1	Release Mechanism	2-2
2.2	Drive and Extension Mechanism	2-4
2.3	Damper System	2-6
2.4	Structure	2-8
2.5	Substrate	2-9
3.0	Analysis	3-1
3.1	System Analysis	3-1
3.2	Structural Analysis	3-12
3.3	Stress Analysis	3-18
3.4	Thermal Analysis	3-24
3.5	Weight Summary	3-33
4.0	Test	4-1
4.1	Downward Deployment Test	4-1
4.2	Humidity Test	4-5
4.3	Vibration Test	4-7
4.4	Spin Deployment Test	4-13
4.5	Brake Test	4-20
5.0	Conclusions and Recommendations	5-1
6.0	New Technology	6-1

LIST OF ILLUSTRATIONS

Figure	Title	Page
1.1	Panel Coordinate System	1-2
2.1	Release System	2-3
2.2	Drive and Extension System	2-5
2.3	Damper System	2-7
2.4	Structural Assembly	2-10
2.5	Tensile Test Specimen	2-12
2.6	Assembly Drawing	2-14
3.1A	Descriptive Diagram	3-3
3.1B	Nomenclature	3-4
3.2	Velocity-Tension vs. Time Curve	3-7
3.3	Velocity vs. Time Curve	3-8
3.4	Velocity-Tension Curve	3-8
3.5	Velocity-Tension vs. Time Curve	3-9
3.6	Velocity vs. Time Curve	3-9
3.7	Summary of Loading Conditions	3-13
3.8	Dynamic Analysis Model (Vibration)	3-14
3.9	Scissors Link Loads	3-19
3.10	Cross Beam 2 and 4 Loads	3-19
3.11	Substrate Roller Loads	3-20
3.12	Screw Jack Loads	3-20
3.13	Boss Loads	3-21
3.14	End Cap (Beam G) Loads	3-21
3.15	Fastener Bolt Loads (A, B, C, D)	3-22
3.16	Fastener Bolt Loads (E)	3-22
3.17	Restraint Mechanism and Shear Pin Loads	3-22
3.18	Summary of Minimum Margins of Safety	3-23
3.19	Scissor-Flex Substrate Configuration	3-24
3.20	Incident Flux Diagram	3-25

LIST OF ILLUSTRATIONS (continued)

Figure	Title	Page
3.21	Cell Temperature, Cross Section A	3-28
3.22	Cell Temperature, Cross Section A	3-29
3.23	Cell Temperature, Cross Section B	3-29
3.24	Cell Temperature, Cross Section B	3-30
3.25	Cell Temperature, Cross Section A	3-30
3.26	Cell Temperature, Cross Section A	3-31
3.27	Cell Temperature, Cross Section B	3-31
3.28	Cell Temperature, Cross Section B	3-32
3.29	Weight Summary	3-33/34
4.1	Downward Deployment Test	4-2
4.2	Downward Deployment Test	4-3
4.3	Downward Deployment Test	4-4
4.4	Downward Deployment Test - Added Weight vs. Time Curve	4-5
4.5	Humidity Test Set-up	4-6
4.6	Vibration Test	4-8
4.7	Vibration Test Instrumentation	4-9
4.8	'G' Level vs. Frequency - X Axis	4-10
4.9	'G' Level vs. Frequency - Y Axis	4-11
4.10	'G' Level vs. Frequency - Z Axis	4-12
4.11	Spin Deployment Test Set-up - Undeployed	4-14
4.12	Spin Deployment Test Set-up - Deployed	4-15
4.13	Test Data 80 RPM Deployment	4-17
4.14	Velocity and Tension vs. Time Curve	4-17
4.15	Test Data 160 RPM Deployment	4-18
4.16	Force Diagram	4-19
4.17	Brake Test Set-up	4-22
4.18	Brake Test Set-up	4-23

LIST OF ILLUSTRATIONS (continued)

Figure	Title	Page
4.19	Damper Spin Deployment Test	4-24
4.20	Static Deployment Test	4-24
5.1	Shear and Moment vs. Deployed Length Curve	5-2
5.2	Tension vs. Deployment Time Curve	5-2
5.3	Area/Weight Ratio vs. Length Curve	5-3
5.4	Area/Volume Ratio vs. Length Curve	5-3

ABSTRACT

A relatively new technique for deploying large area solar arrays has been developed for the Goddard Space Flight Center by the Fairchild Hiller Corporation. This design incorporates a flexible substrate to which are fastened silicon solar cells. The array can thus be packaged within a very small volume by rolling it onto a drum or reel.

During Phase I of this project, a "proof-of-principle" model was designed, fabricated and tested. The design consisted of two flexible, parallel arrays, mounted on synchronized rollers, and deployed outward from a spinning body. The area of each substrate was 8 ft.^{2}. Stabilization of the substrate was accomplished by an extendible scissors linkage between the arrays. Total volume of the sixteen square feet of packaged solar cells was approximately 13-1/2 pounds. An analysis of the deployment, launch, vibration, solar radiation, and induced stresses was also completed.

The contract was a follow-on to NAS 5-3988, a previous study contract, to determine the optimum system for extending a solar array from a spinning spacecraft. The study showed that the flexible array is generally more favorable where packaged volume and weight are primary considerations.

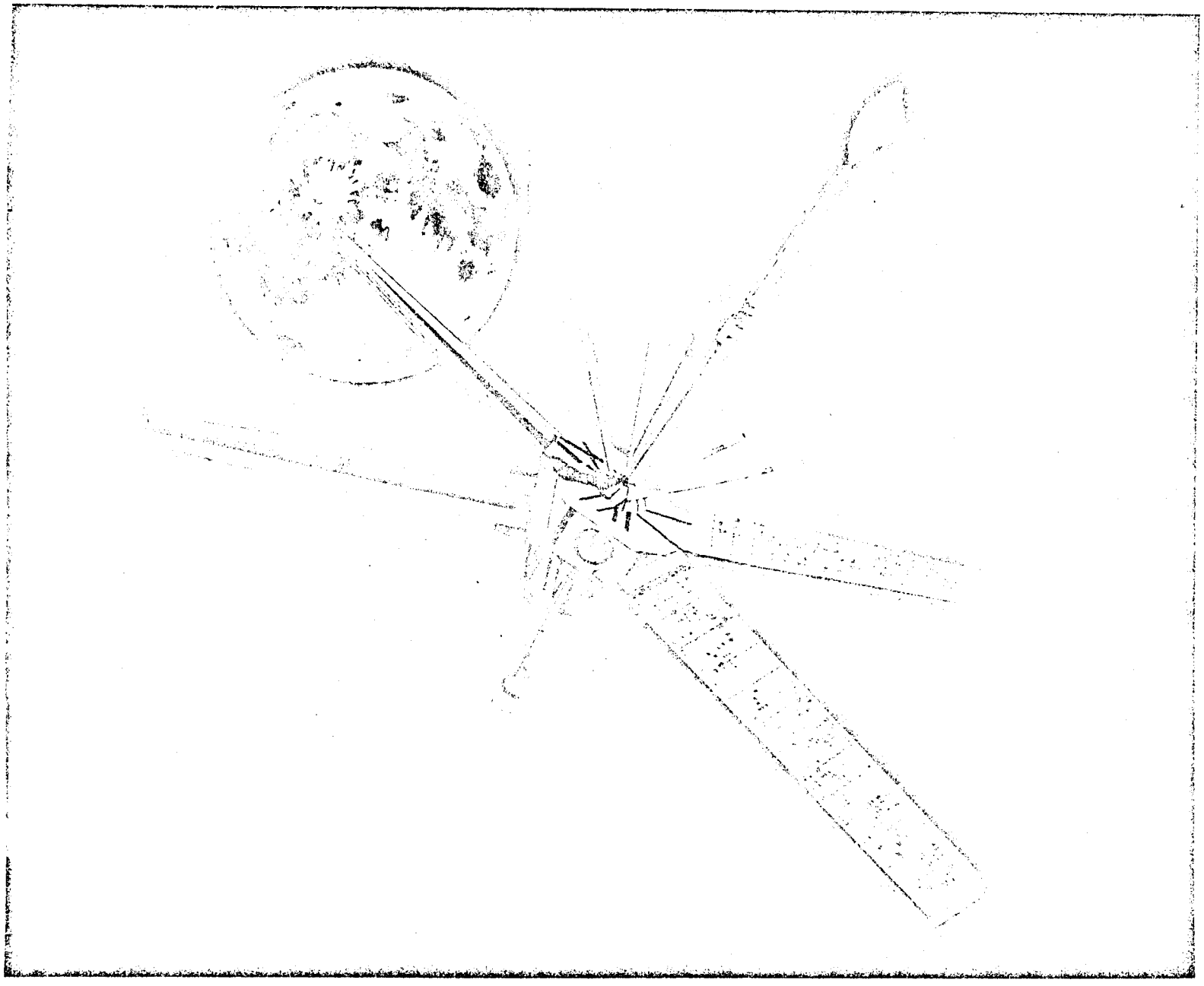

FRONTISPIECE

1.0 INTRODUCTION

Fairchild Hiller, Space Systems Division, has just concluded a Phase I effort on the development of a spaceborne solar cell array. The effort was directed toward designing, fabricating and testing a new concept in solar power. This concept utilized a flexible substrate upon which were mounted silicon solar cells. The advantage of this technique is its greater packaging efficiency and high power-to-weight ratio.

The design of the proof-of-principle model was evaluated in a previous study for the Goddard Space Flight Center. The design arrived at during the study utilized a flexible substrate upon which silicon solar cells, cover glass and inter-connections were bonded. The entire array was then deployed from a pair of synchronized roller assemblies. The arrays were placed back-to-back to provide a 360° field of view. Stabilization for the arrays was provided by a scissored linkage system. This approach was shown in the study to offer the best packaging efficiency and the lowest weight of several configurations studied. The design criteria for the study, and also for the fabrication phase, are listed below:

- The solar array package dimensions were to be no greater than 13 x 25 x 4 inches. When fully deployed, the array was to be 8' long, 1' wide, and have solar cells mounted to provide a 360° field of view. The deployment mechanism should be capable of maintaining a rigid configuration when fully deployed. The relationship between the array and the spacecraft are given in Figure 1.1.
- The array is to deploy while spinning at rates (before deployment) of 80 and 160 r.p.m.
- Target weight of the mechanism, wiring, inter-connectors, and solar cells was 12 lbs.

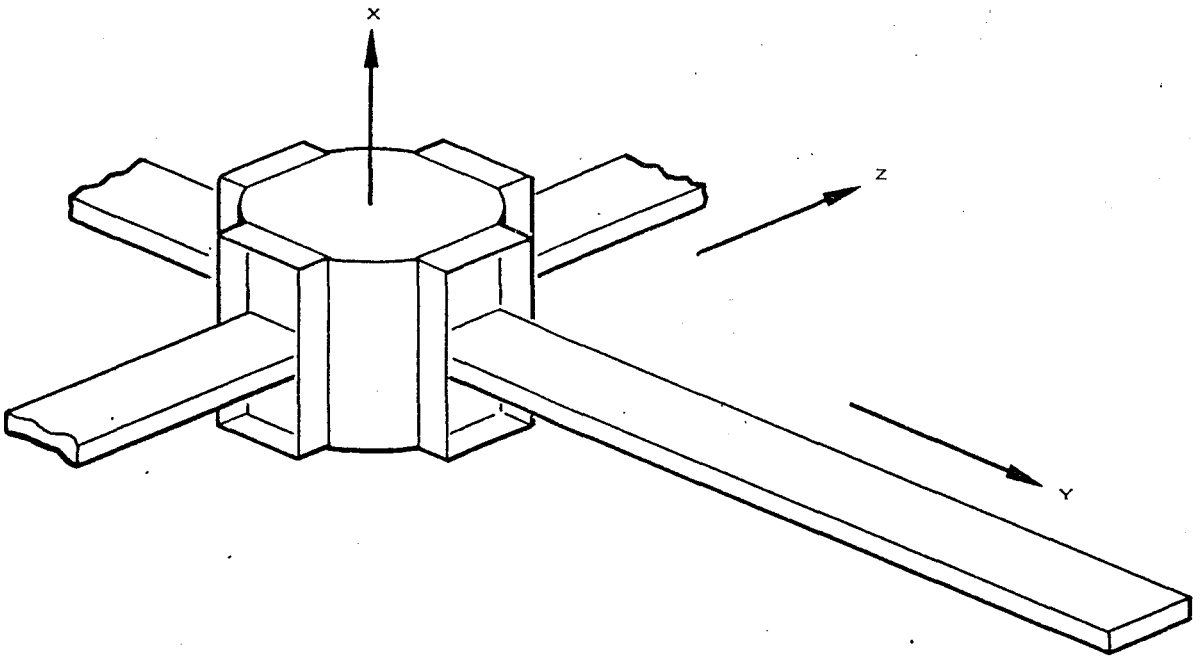

FIGURE 1.1 PANEL COORDINATE SYSTEM

- The deployment mechanism was to be capable of reliable operation in space.
- The substrate surfaces were to be compatible with RTV-40, or similar cell bonding materials.
- The packaged array must be able to withstand the shock, vibration, and accelerations of launch.
- Materials used in fabricating the system must be non-magnetic, capable of withstanding radiation and humidity.
- The packaged array was to be capable of long term storage at temperatures which may vary from $-20^{\circ}C$ to $+60^{\circ}C$ and also capable of withstanding partial vacuum conditions for extended periods without excessive deterioration.
- The extended array was to be capable of withstanding a thermal cycling test at 10^{-7} Torr pressure from $-70^{\circ}C$ to $+70^{\circ}C$ for a thousand cycles at a nominal rate of 2 hours per cycle.

- The structure was to be capable of meeting the above conditions without degrading the performance of the test cells.

In addition to developing hardware for the flexible solar array, a study was also conducted on the possibility of enlarging the area of this array to determine growth possibilities of the array as compared to other rigid systems. The data used in the study is actual data from the hardware program.

Since completion of the proof-of-principle model, several design changes are contemplated to improve the performance of the mechanism and to reduce its weight. Improvements are also being considered in the manufacture and handling of the flexible array which was found to be a delicate operation during the proof-of-principle model development.

2.0 DESIGN

Phase I of the Deployable Solar Array Project concentrated on developing hardware for deploying a 1' x 8' array of solar cells. The design criteria is covered in Section 1.0.

As previously mentioned, the solar cells are attached to flexible substrates. Two arrays, back-to-back, are necessary for the field of view required. The arrays are packaged on separate rollers to prevent the cells from coming in direct contact with each other when wound up. In addition, it was found difficult to wind a substrate with cells on both sides because of the considerable strain on the electrical inter-connection between the cells. In the design currently being used, a layer of thin polyurethane foam is bonded to the back of the substrate to provide a shock resistant buffer between the face of the solar cell and the back of the next outer layer. This has proved to be sufficient protection and, in addition, has provided considerable damping to the system. A synchronizing gear train was used to insure that both substrates are deployed at the same rate.

When deployed the substrate is supported, for load conditions normal to the array, by a scissors type linkage. For a spinning vehicle, however, it is theoretically possible that none would be needed. A spring motor and screw jack system provides deployment energy in addition to the centrifugal force.

A centrifugal brake is used to limit the deployment rate of the substrate and thereby reduce side loads on the system caused by Coriolis forces. The brake is directly coupled to the substrate synchronizing system.

The forces for deployment are the centrifugal force acting on substrate and linkage plus the force imposed by the negator spring driving the screw jacks and the scissors brake.

2.1 RELEASE MECHANISM

The release mechanism is primarily to provide 3-axis support for the extension linkage during the boost phase of flight. It is also to keep the rollers from deploying the solar arrays prematurely.

The mechanism chosen for this application is shown in Figure 2.1. It consists of two sets of clamping hooks attached to the end plates of the structure. These restrain the front plate of the mechanism. They are arranged so that release of both sides is nearly simultaneous. Unsymmetrical loads would otherwise occur at the beginning of deployment. The energy for the deployment was intended to be pyrotechnic devices. But, due to the many deployments felt necessary for development tests, an electrical solenoid device was substituted. The solenoid, when activated, pulls a sliding cam upward as shown in the figure. This cam in turn activates the push rod. Attached to the push rod are two locking blocks circular in shape and extending through the end plates. (The rod is also supported in the center on one of the screw jack support posts to improve the structural stability.) When this push rod is displaced, the restraint levers are free to rotate and release the tension on the tension rod. The released energy then pushes forward on the toggle linkage, opening the clamping hooks, thus releasing the forward plate. The linkage and substrate are then free to deploy. The clamping hooks are fabricated to form a cam that will open under the centrifugal force whether or not the release spring is active. All parts of the mechanism are of aluminum, with the exception of some hinge pins, etc. which are made of beryllium copper or non-magnetic stainless steel. To keep the substrate from unraveling, the substrate synchronizing gear train is locked by the gear latch on the sliding cam rod.

The original concept proposed in the study was to use a double-cable cutting device which would latch the front plate with a set of "fingers". This was discarded for several reasons:

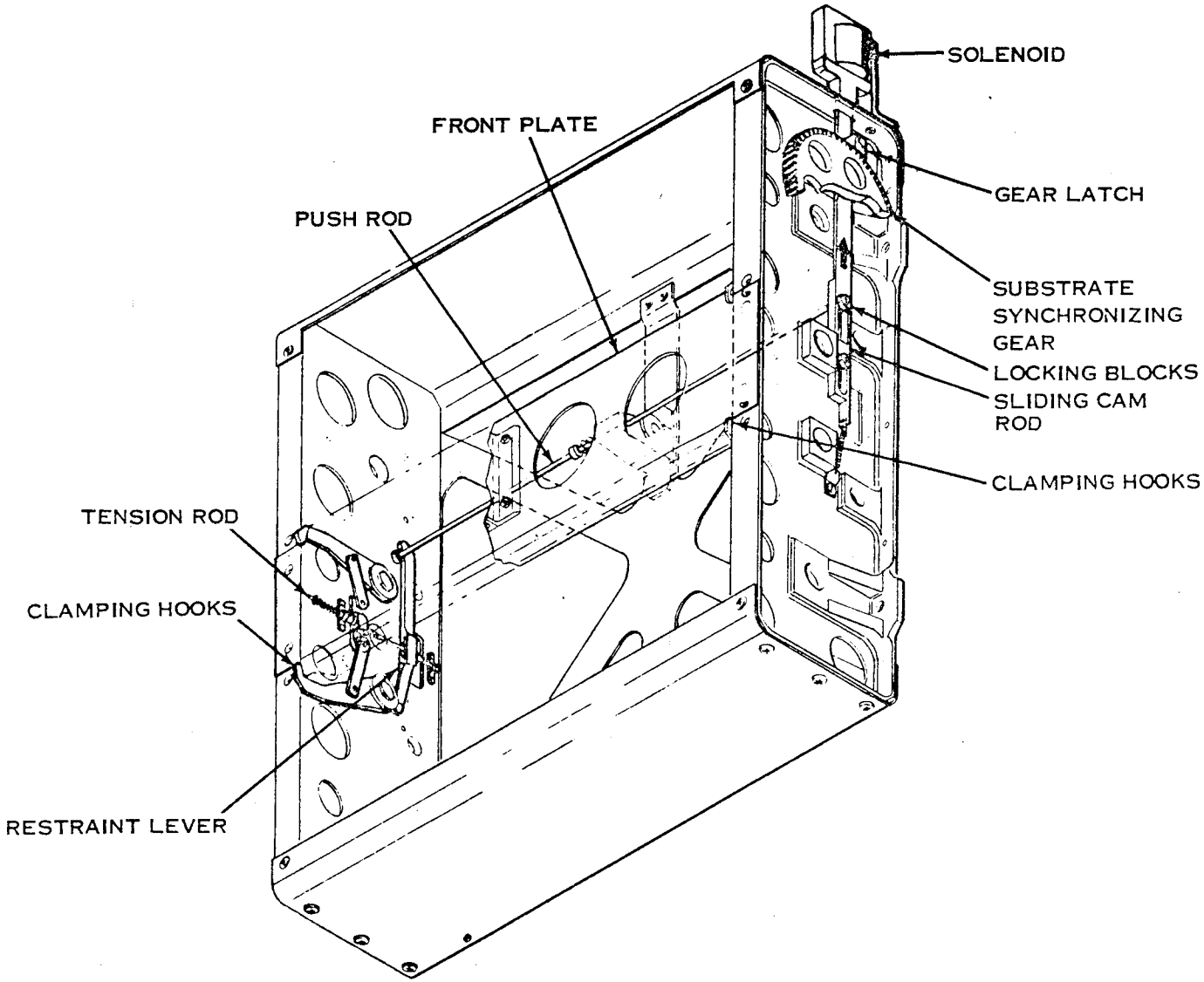

FIGURE 2.1 RELEASE SYSTEM

- The cable would have a tendency to be free and perhaps jam the mechanism.
- Fragments of the cut cable could interrupt other systems on the spacecraft if it came into contact with them.

The present release mechanism is a design which can be extrapolated to much larger assemblies. The only probable modification needed for a larger array would be strengthening of the front plate and perhaps spreading the clamping hooks further apart to accommodate deeper scissors linkages.

2.2 DRIVE AND EXTENSION MECHANISM

For a spinning vehicle, and with the particular requirements for the Deployable Solar Array, it is theoretically possible that no drive and extension mechanism is necessary. Because of ground handling and the possibility of complete spacecraft despin, however, it was felt that some system of support must be provided for the flexible arrays. The system chosen was the motor spring and screw jack drive system shown in Figure 2.2. The linkage itself consists of 8-1/2 box links, hinged end-to-end. The inboard box link is attached to a set of ball screws. Additionally, upper and lower channel links are attached to the box links in such a manner as to form an expandable scissors structure. The screw jacks to which the linkage is attached are fastened on their ends to the structural endplates and in its mid-span to a set of pillow blocks. The pillow blocks are intended to be fastened directly to the spacecraft structure. In this manner, the moment due to the weight of the array, under a 1g environment, can be directly transferred into the spacecraft, and thereby not induce large loads to the solar array structure.

The screw jacks are driven by a gear train, the central gear of which is attached to a Negator spring drum. Upon deployment, the spring imparts a torque to the screw jacks. The screw jacks are left and right hand threads so that an applied torque will supply a pinching motion of the linkages.

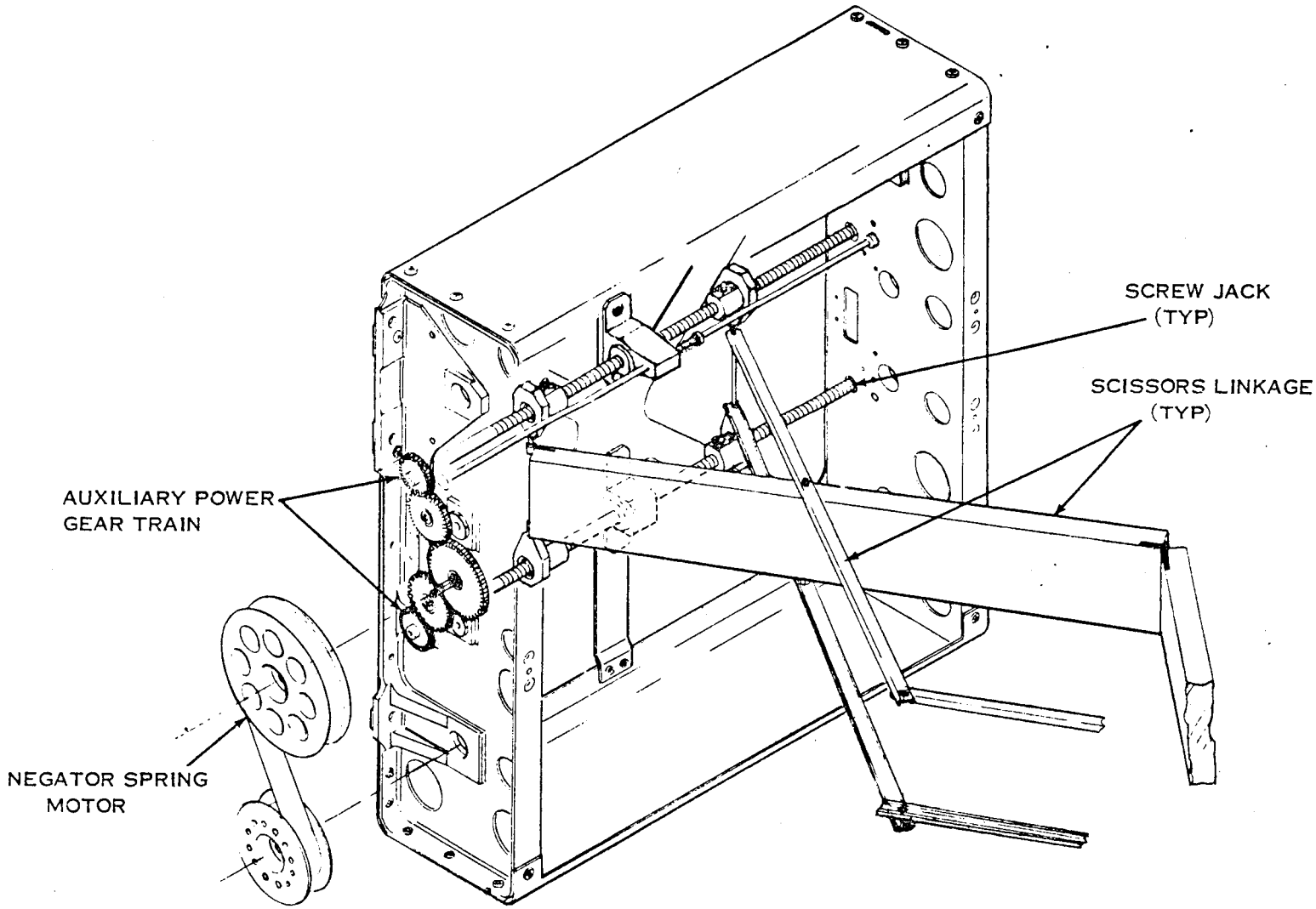

FIGURE 2.2 DRIVE AND EXTENSION SYSTEM

The box linkages are manufactured of magnesium frames to which are bonded aluminum face sheets. The inboard three lengths have face sheets of .016 inch thickness and, in addition, have a polyurethane rigid foam core for face sheet stability. The next three adjacent outboard links are the same construction, but due to the decreased loads the foam core was deleted. The next two and one-half outboard lengths are the same in construction as the preceding three, except that the face sheets are .008" thick. The upper and lower drive links are made of aluminum extrusions. The screw jacks for the proof-of-principle model are purchased parts and are made of cold rolled steel, heat treated to 125,000 psi. The ball nuts are of the same material. These do not meet the non-magnetic requirement, and their selection was based on cost and delivery schedule. For the prototype models, both of these items will be manufactured of titanium as per the study. The gear train on the end of the screw jack assemblies are phenolic. Both drums to run the Neg'ator* motor are magnesium. The Neg'ator spring was intended to be beryllium copper, but during the check-out of the mechanism it proved to be inadequate. Therefore, a stainless steel unit was substituted. A stainless steel spring will also be used for the prototype model.

2.3 DAMPER SYSTEM

The damper system on the Deployable Solar Array was intended to delete, or to eliminate as far as possible, the side loads due to despin of the spacecraft. An additional reason for damping the deployment is to eliminate a large shock at the termination of array travel.

The damping system as sketched in Figure 2.3 consists of two substrate rollers, their synchronizing gear train, and the centrifugal brake. It will be noticed that in addition to synchronizing the rollers there is also a power transfer through the gear train. The force in the substrates is due to the centrifugal force caused by the spinning spacecraft and also the force exerted by the scissors linkage.

* Registered trade mark of the Hunter Spring Co.

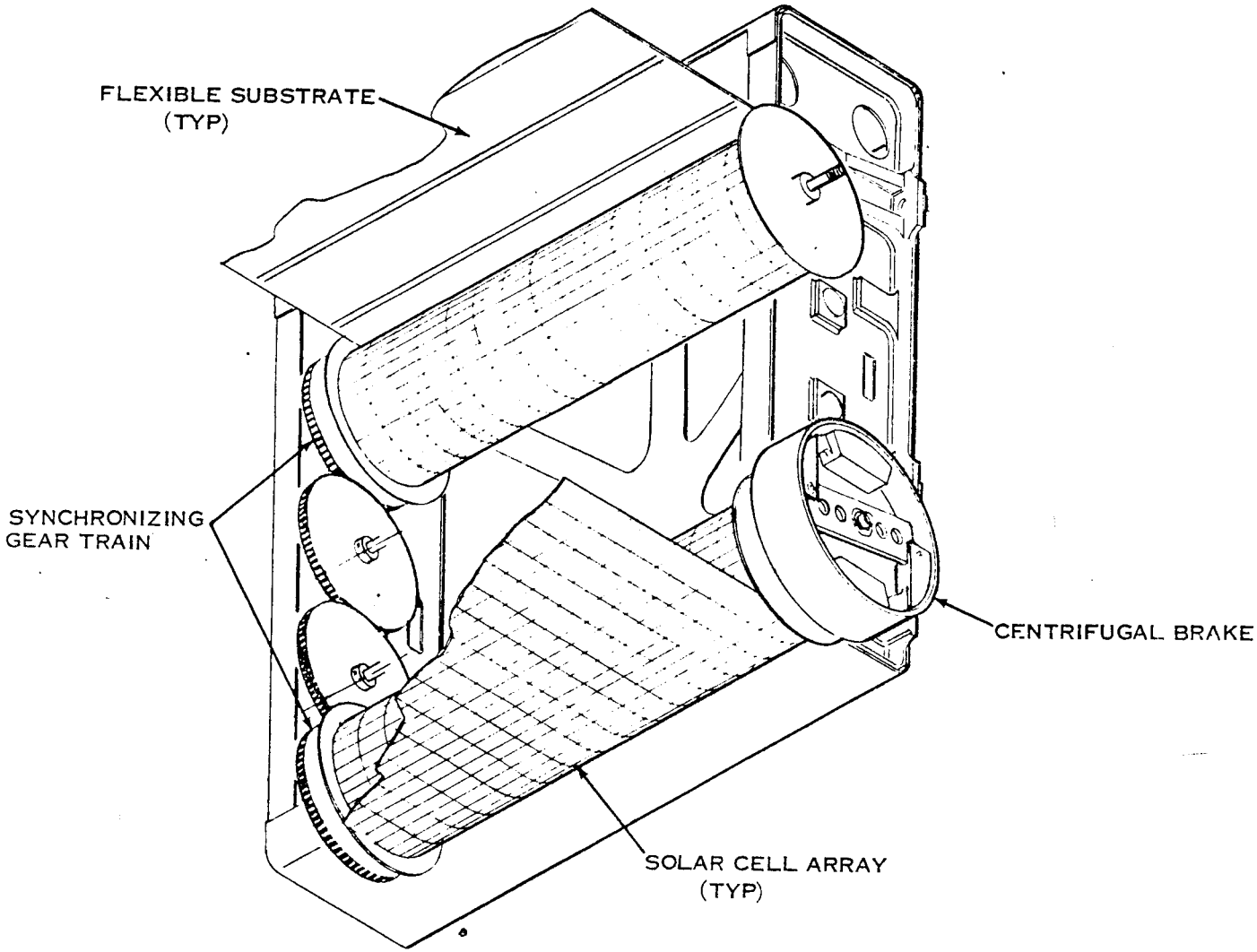

FIGURE 2.3 DAMPER SYSTEM

The brake contains a planetary gear drive which rotates the brake shoes at a much higher rate than the rollers. The brake shoes are of a self-energizing type. The repeatability of the centrifugal brake is good under similar operating conditions. The brake is a proven mechanical device and little difficulty is involved in analyzing its performance. The force/velocity ratio of the centrifugal brake is also optimum for this application in that it is a V^2 type damper, i.e., the harder the substrate is pulling, the more braking is supplied by the damper. Due to its simplicity, the cost of fabrication is relatively small. The centrifugal brake was also chosen because it offered the wide choice of adjustments for regulating the velocity of the substrate. This adjustment can be in several ways. The most obvious, of course, is changing the friction pads to a different coefficient of friction on the brake shoe. Another method is to increase the mass of the fly weight. A third method, which has the greatest effect but which is hardest to incorporate, is changing the gear ratio of the brake.

The materials used in this system are all non-magnetic. The rollers are fabricated of aluminum tubing with aluminum end fittings. The synchronizing gear train is also aluminum as well as the housing for the brake and all other brake parts (with the exception of the fly weights). Brass was chosen in order to obtain a high density.

2.4 STRUCTURE

The housing on the Deployable Solar Array is to support the mechanism and the substrate for vibration, spin, launch and handling loads. The structure is rigid enough to provide for deployment without binding of the mechanisms and is also lightweight and relatively simple to manufacture. A minimum of dissimilar metals has been used to alleviate galvanic action and differential thermal expansion.

A bearing mount in the end plates was necessary because of mounting of the rollers, drive screws, etc. The easiest way to do this, it was felt, was to

use a machined part since it is not excessively large. The material selected was a magnesium billet. The top and the bottom covers of the structure are also of magnesium, but of .032 sheet metal. The backplate, which affords only stability for handling and is not actually a part of the structural design, is also .032 magnesium sheet. A sketch of the structure is shown in Figure 2.4.

Growth possibilities for this structure are good since very little weight increase is involved in extending the upper, lower, and backplates to make a much wider structure; nor does the depth of the box need to become much greater to accommodate a larger array.

2.5 SUBSTRATE

It was determined during the study phase of this program that a practical flexible solar cell array should be flexible only in the direction normal to the roller from which it deploys. This will prevent the substrate from sagging across its width and inducing unnecessary loads into the cell interconnects. To satisfy these requirements, consideration was given during the study to the details of design, material selection, fabrication feasibility, and functional reliability of the array.

The study recommendations were followed during the Phase I fabrication of the proof-of-principle dummy arrays. Although some tests were run during the study, additional work was done early in Phase I of this program to further validate the study results. Tests led to the design of the flexible array using 3 mil Kapton polymide film substrate. Bonded on the forward side were .025 aluminum chips, and on the reverse side .025 magnesium stiffeners were added intermittently. A foam backing was then applied across the complete aft side of the array to prevent scuffing of the solar cells against the stiffeners and the back of the film.

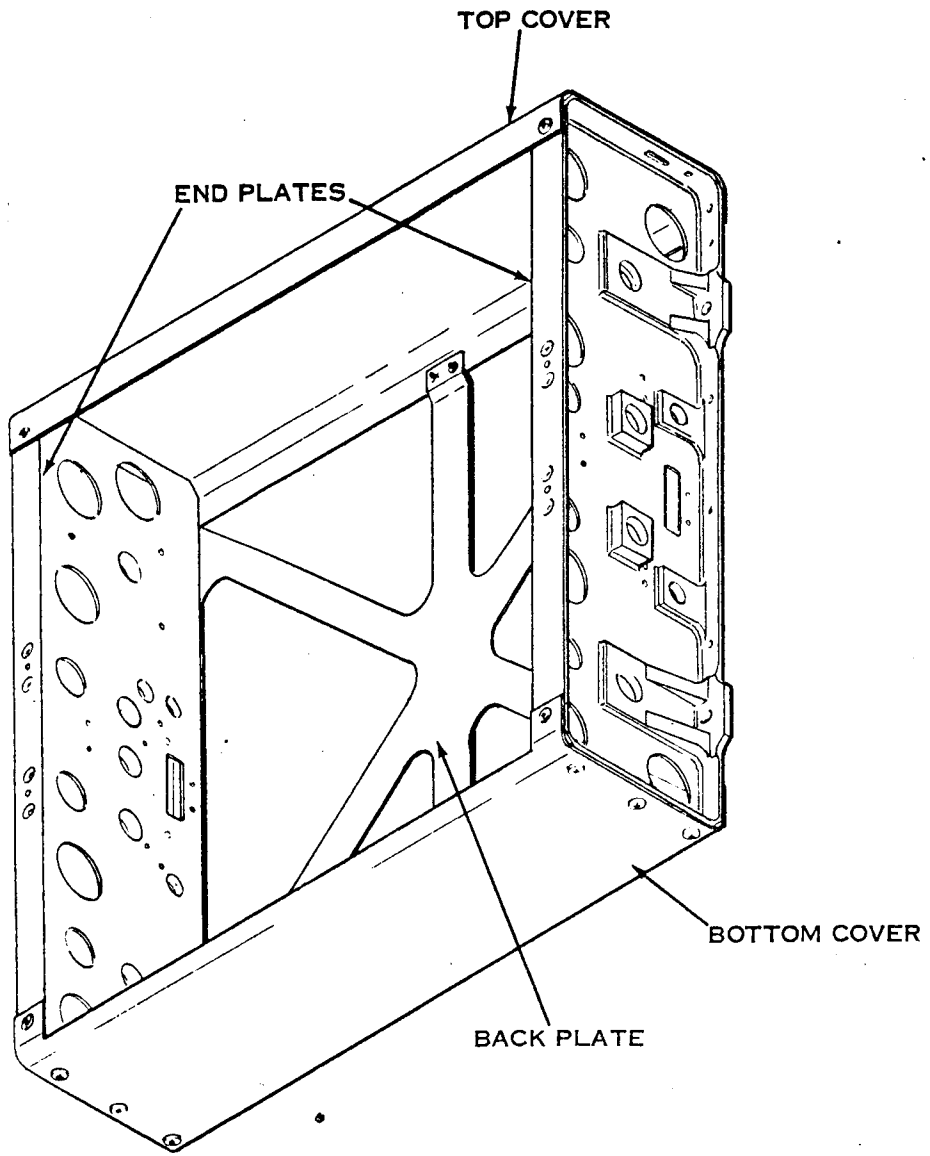

FIGURE 2.4 STRUCTURAL ASSEMBLY

Three materials were considered for the substrate: Kapton, Mylar, and Fiberglass cloth impregnated with silicon rubber. The Kapton was selected because of its high strength for a wide temperature range coupled with a very light weight.

The fiberglass and rubber combination could not be made in light enough gauges to compete with the films for this application. In addition, the Kapton has good dielectric properties, good folding endurance, and is more radiation resistant than the mylar. One drawback with the Kapton seemed to be its notch sensitiveness. This was, however, felt to be acceptable with the loads anticipated on the array.

The aluminum chips used to simulate the 13 mil cells plus their 6 mil cover glass were .025 thick. This is slightly heavier than the cell and cover glass combination, but was felt to be adequate for ballast.

The stiffeners intermittently installed on the back of the array were .025 magnesium. Other materials considered included fiberglass reinforced plastic, beryllium, aluminum, and beryllium copper. Beryllium would have been the best choice structurally, but its cost was prohibitive.

The foam backing on the aft side of the array was a .032 thick polyurethane bonded to the aft side of the array with an epoxy adhesive. This combination seemed to be adequate and very little scuffing of the foam or marring of the simulated cells was found during subsequent handling and testing.

A test program was initiated to find the proper combination of film, adhesive primers, surface preparations, etc. In this test 3 and 5 mil specimens to the shape shown in Figure 2.5 were selected for test. Several adhesives were tried. These included RTV-40's, Epoxy 828 with a plasticizer, and Dow 92-018. Surface preparation included mechanically roughing the surface

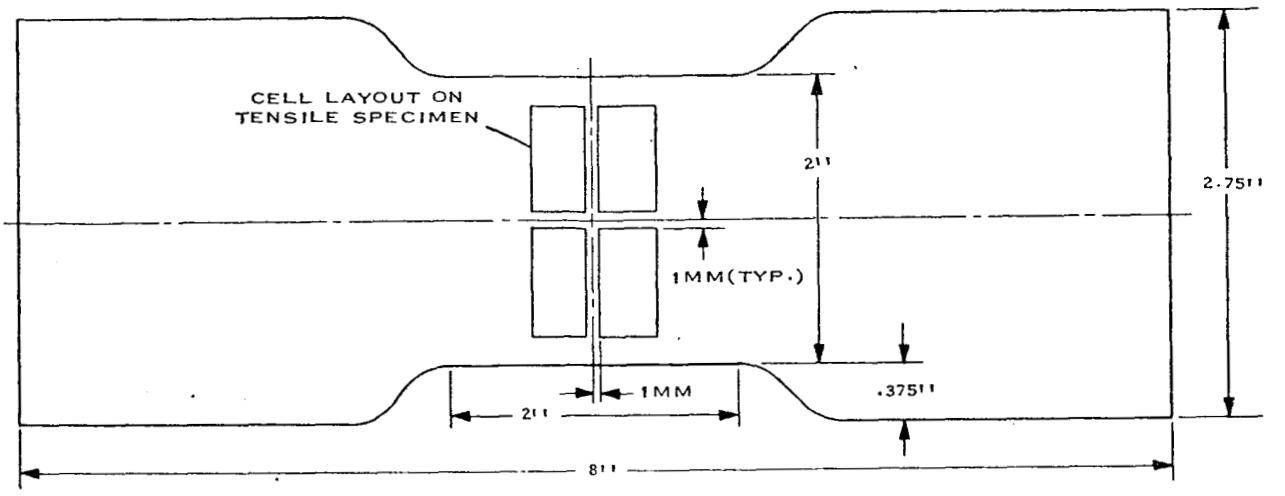

FIGURE 2.5 TENSILE TEST SPECIMEN

of the Kapton and adding a primer for the RTV series. Surface preparation for the other adhesives included buffing the surface and cleaning with MEK.

The results of these tests indicated that the RTV-40 would not adhere well to the film and would peel very easily. The Dow 92-018 was equally poor and cells came off relatively easily. The epoxy was brittle but the plasticizer seemed to alleviate this condition somewhat. The epoxy was selected although it was not felt to be the best possible solution. However it looked adequate for use on the test substrates. One curious effect of bonding with the epoxy on the Kapton film was the lower strength exhibited by the film during the test. This was probably due to some chemical interaction between the epoxy and the film. The loss in strength was approximately 10% over an unbonded test specimen. The Kapton film also seemed to be fairly notch sensitive during this test, so great care was given during the fabrication of the dummy substrates to putting on very smooth edges. The epoxy bonding

of the cells to the film is not considered to be the final solution, and greater effort will be put into developing a better system during Phase II when live cells also will be attached to the substrate.

During the testing of the unit, several cells came off; but a great deal more were damaged by just handling of the array in its deployed condition. This points up the problem of developing sufficient handling equipment for a flexible array of this or any other configuration.

The array was fastened to the substrate roller by bonding with the epoxy adhesive. To provide greater reinforcement it was also doubled back upon itself at the frontplate attachment as well as at the rollers. Epoxy was used for this but proved to be very unsatisfactory in that it stiffened the substrate a great deal and made the problem of popping the cells off much greater.

Figures 2.6A, 2.6B, and 2.6C are the assembly drawings of the Deployable Solar Array. They are reduced prints of FHC Drawing 528-00000.

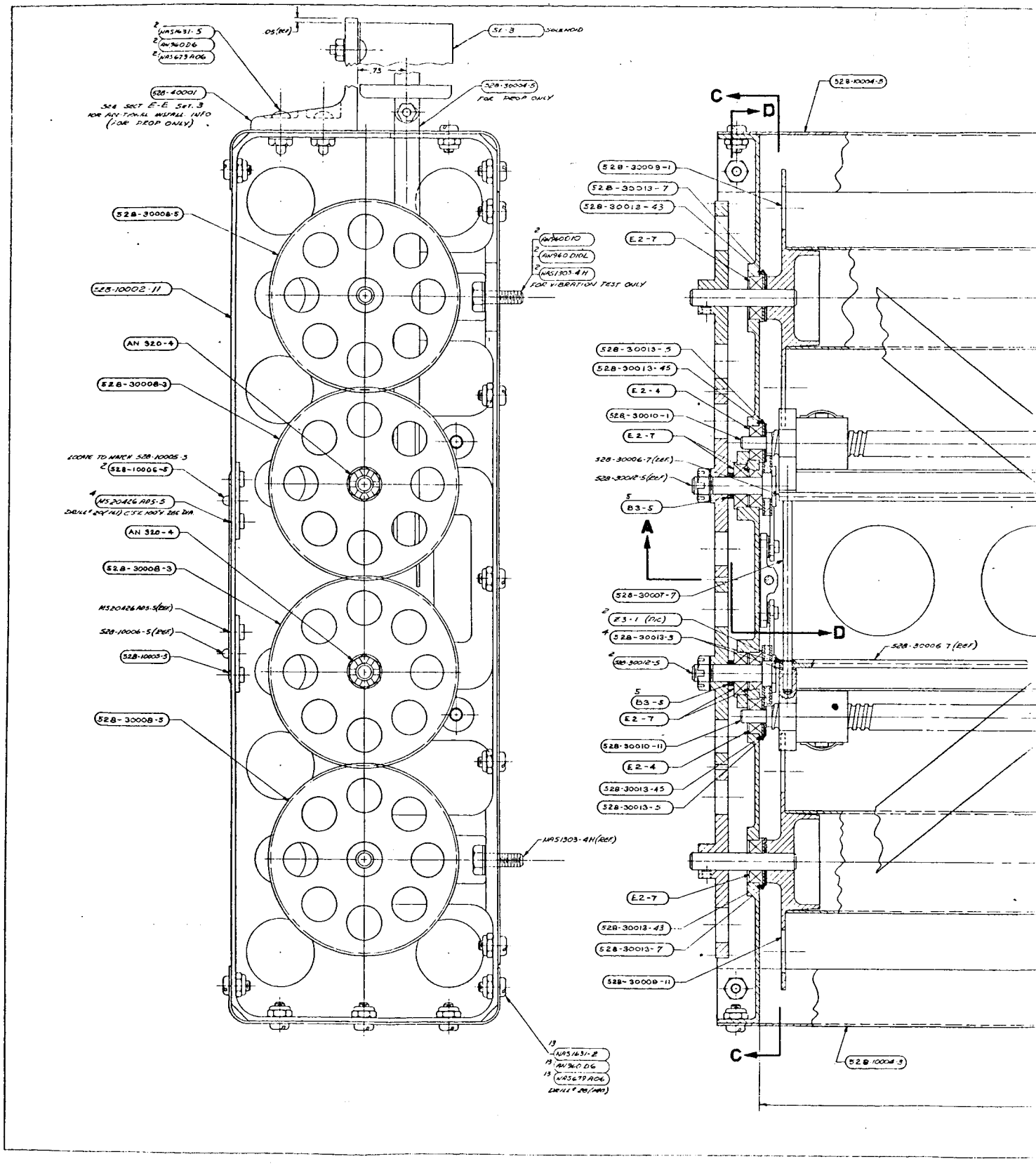
2 NAS1631-5
2 AN960D6
2 NAS679A06
.05(REF)
.75
S1-3 SOLENOID
528-40001
SEE SECT E-E SHT. 3 FOR ADDITIONAL INSTALL INFO (FOR PROP ONLY)
528-30004-5 FOR PROP ONLY
528-30008-5
528-10002-11
AN 320-4
528-30008-3
LOCATE TO MATCH 528-10005-3
2 528-10006-5
4 MS20426AD5-5
DRILL #20(.161) C'SK 100°V .286 DIA.
AN 320-4
528-30008-3
MS20426AD5-5(REF)
528-10006-5(REF)
528-10005-3
528-30008-5
2 AN960D10
2 AN960D10L
2 NAS1303-4H
FOR VIBRATION TEST ONLY
NAS1303-4H(REF)
13 NAS1631-2
13 AN960D6
13 NAS679A06
DRILL #28(.140)
C
D
528-10004-3
528-30009-1
528-30013-7
528-30013-43
E2-7
528-30013-5
528-30013-45
E2-4
528-30010-1
E2-7
528-30006-7(REF)
528-30012-5(REF)
5 B3-5
A
528-30007-7
2 #3-1 (P/C)
4 528-30013-5
2 528-30012-5
528-30006-7(REF)
5 B3-5
E2-7
528-30010-11
E2-4
528-30013-45
528-30013-5
E2-7
528-30013-43
528-30013-7
528-30009-11
C
528-10004-3

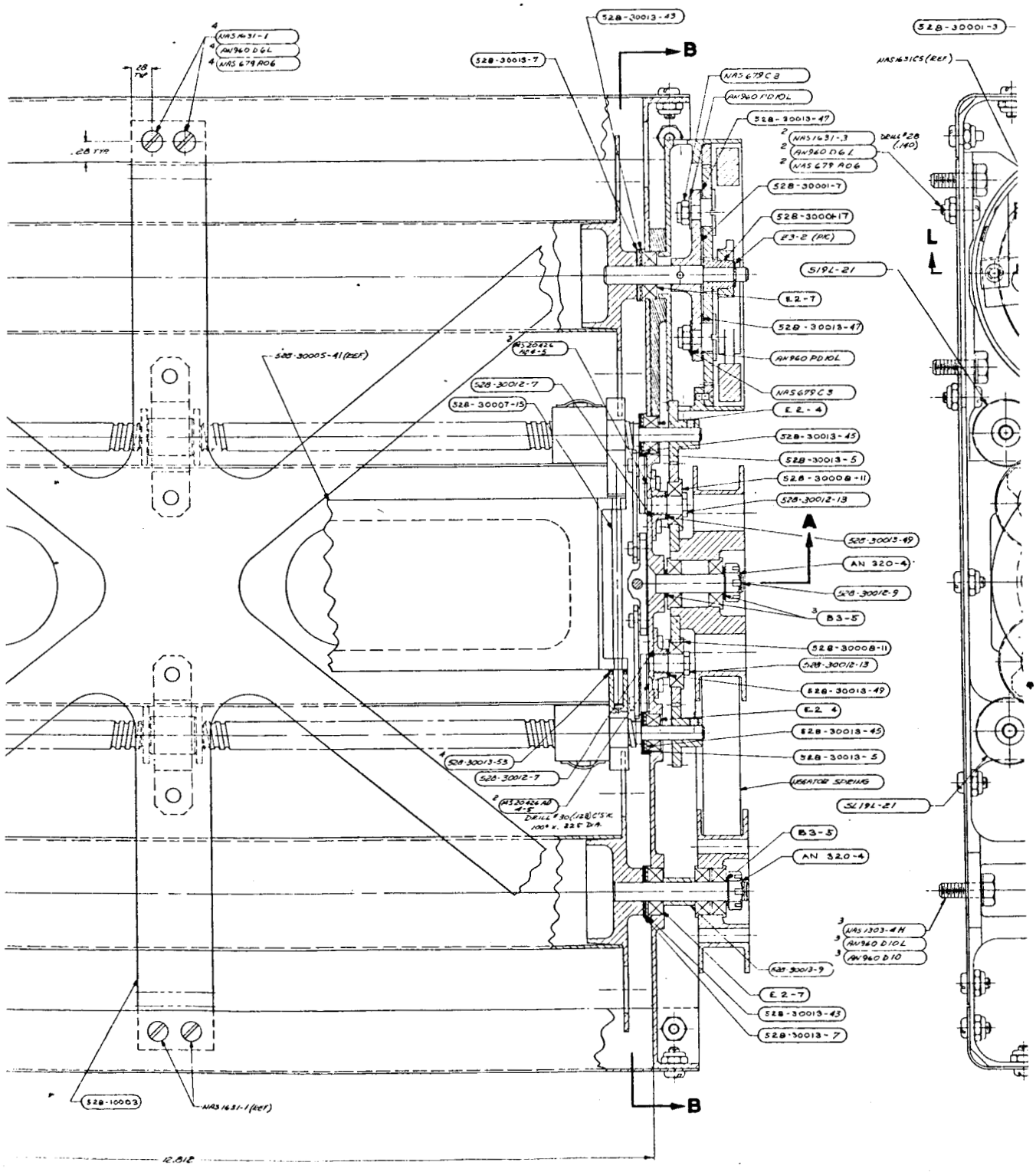
4 NAS1631-1
4 AN960D6L
4 NAS679A06
.28 TYP
.28 TYP
528-30013-43
528-30013-7
B
NAS679C3
AN960PD10L
528-30013-47
2 NAS1631-3
2 AN960D6L
2 NAS679A06
DRILL #28 (.140)
528-30001-7
528-30001-17
F3-2 (PIC)
519L-21
E2-7
528-30013-47
AN960PD10L
NAS679C3
E2-4
528-30013-45
528-30013-5
528-30008-11
528-30012-13
A
528-30013-49
AN 320-4
528-30012-9
3 B3-5
528-30008-11
528-30012-13
528-30013-49
E2-4
528-30013-45
528-30013-5
VIBRATOR SPRING
SL19L-21
B3-5
AN 320-4
3 NAS1303-4H
3 AN960D10L
3 AN960D10
528-30013-9
E2-7
528-30013-43
528-30013-7
528-30001-3
NAS1631C5 (REF)
L
L
528-30005-41 (REF)
3 NAS20426 AD8-5
528-30012-7
528-30007-13
4 528-30013-53
528-30012-7
2 NAS20426 AD 4-5
DRILL #30 (.128) C'SK 100° x .225 DIA.
528-10003
NAS1631-1 (REF)
B
12.812

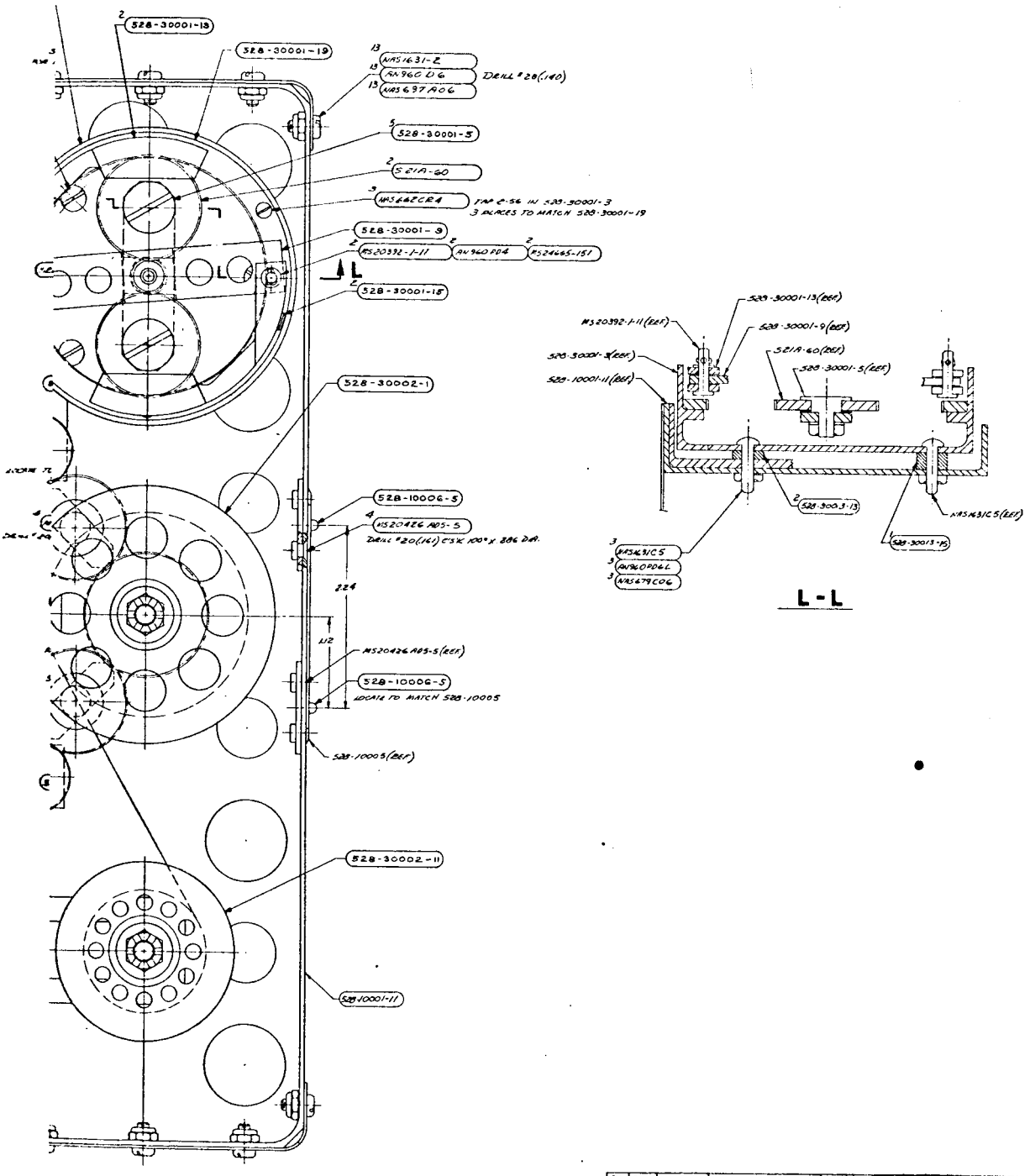
528-30001-18
528-30001-19
NAS1631-2
AN960 D6
NAS697A06
DRILL #28(.140)
528-30001-5
521A-60
NAS682CR4
FOR 2-56 IN 528-30001-3
3 PLACES TO MATCH 528-30001-19
528-30001-9
MS20392-1-11
AN960PD4
MS24665-151
L
528-30001-15
528-30002-1
528-10006-5
MS20426AD5-5
DRILL #20(.161) CSK 100° X .386 DIA.
224
112
MS20426AD5-5(REF)
528-10006-5
LOCATE TO MATCH 528-10005
528-10005(REF)
528-30002-11
528-10001-11
528-30001-13(REF)
MS20392-1-11(REF)
528-30001-9(REF)
528-30001-3(REF)
521A-60(REF)
528-30001-5(REF)
528-10001-11(REF)
528-30013-13
NAS463C5(REF)
528-30013-15
NAS463C5
AN960PD6L
NAS679C06
L-L
ITEM NO REQD PART NO DESCRIPTION MATERIAL SPECIFICATION
LIST OF MATERIALS
MATERIAL
HEAT TREATMENT
FINISH
ALL TOLERANCES ±
APPROVAL
DATE
FAIRCHILD HILLER SPACE SYSTEMS DIVISION WASHINGTON, D.C. AREA
FINAL ASSEMBLY-
DEPLOYABLE SOLAR
ARRAY
CODE IDENT NO 52B
17232
SCALE 2/1
SHEET 2
REV ASSY REVISION APPROVAL
APPLICATION QTY

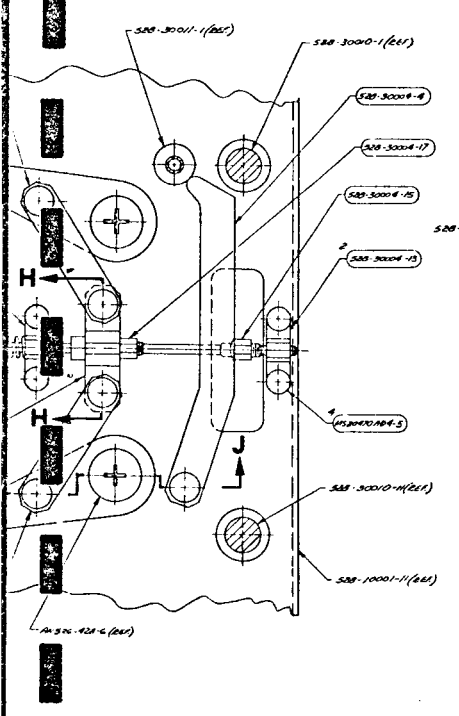

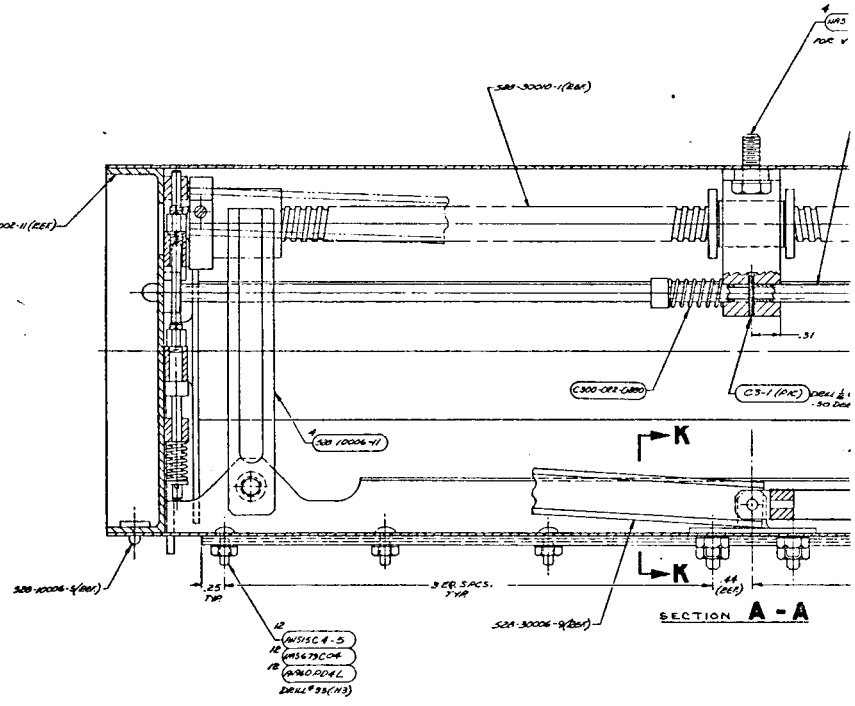

SECTION A - A

SECTION B - B

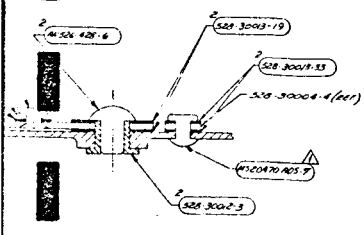

SECTION J - J

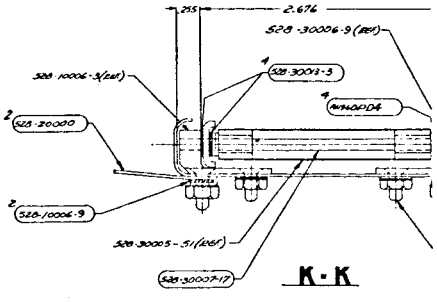

K - K

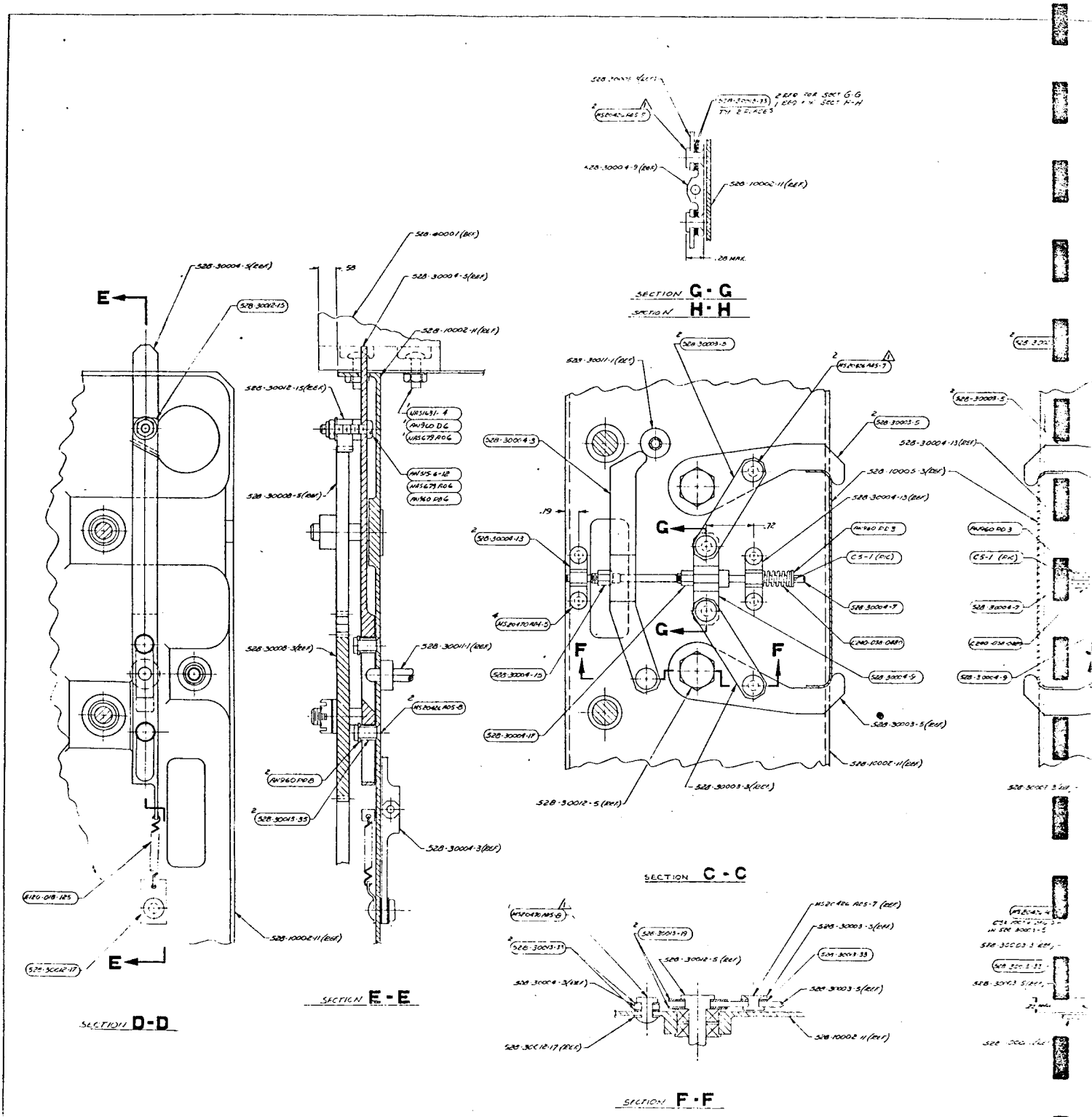
SECTION G-G
SECTION H-H
SECTION D-D
SECTION E-E
SECTION C-C
SECTION F-F
528-30004-5(REF)
528-30012-15
528-40001(REF)
528-30004-5(REF)
528-10002-11(REF)
528-30012-15(REF)
528-30008-5(REF)
528-30008-3(REF)
528-30011-1(REF)
528-30004-3(REF)
528-10002-11(REF)
528-30011-1(REF)
528-30003-5
528-30004-3
528-30004-13
528-30004-17
528-30012-5(REF)
528-30003-3(REF)
528-10005-3(REF)
528-30004-13(REF)
528-30004-9
528-30003-5(REF)
528-10002-11(REF)
528-30012-17(REF)
528-30012-17(REF)
528-30012-5(REF)
528-30003-3(REF)
528-10002-11(REF)

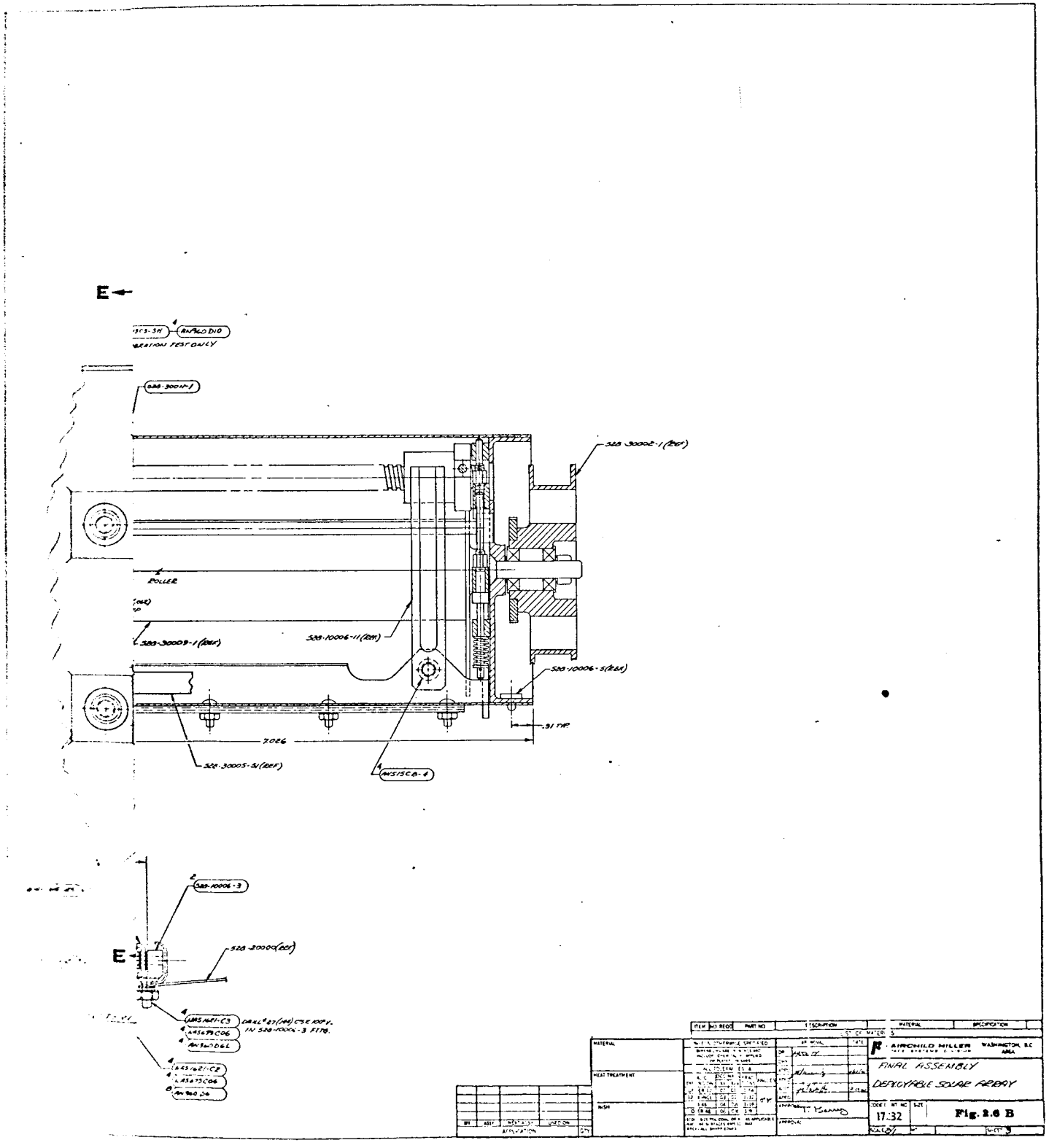
E
ROLLER
.31 TYP
7.026
E
FINAL ASSEMBLY
DEPLOYABLE SOLAR ARRAY
AIRCHILD MILLER
WASHINGTON, D.C. AREA
17.32
Fig. 2.6 B

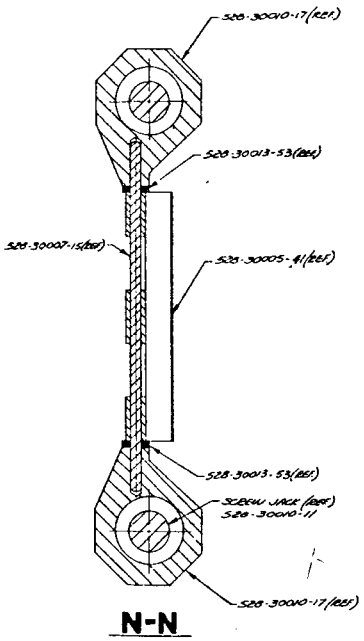

N-N

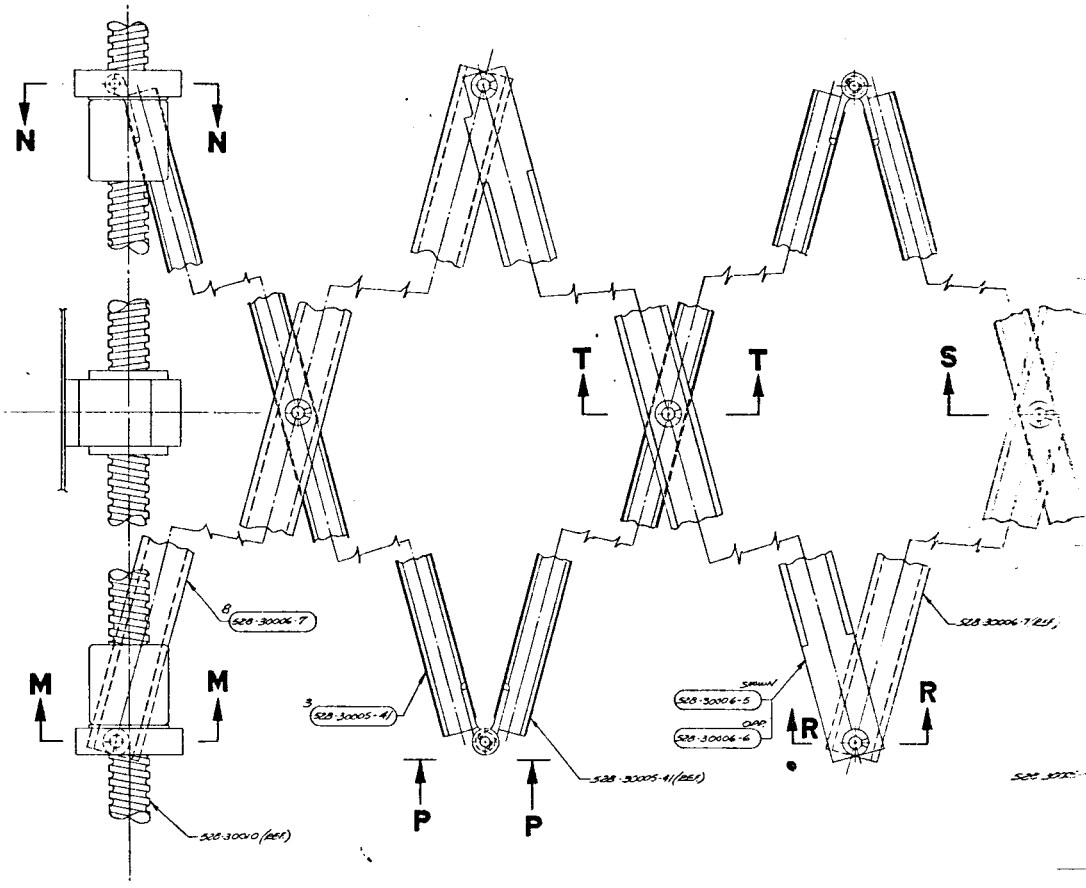

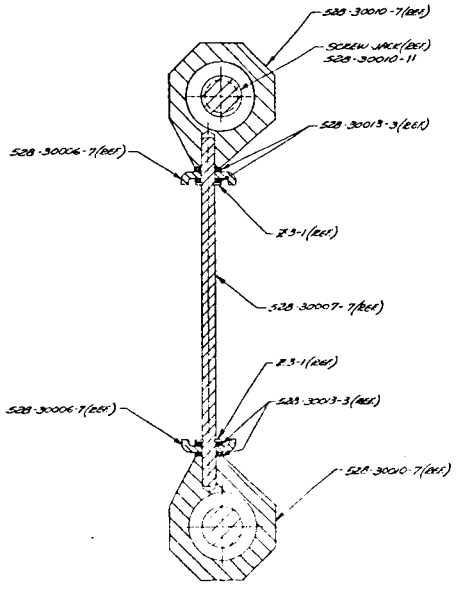

M-M

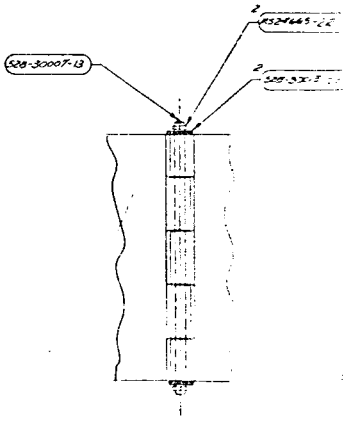

P-P

(6 PLACES)

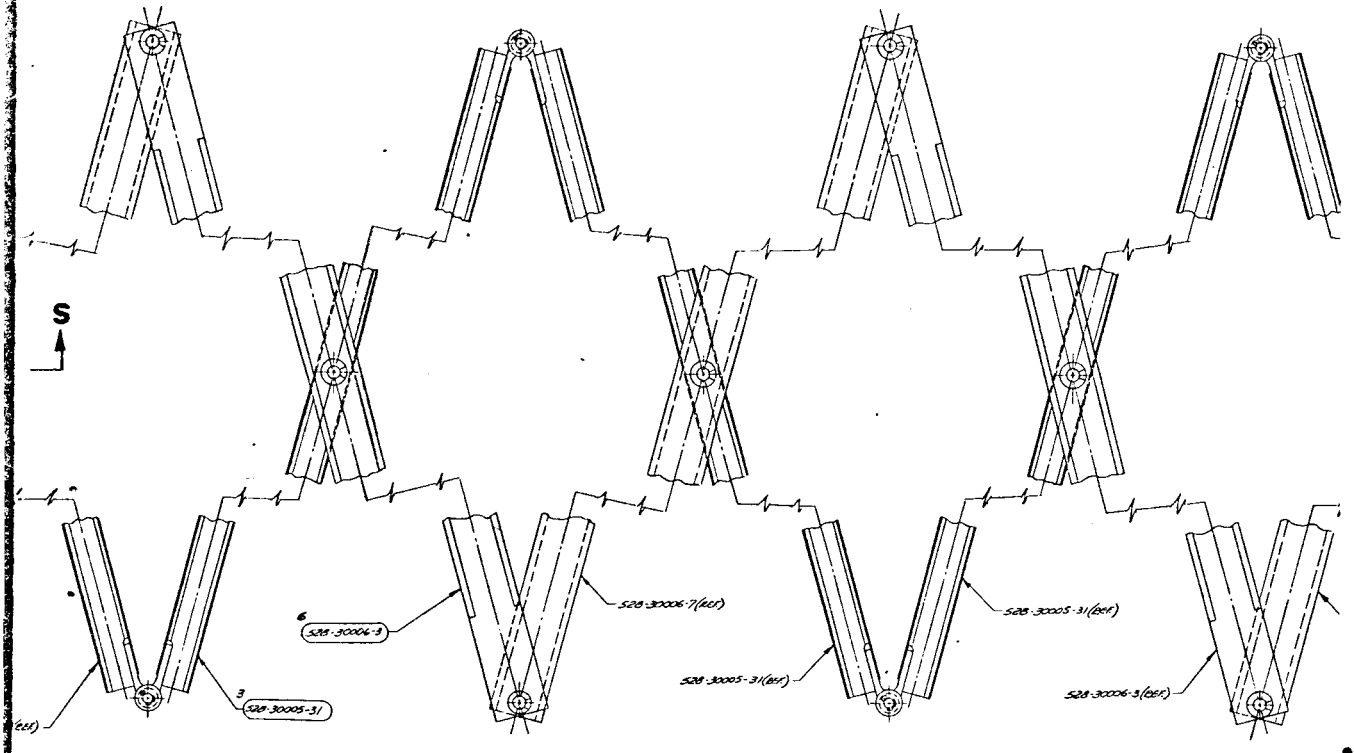

VIEW OF LINKS WITH LINKS PARTIALLY DEPLOYED

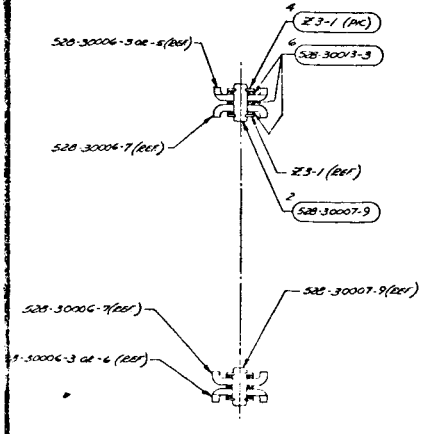

R-R

TYP HINGE INSTALL FOR CHANNEL LINKS
(8 PLACES)

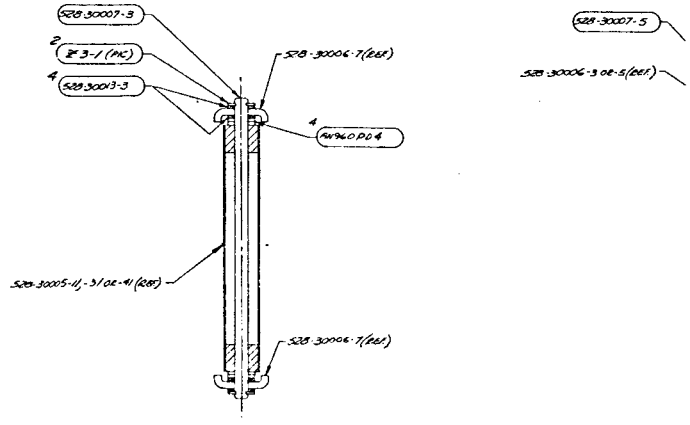

S-S

TYP 4 PLACES

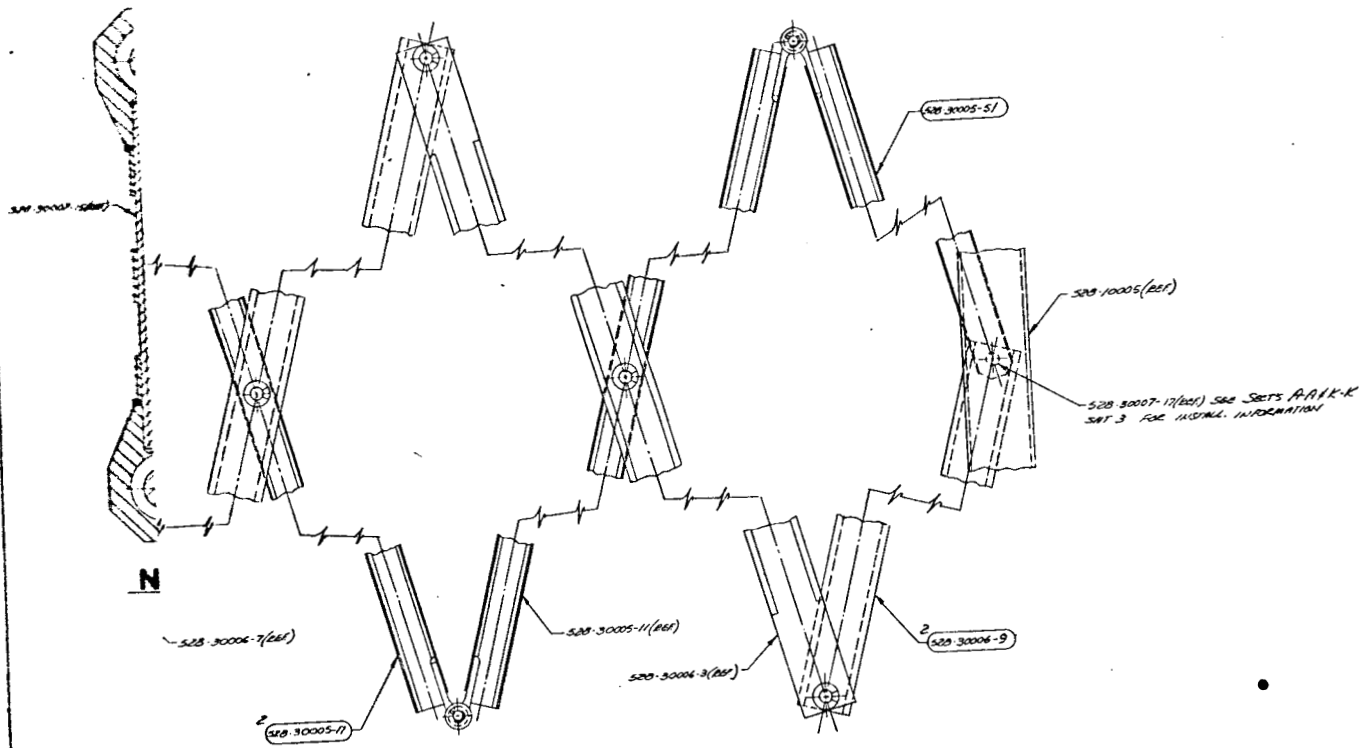

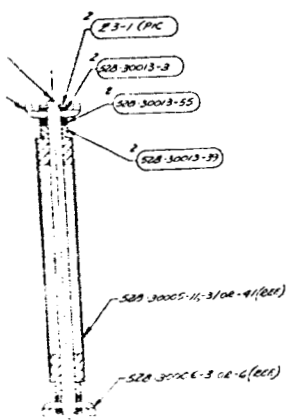

T-T

TYP 4 PLACES

UNLESS OTHERWISE SPECIFIED DIMENSIONS ARE IN INCHES TOLERANCES ON DECIMALS ANGLES	APPROVAL	DATE	FAIRCHILD HILLER SPACE SYSTEMS DIVISION WASHINGTON, D.C. AREA
	DR J. Gonzalez	3/11/65	FINAL ASSEMBLY
	CHK		DEPLOYABLE SOLAR ARRAY
	APP Hamm	3/11/65	
	APP		
	APPR J. Bailey	3/11/65	
BASIC DIMENSION ±X ±Y ±Z ±N ANGLES	APPROVAL T. Banning		CODE IDENT NO. 17232 SIZE
UNDER 12 0.1 0.05 0.02 0.01 0°30'	APPROVAL		Fig. 2.6 C
12-24 INCL 0.2 0.10 0.03 0.02			SCALE 5/1 SHEET 4
24-48 0.4 0.15 0.04 0.04			
OVER 48 0.6 0.20 0.06 0.06			
STOP & FIT FILE, UNLESS OTHERWISE SPECIFIED REMOVE BURRS, SHARP EDGES			

3.0 ANALYSIS

Several analyses were performed during the course of Phase I to support design of the deployable array. They are presented in this section in the order by which they affected the detail design. These were the deployment analysis, the dynamic vibration analysis, and a detailed analysis of the structure and mechanism due to the loads imposed by the spin deployment, the vibration, and the deployment under 1g conditions.

3.1 SYSTEM ANALYSIS

This section reviews the equations of motion necessary to describe the deployment dynamics of the Deployable Solar Array. The non-linearity of the problem dictates a digital solution of the final equations.

The following assumptions were used in the analysis:

- Rigid body dynamics.
- Deployment occurs in a zero gravity field.
- Aerodynamic phenomena do not exist.
- Angular velocity vector remains coincident with the spin axis.
- Dynamic system is symmetric about the spin axis.

The mathematical model for which the program was developed consists of a centerbody housing four (4) uniformly spaced deployable arms. Upon release, the solar arrays are deployed under the influence of centrifugal force and four constant force scissors mechanisms. Self-energizing brakes, geared to the substrates, are used to limit the deployment speed.

Figure 3.1A is a diagrammatic sketch of the system. The dimensional nomenclature symbols and definitions used in this analysis are presented in Figure 3.1B.

3.1.1 Equations of Motion

Denoting the total angular momentum of the system before deployment begins as:

$$C = \omega_{c_o} I_o \tag{1}$$

it follows that the instantaneous angular velocity at any time during deployment is:

$$\omega_c = C/I \tag{2}$$

and

$$\dot{\omega}_c = -C\dot{I}/I^2 \tag{3}$$

where

$$I = \left\{ \left[\frac{W_c}{2} + 4W_B + \frac{4}{3} W_P + 4W_R + \frac{8}{3} \mu R_c \right] R_c^{\,2} + \frac{4}{3} W_P X_e^{\,2} + \frac{4}{3} W_P X_e R_c - 4\mu X_e R_c^{\,2} + \frac{4}{3} \mu X_e^{\,3} \right\} \Big/ g \tag{4}$$

$$\dot{I} = 4 \left[\mu (X_e^{\,2} - R_c^{\,2}) + \frac{W_P}{3} (2X_e + R_c) \right] \dot{X}_e \Big/ g \tag{5}$$

The development of equations (4) and (5) are found in Appendix A of the study report.

Having described the angular motion of the entire unit, the equilibrium equation for each deploying panel can now be defined. The radial forces tending to aid or restrict deployment of the flexible substrate are as follows:

3.1.1.1 Centrifugal Force

The centripetal acceleration at any point on the deployed panel is:

$$a_N = -X \omega_c^{\,2} \tag{6}$$

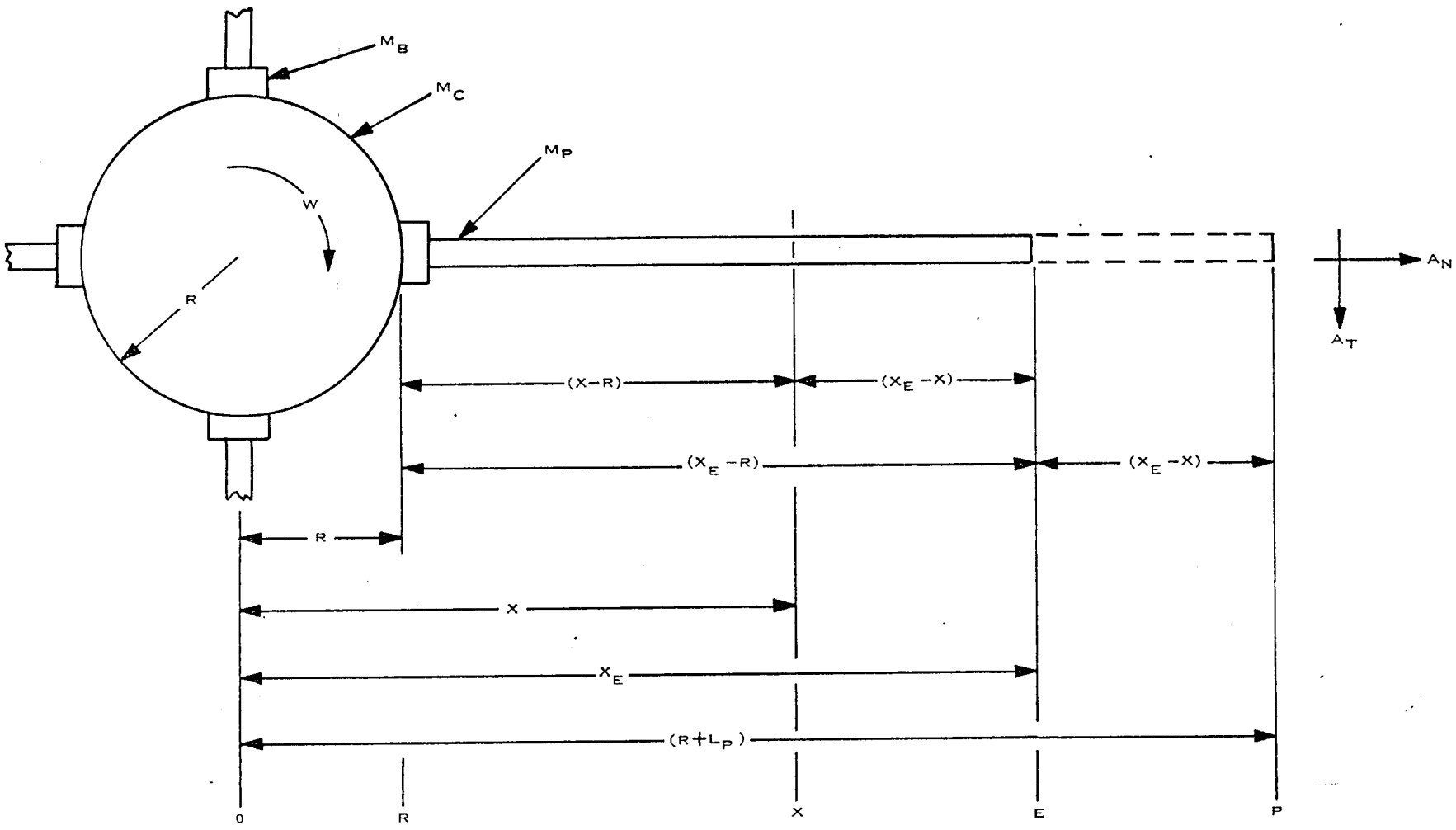

FIGURE 3.1A DESCRIPTIVE DIAGRAM

a	Linear acceleration, ft./sec.^{2}
C	Total angular momentum, ft. lb. sec.
C_f	Friction coefficient, lb./lb.
F	Force, lb.
g	Gravity acceleration, 32.2 ft./sec.^{2}
I	Mass moment of inertia about spin axis, ft. lb. sec.^{2}
L_p	Total length of substrate, ft.
N	Number of scissors links
R	Radius, ft.
S	Gear ratio, brake speed and substrate roller speed
t	Time, sec.
W	Weight, lb.
X	Radial station measured from spin axis, ft.
X_e	Distance of outermost point on deploying panel from spin axis, ft.
θ_1	Radial angle between speed brake mass hinge and friction point
θ_2	Radial angle between speed brake mass hinge and mass C.G.
μ	Substrate weight per linear foot, lb./ft.
ω	Angular velocity, rad./sec.

Subscripts

b	Refers to stationary housing boxes
c	Refers to cylindrical centerbody
e	Refers to outermost point on deploying panel
f	Refers to speed brake friction device
n	Refers to normal or radial direction
p	Refers to scissors
r	Refers to substrate (rolled and/or extended portion)
t	Refers to tangential direction
1	Refers to length

FIGURE 3.1B NOMENCLATURE

3.1.1.4 Speed Brake Force

$$F_f = - \frac{C_f S^3 W_f R_1 R_f^2 \dot{X}_e^2 \sin \theta_2}{g \left[R_f \sin \theta_1 - C_f (R_1 - R_f \cos \theta_1) \right] R_R^3} \tag{13}$$

3.1.1.5 Summation of Equations

The equation of motion for the radial motion of the deploying panels, then, can be written by summing equations (7) through (13).

$$F_{I_P} + F_{I_R} + F_{I_f} + F_P + F_{N_R} + F_{N_P} + F_f = 0 \tag{14a}$$

or

$$\left[\frac{W_P + W_R + \mu (X_e - R_c) + (2S^2 W_f R_f^2 / R_R^2)}{2g} \right] \ddot{X}_e$$

$$- \left[\frac{F_f}{\dot{X}_e^2} \right] \dot{X}_e^2 - F_P - F_{N_R} - F_{N_P} = 0 \tag{14b}$$

Solving equations (14) for $\ddot{X}_e$ and integrating twice to obtain $\dot{X}_e$ and X_e gives the following equations

$$\ddot{X}_e = \frac{2g \left(\frac{F_{y_s} \tan \phi}{N} + F_{N_R} + F_{N_P} + F_f \right)}{\left[W_P + W_R + \mu (X_e - R_c) + \frac{2S^2 W_f R_f^2}{R_R^2} \right]} \tag{15}$$

$$\dot{X}_e = \int_0^t \ddot{X}_e \, dt + \dot{X}_{e_o} \tag{16}$$

$$X_e = \int_0^t \dot{X}_e \, dt + X_{e_o} \tag{17}$$

where

$$\tan\phi = (X_e - R_c) \Big/ \sqrt{N^2 R_p^{\,2} - (X_e - R_c)^2} \tag{18}$$

$$R_R = \sqrt{R_{R_e}^{\,2} + \frac{t_R (l_p - X_e + R_c)}{\pi}} \tag{19}$$

R_{R_e} = Radius of spool on which the substrate is rolled.

Figures 3.2 through 3.6 are the result of iterating these equations with equations (2) and (4) for the conditions noted on the figures.

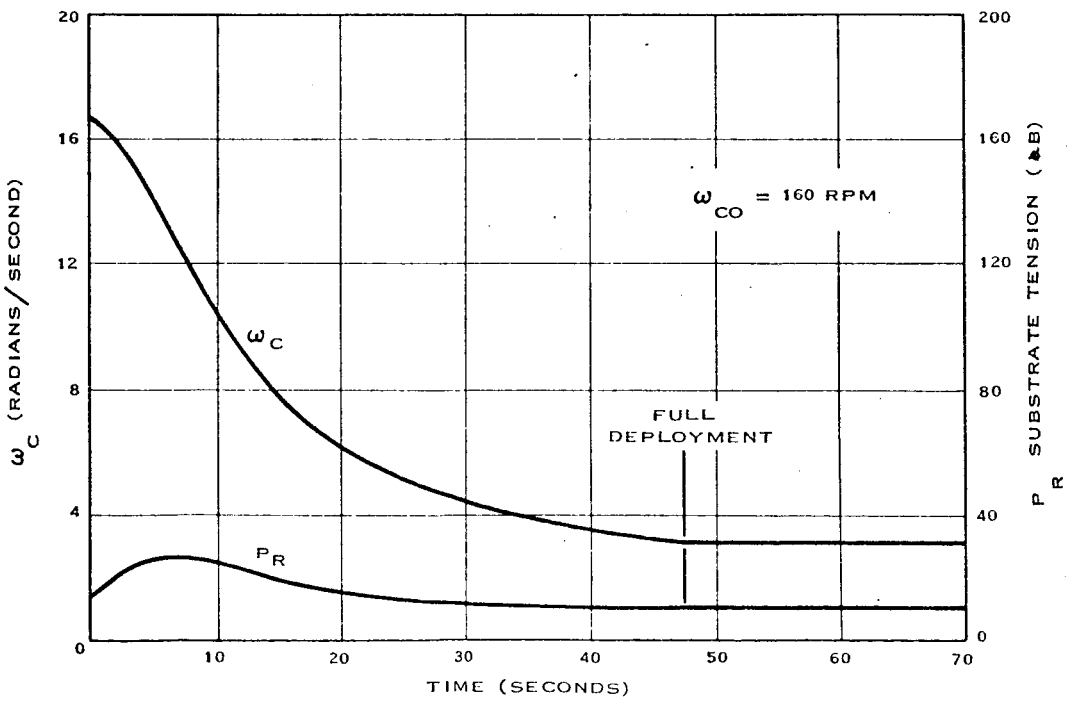

FIGURE 3.2 ANGULAR VELOCITY AND SUBSTRATE TENSION VS TIME, 4 ARRAYS MOUNTED ON SPACECRAFT

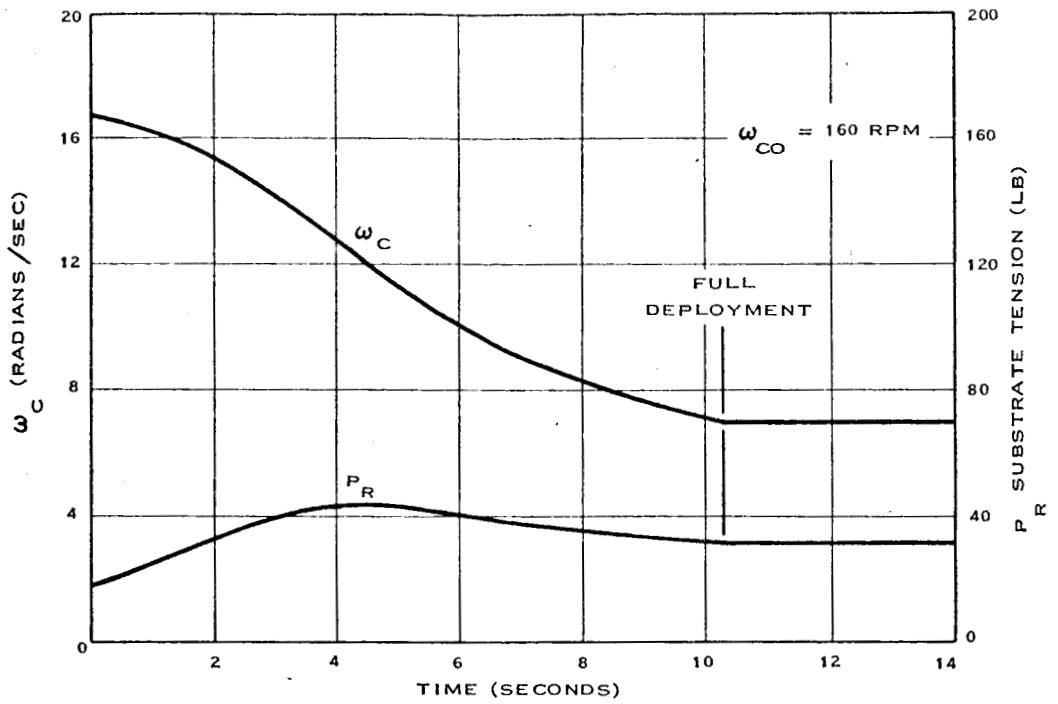

FIGURE 3.3 ANGULAR VELOCITY VS TIME
SPACECRAFT WITH 1 ARRAY

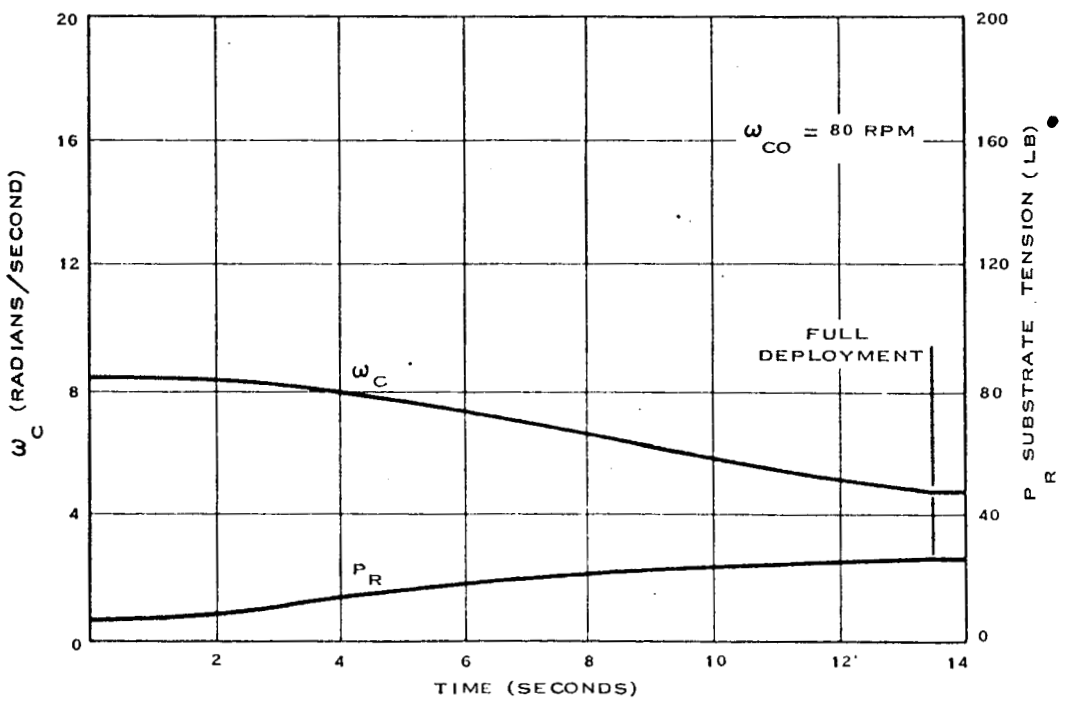

FIGURE 3.4 ANGULAR VELOCITY AND SUBSTRATE TENSION,
528 — 80000 TEST FIXTURE

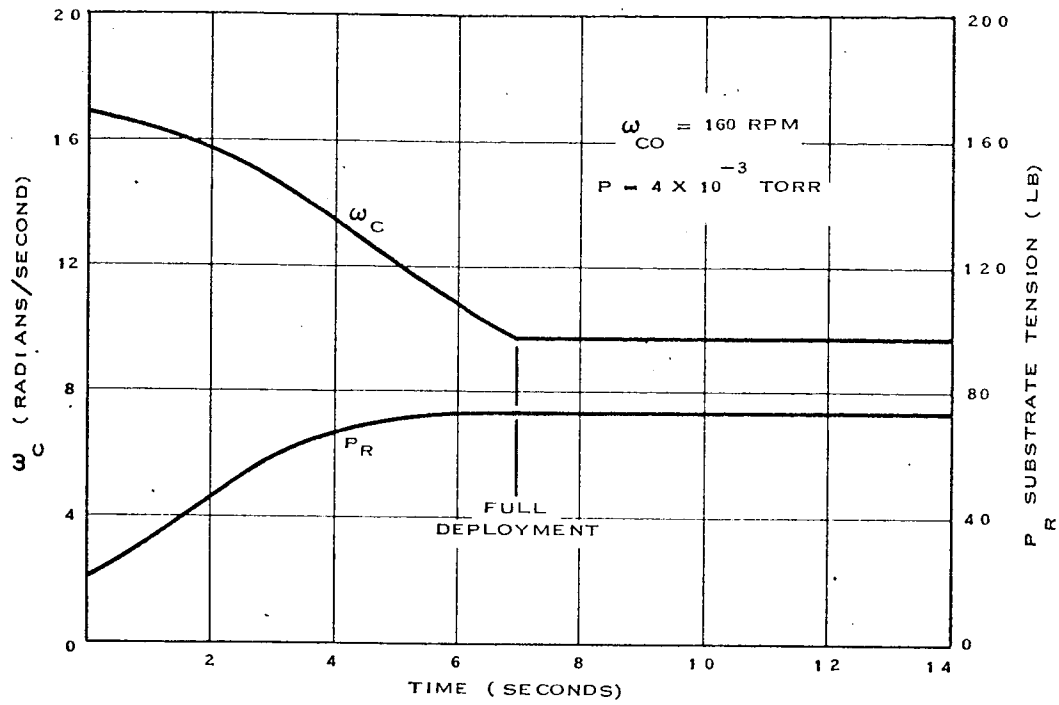

FIGURE 3.5 ANGULAR RATE AND SUBSTRATE TENSION VS TIME, 528–80000 TEST FIXTURE

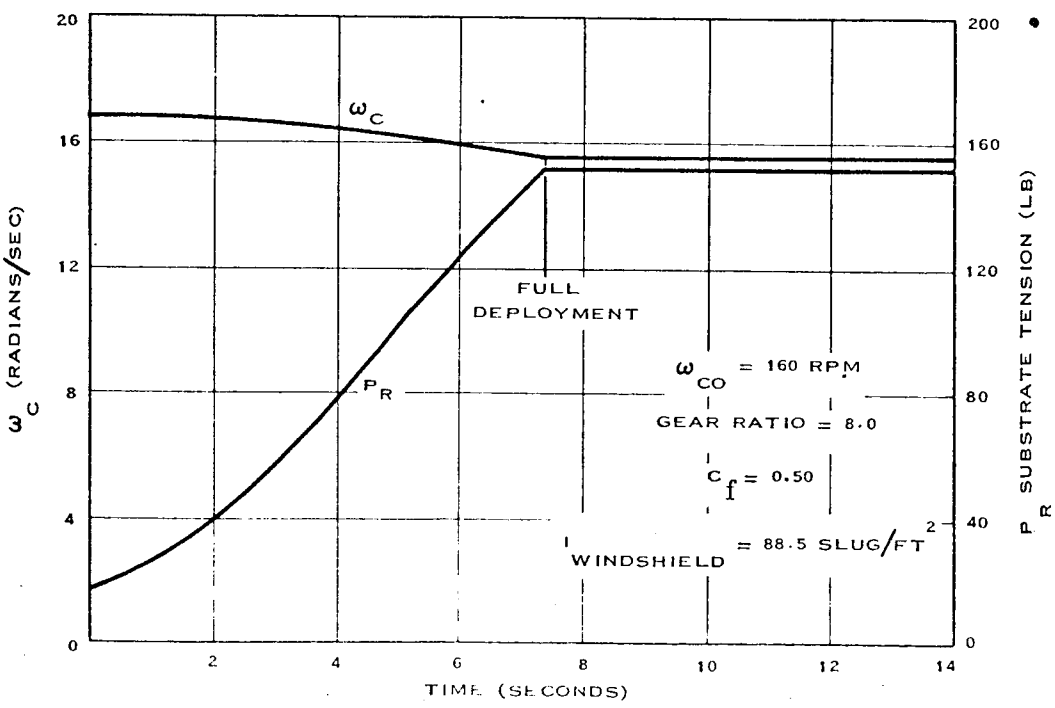

FIGURE 3.6 ANGULAR VELOCITY VS TIME, WINDSHIELD FIXTURE

3.1.2 Loading Equations

The loads of primary interest in the deploying panels are tangential (in-plane) shear and bending moments in the linkage and the tension in the flexible substrate.

3.1.2.1 In-Plane Loads

The in-plane loadings on the panels are a result of local tangential accelerations caused by the angular acceleration of the entire unit about the spin axis (equation (3)) and the corriolis acceleration caused by the instantaneous deployment velocity $\dot{X}$. The total tangential acceleration at any point on the panel is

$$a_T = \dot{\omega}_c X + 2\,\omega_c \dot{X} \tag{20}$$

Since the scissors unit is fixed to the centerbody at a point which does not move radially, it is seen that

$$\dot{X}_p = \left(\frac{X - R_c}{X_e - R_c} \right) \dot{X}_e \tag{21}$$

The substrate, however, will deploy at the same rate as $\dot{X}_e$ since it is being unwound from a roll.

$$\dot{X}_R = \dot{X}_e \tag{22}$$

The shear, then, at a point X on the deployed panel can be found by integrating the inertia forces outboard of that point.

$$a_T = \left(\frac{X}{X_e} \right) a_{T_e}$$

$$dV = -a_T\, dm = -\left(\frac{X}{X_e} \right) a_{T_e} \left[\frac{W_p}{X_e - R_c} + \mu \right] dX \Big/ g \tag{23}$$

$$V = - \frac{a_{T_e} \left[W_p + \mu \, (X_e - R_c) \right]}{X_e \, (X_e - R_c) \, g} \int_X^{X_e} X \, dX$$

$$V = - \frac{a_{T_e} \left[W_p + \mu \, (X_e - R_c) \right] \, (X_e^2 - X^2)}{2X_e \, (X_e - R_c) \, g} \qquad (23) \text{ cont'd}$$

Integrating equation (23) from X to X_e yields the following equation for the in-plane bending moment at a point X.

$$M = - \frac{a_{T_e} \left[W_p + \mu \, (X_e - R_c) \right] \, (2X_e^3 - 3XX_e^2 + X^3)}{6X_e \, (X_e - R_c) \, g} \qquad (24)$$

For both equations (23 and (24)

$$R_c \leq X \leq X_e$$

3.1.2.2 Substrate Tension Load

It is assumed the substrate material will not react tangential loads and will withstand only tension and inertia loads caused by $\ddot{X}_e$. The inertia loads of the speed brake and the undeployed (roller) portion of the substrate is expressed as follows:

$$F'_{I_R} = - \left[W_R - \mu \, (X_e - R_c) \right] \ddot{X}_e \, / \, 2g \qquad (25)$$

Combining the speed brake force, expressed in equation (13) with the inertia forces, the tension in the individual substrates can be expressed as follows:

$$P_R = \frac{F_f}{2} + \left\{ \frac{W_R - \mu \, (X_e - R_c)}{4g} + \frac{S^2 \, W_f \, R_f^2}{2g \, R_R^2} \right\} \ddot{X}_e \qquad (26)$$

Calculated values of P_R for various conditions is shown on Figures 3.2 thru 3.6.

3.2 STRUCTURAL ANALYSIS

A structural analysis was performed on the Deployable Solar Array to establish its structural integrity. It consisted of forced vibration and frequency analysis to determine the vibratory loads in the packaged configuration and deployment analysis to determine the loads and deflections developed during deployment and in the fully deployed condition. The results of the spin deployment analysis in the previous section were used to determine lateral loading and substrate tension during deployment. A detail stress analysis was conducted to prove the ability of the structure to withstand the loads acting on it.

3.2.1 Load Analysis

Three basic loading criteria were studied for the structure:

1) Vibration in packaged condition
2) Static deployment
3) Spin deployment

Several load conditions exist for each of the load criteria above and are identified in Figure 3.7.

3.2.1.1 Vibration Analysis

The dynamic response of the Deployable Solar Array in the packaged configuration was determined by representing the structure as a spring-mass-damper-system. The dynamic model is shown in Figure 3.8 . The rollers and substrate were represented by two beams (K and L) with three masses on each beam. The damper and Neg'ator spring spool were represented as masses hanging on the ends of the roller beams K and L respectively. The scissor links were represented by two masses on beams H and I. The scissor beams H and I are resting on the cross beams 2 and 4 which are

Condition	Direction	Frequency cps	± g Input
a	Z	130.38	10.7
b	Z	183.44	10.7
c	Z	186.6	10.7
d	Z	425	10.7
e	Z	443.4	10.7
f	Z	541.6	21.0
g	Z	629.2	21.0
h	X	99.7	2.1
i	X	130.38	2.1
j	X	142.2	2.1
k	X	183.9	2.1
l	X	422.1	2.1
m	X	443.4	2.1
n	Y	31.88	0.9
n_a	Y	77.5	2.1
o	Y	34.38	0.9
p	2.0 g Dynamic Deployment		
q	2.0 g Static Fully Deployed		

FIGURE 3.7 SUMMARY OF LOAD CONDITIONS

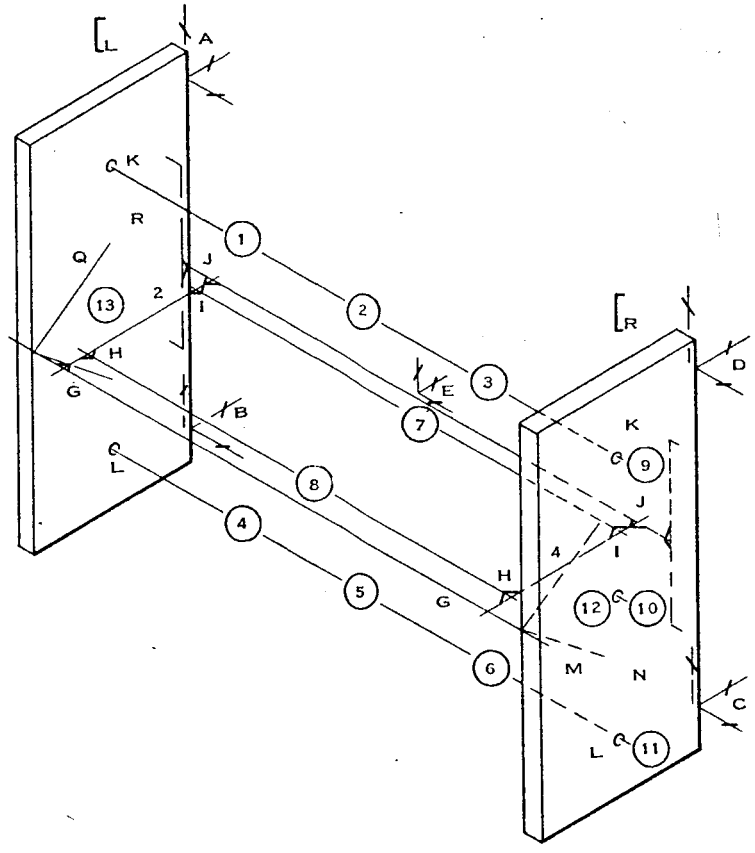

FIGURE 3.8 DYNAMIC ANALYSIS MODEL (VIBRATION)

supported by the screw jack beam J towards the back and the front plate G towards the front. Scissor link H is also tied to front plate G at the mid-point and screw. The two rollers (K and L), the screw jack J, and front plate G are all simply supported at their ends by end channels $[_R$ and $[_L$ and screw jack J has an additional support at reactions E. The end channels $[_R$ and $[_L$ are supported at reactions A, B, C, and D and act as deep shear beams bending about both principal axes. The total system consists of 13 masses each with three degrees of freedom in an xyz coordinate space, giving a total of 39 degrees of freedom.

A structural analysis was performed using the method of least work to determine the load distribution for the model with three degrees of indeterminacy. A three-dimensional influence coefficient matrix was developed

giving the deflection of each mass point in each of three mutually perpendicular directions for a unit load applied at any mass point. The analysis was performed on the 7090 computer. The influence coefficients were in the matrix form:

$$\left[\delta\right] = \begin{bmatrix} \delta_{xx} & \delta_{xy} & \delta_{xz} \\ \delta_{yx} & \delta_{yy} & \delta_{yz} \\ \delta_{zx} & \delta_{zy} & \delta_{zz} \end{bmatrix}$$

where the first subscript refers to the deflection of the mass point and the second subscript refers to the direction of a unit load.

A frequency analysis was performed in which the matrix equation

$$\left\{X\right\} = \omega^2 \left[\delta\right] \left[M\right] \left\{X\right\}$$

was solved by iteration on a computer to give the first 15 natural frequencies and the associated mode shapes.

The iterative process is initiated by assuming values of X on the right hand side of the equations and calculating the values of X on the left hand side. Successive iterations are performed until the computed X is equal to the assumed X.

where X = column matrix of deflections of masses

ω = natural frequency (Rad/sec)

$\left[\delta\right]$ = square matrix of influence coefficients

$\left[M\right]$ = diagonal matrix of lumped masses

A study of the mode shapes indicated which mass motions were predominate for each of the natural frequencies and forced vibrations analyses were

conducted for simusoidal input of ±1g in the x, y, and z directions separately for the appropriate frequencies. In the forced vibration analysis, structural damping was introduced with a damping coefficient of .05. For each of the x and y and z analyses, transmissibilities in the x, y, and z directions were computed by use of the matrix equation

$$\left\{T\right\} = (1 + i\,g)\left[(1 + i\,g)\left[1\right] - \omega^2\left[\delta\right]\left[M\right]\right]^{-1}\begin{Bmatrix} V_x \\ V_y \\ V_z \end{Bmatrix}$$

where T = transmissibility of each mass

= structural damping coefficient

$i = \sqrt{-1}$ = (introduced to represent phase relationship)

The input vibration levels are given below.

VIBRATION LEVELS

Sinusoidal Tests

Frequency (cps)	Thrust Axis (z) (g's)	Transverse Axis (x & y) (g's)
5-50	2.3	0.9
50-500	10.7	2.1
500-2000	21.0	4.2
2000-3000	54.0	17

Constant sweep rate of 2 octaves/minute

Random Test (each axis)

Frequency Range (cps)	PSD Amplitude (g^2/cps)	(g-rms)	Duration Min.
20-2000	.07	11.5	4.0

The internal loads resulting from the vibration environment were determined using the transmissibilities from the dynamic analysis and the internal load distribution from the structural analysis. The critical load conditions for each element of the structure are summarized in Section 3.2.1.4. A list of the frequencies and the associated direction is given in Figure 3.7.

3.2.1.2 Static Deployment Analysis

A load and deflection analysis was performed for static deployment. As the scissors linkage and substrate deploy, the gravity loads are resisted by bending and torsion of the scissors links. The deployment is characterized by the fact that the portion of the load carried by bending and torsion changes with the degree of deployment. The static deployment load analysis is described in Section 3.2.1.4. The load and deflection analysis was based on the slightly conservative assumption that all of the vertical load is carried by the box extension links.

3.2.1.3 Spin Deployment Analysis

The results of a spin deployment analysis were used to determine lateral loading on the linkage and substrate tension during deployment. The internal loads resulting from spin deployment are included in the internal loads section.

3.2.1.4 Internal Loads

The most critical loads resulting from vibration (packaged), static deployment (fully deployed), and spin deployment were determined and are

summarized in Figures 3.9 through 3.17. The limit loads for static deployment are based on 1.33 g in order that ultimate loads will be for 2 g.

3.3 STRESS ANALYSIS

A detailed stress analysis was conducted on each element of the structure in order to establish the ability of the structure to resist the loads which will come to act upon it. Yield margins of safety were based on loads of 1.15 times limit loads and ultimate margins of safety are based on 1.5 times limit load. A summary of minimum margins of safety is presented in Figure 3.18.

Additionally, a deflection analysis under 1 g was completed for both static and rotating conditions. These are not included in this report in the interest of brevity but can be obtained from Fairchild Hiller Document DSA-SA-1, "Design Study Analysis of Deployable Solar Array".

Cond.		Transmiss.		Input g		Acc g		Max. Bending Mom. (lb-in)			
								Scissor H (8)		Scissor I (7)	
		X	Z	X	Z	X	Z	M_x	M_z	M_x	M_z
a	7	---	2.0	---	10.7	---	21.4	65	---	90	---
	8	---	1.1	---	10.7	---	11.8				
b	7	0.3	18.3	10.7	10.7	3.2	191	600	---	796	---
	8	0.1	2.7	10.7	10.7	1.07	29				
c	7	0.3	21.0	10.7	10.7	3.2	224	690	---	910	---
	8	0.1	2.5	10.7	10.7	1.07	26.8				
f	7	---	2.0	---	21.0	---	42	208	---	170	---
	8	---	18.6	---	21.0	---	390				
i	7	5.5	---	2.1	---	11.5	---	---	18	5.7	52.5
	8	1.9	---	2.1	---	4.0	---				
j	7	18.9	---	2.1	---	39.8	---	---	---	27	180
	8	1.4	---	2.1	---	2.94	---				
h	7	2.5	---	2.1	---	5.25	---	---	196	26.2	24.2
	8	16.7	---	2.1	---	35	---				

FIGURE 3.9 SCISSORS LINK LOADS

Maximum Bending and Shear Bm 2 or 4				
Cond.	Max. Mom. for 1g	Input ±g	Bend. Mom. lb-in	Shear lbs.
b	6.8	10.7	72.9	60.6
c	7.9	10.7	84.5	70.5

FIGURE 3.10 CROSS BEAM 2 AND 4 LOADS

Bending

Location	Condition a		Condition b		Condition i	
	M_x	M_y	M_x	M_y	M_x	M_y
Kor L-1	--	--	0	--	0	0
Kor L-2	135	--	1340	--	1.8	254
Kor L-3	184	--	1890	--	2.5	362
Kor L-4	134	--	1340	--	1.8	256
Kor L-5	3.1	--	25	--	0	5.0

Limit Moment in lb-in

FIGURE 3.11 SUBSTRATE ROLLER LOADS

Axial

Peak Axial Load = 82 lbs. (Cond.n)

Peak Axial Load = 26 lbs. (Cond.o)

(Axial load is almost zero for all other load conditions)

Design Condition is Cond. b (183.44 cps Z; input = 10.7g)

Cond.	Bending Screw Jack lb.-in.		
	J-2	J-3	J-4
b	49.2	8.9	49.2
c	56.7	10.3	56.7
q	162	---	162

FIGURE 3.12 SCREW JACK LOADS

Cond.	Roller boss(K or L) lbs.			Screw Jack (J) lbs.		
	X	Y	Z	Y	Z	X
b	--	--	410	--	25	--
c	--	--	340	--	29	--
h	6.5	--	--	--	--	--
i	42	--	13.74	--	--	--
k	78	--	--	--	--	--
n	--	89	--	1.3	--	--
p	40	--	--	--	--	81.5
n_a	--	208	--	3.4	--	--

FIGURE 3.13 BOSS LOADS

Bending and Shear (Limit Loads)

Pt. / Cond	Mom. about X axis lb-in			Mom. about Z axis lb-in			Max Shear	
	2	3	4	1A	3	4A	V_z(lbs)	V_x(lbs)
a	18.7	136	18.7	--	--	--	25	--
b	106	820	106	--	--	--	14.9	--
c	117	910	117	1.8	15.5	1.8	16.6	2.82
f	270	1675	270	--	--	--	305	--
h	--	--	--	15	10.5	15	--	2.0
p	--	--	--	--	124.5	--	--	41.5

FIGURE 3.14 END CAP (BEAM G) LOADS

Cond.	Load in bolt A or D lbs.			Load in bolt C or B lbs.		
	X	Y	Z	X	Y	Z
b	158	---	470	158	---	470
i	56	---	29.6	56	---	29.6
n	7.65	92.6	---	---	69	---
p	81.5		---	81.5	---	---
n_a	1718	216	---	1700	161	---

FIGURE 3.15 FASTENER BOLT LOADS (A, B, C, D)

Cond.	Bolt load (E) lbs.		
	X	Y	Z
b	23	---	---
q	155	---	---
p	93.5	---	---

FIGURE 3.16 FASTENER BOLT LOADS (E)

Cond.	Restraint Mech. load lbs.	Shear Pin loads lbs.
a	---	19.2
b	3.4	106.5
c	3.8	117
f	---	271
h	30	---
j	29.4	---

FIGURE 3.17 RESTRAINT MECHANISM AND SHEAR PIN LOADS

Element	Mode of Failure	Load Cond.	Min. M. S. Y = Yield U - Ultimate
Roller boss in end plate L_{left} L_{right} K_{left} (Proto.)	Compressive yield due to bending	N_A	+0.10 Y
Roller boss in end plate K_{left} (Prop. only)	Shear failure in bonding of doubler	N_A	+0.45 U
Roller boss in end plate KR (Brake side)	Tension yield due to bending	N_A	+0.14 Y
Substrate roller	Comp. crushing of tube wall due to bending	b	+0.01 U
Substrate retainer pl.	Bending	N_A	+0.13 U
Roller pins	Torsion	P	+0.00 U
Front plate (6)	Crippling of element	f	+0.41 U
Cross beams (2 & 4)	Bending	C	+0.11 U
Screw jack	Bending	P	+0.26 U
Box extension link	Bending (comp.)	Q	+0.28 Y
Hinge pins Box link to box link	Shear	Q	+0.46 U

FIGURE 3.18 SUMMARY OF MINIMUM MARGINS OF SAFETY

3.4 THERMAL ANALYSIS

The thermal analysis was performed on the Scissor-Flexible Substrate configuration shown in Figure 3.19.

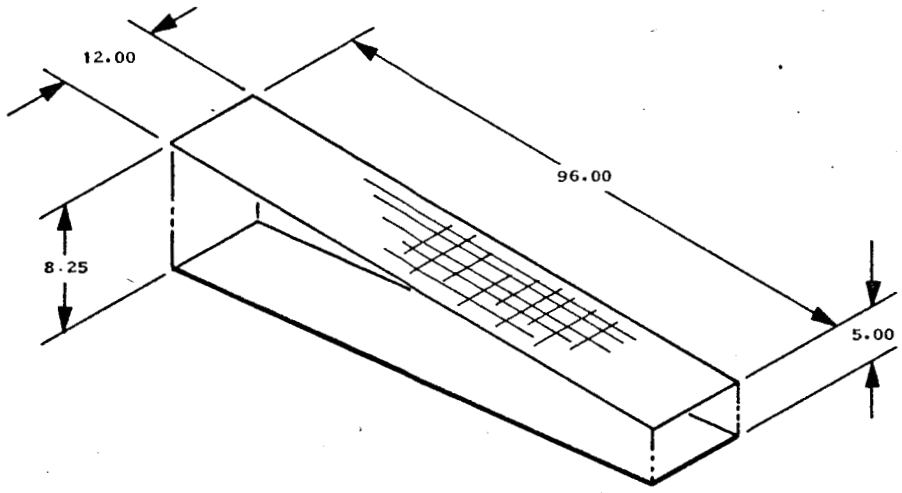

FIGURE 3.19 SCISSOR – FLEX SUBSTRATE CONFIGURATION

The analysis considered a spacecraft with an altitude of 600-700 statute miles. The vehicle was assumed to be stationary along the earth-sun line, spinning about an axis perpendicular to the plane of the solar arrays. Incident solar, albedo and earth heat fluxes were considered. The nominal values in a 3σ variation were assumed in the calculations. The analysis was performed in parametric form since various parameters are uncertain or unknown at this time.

One of the major parameters of concern is the incidence angle of the solar vector since it not only effects the power output of the cell but also the solar cell temperature. The temperature is affected in two ways:

(1) The incident solar flux is reduced by the cosine of the angle (see Figure 3.20).

(2) The parallel plate configuration allows solar flux to be incident upon the backface of the substrate.

The latter tends to reduce the amount of radiant-interchange between the substrate and therefore increases the solar cell temperature. The values of $\phi = 80^{\circ}$, 60°, 40° and 20°.

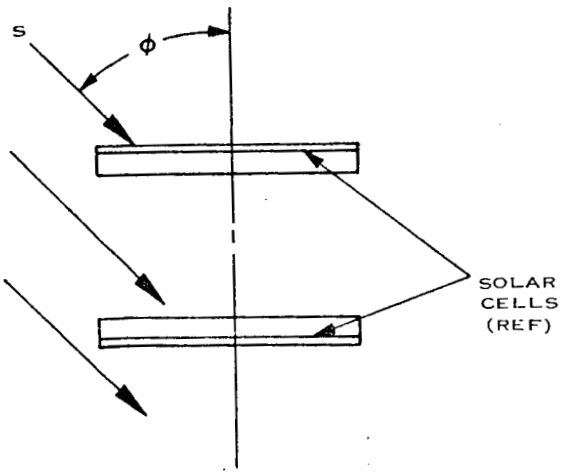

FIGURE 3.20 INCIDENT FLUX DIAGRAM

The distance between the substrates is another major parameter. This affects the configuration factor. The magnitude of this factor is directly proportional to the amount of radiant interchange between the plates. This is seen from the relation

$$Q_{rad} = \sigma F_A F_E T^4$$

where:

F_A - configuration factor

F_E - emissivity factor

As the distance between the plates decreases, the configuration factor decreases. The distances considered in this analysis are: y = 8.25 inches and y = 5.0 inches which are the maximum and minimum of the design.

The third significant parameter is the substrate material cross section. The solar array has the greater portion of solar cells made up of the following materials. (All dimensions in inches.)

0.006 Quartz Cover Glass
0.003 RTV Adhesive
0.013 Silicon Solar Cell
0.005 RTV Adhesive
0.003 H-Film Substrate
0.032 Flexible Foam Cushion

Cross Section A

Certain portions of the array have an additional stiffener of a magnesium strip. The material cross section is,

0.006 Quartz Cover Glass
0.003 RTV Adhesive
0.013 Silicon Solar Cell
0.005 RTV Adhesive
0.003 H-Film Adhesive
0.005 RTV Adhesive
0.025 Magnesium Stiffner
0.032 Flexible Foam Cushion

Cross Section B

Since the incident solar flux will "see" the polyurethane foam on the back of the aft substrate, its absorptance and emittance characteristics must be known, and is the fourth major parameter to be considered. The values of absorptance and emittance of polyurethane foam are not well known therefore a selection of variable α and constant ϵ was selected from available data as the parameters in the analysis. The values chosen were: α = 0.2, 0.4, 0.6 and 0, with ϵ = 0.8. The effects of low ϵ must be considered. However, a case with an ϵ = 0.2 and the α = 0.2, 0.4, 0.6 and 0.8 was chosen for comparison.

Using these four parameters, 128 cases were on a Heat Transfer Computer program to determine the maximum operating temperatures. The results are shown in Figures 3.21 thru 3.28.

CONCLUSIONS:

Conclusions which can be drawn from this analysis are:

- Solar cell temperature is independent of the absorptivity of the foam cushion.

- Solar cell temperature is independent of the emittance of the foam cushion.
- Difference in material cross section has little effect on the solar cell temperature.
- Separation distance between the substrates has little effect for small distances.
- Solar cell temperature is chiefly dependent on the solar heat flux angle of incidence and is the cause of the most significant changes in solar cell temperature.

A parameter which could reduce the solar cell temperature is the separation distance between the solar cells. A significant increase in this distance would have to be realized, however, before any sizeable change in cell temperature would occur.

It should be noted that this analysis purposely selected the worst heating condition which would occur for the Deployable Solar Array and therefore the temperature for any other case would be less.

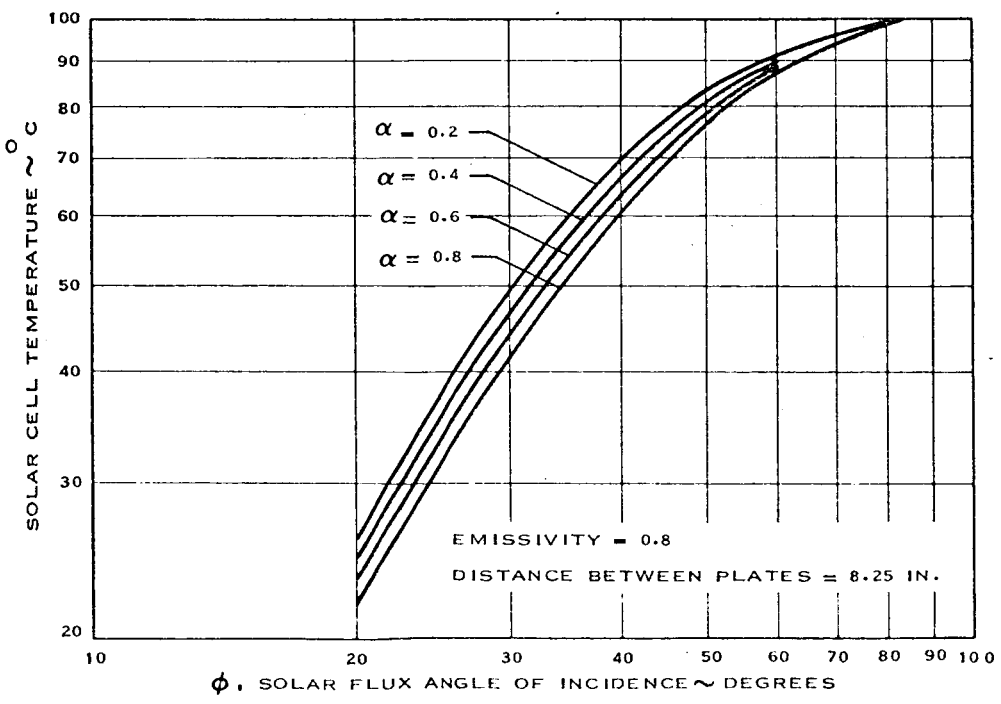

FIGURE 3.21 CELL TEMPERATURE, CROSS SECTION A

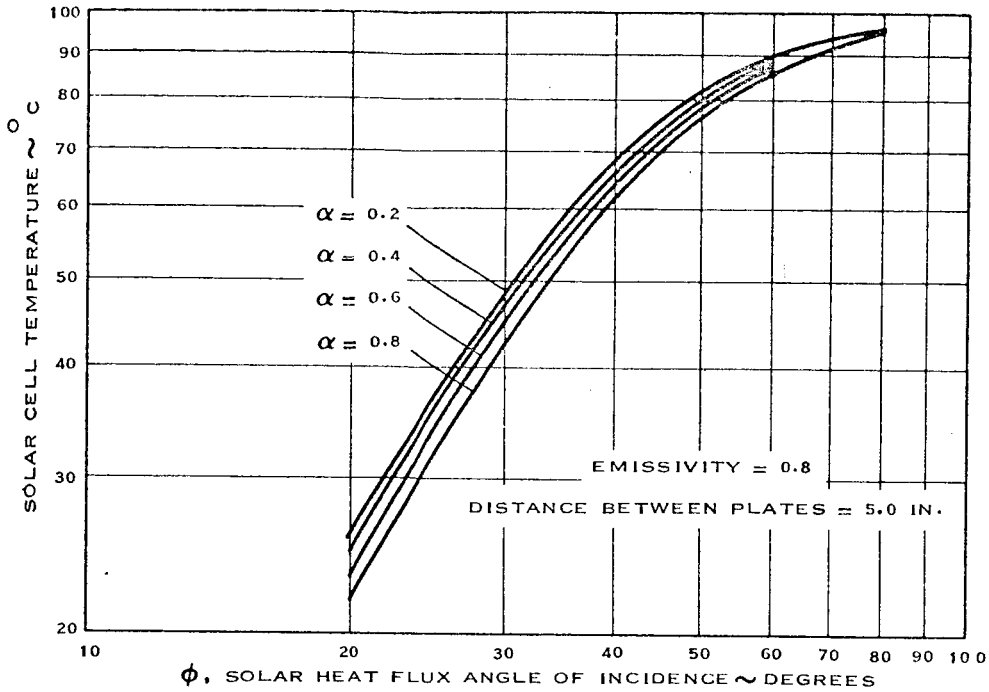

FIGURE 3.22 CELL TEMPERATURE, CROSS SECTION A

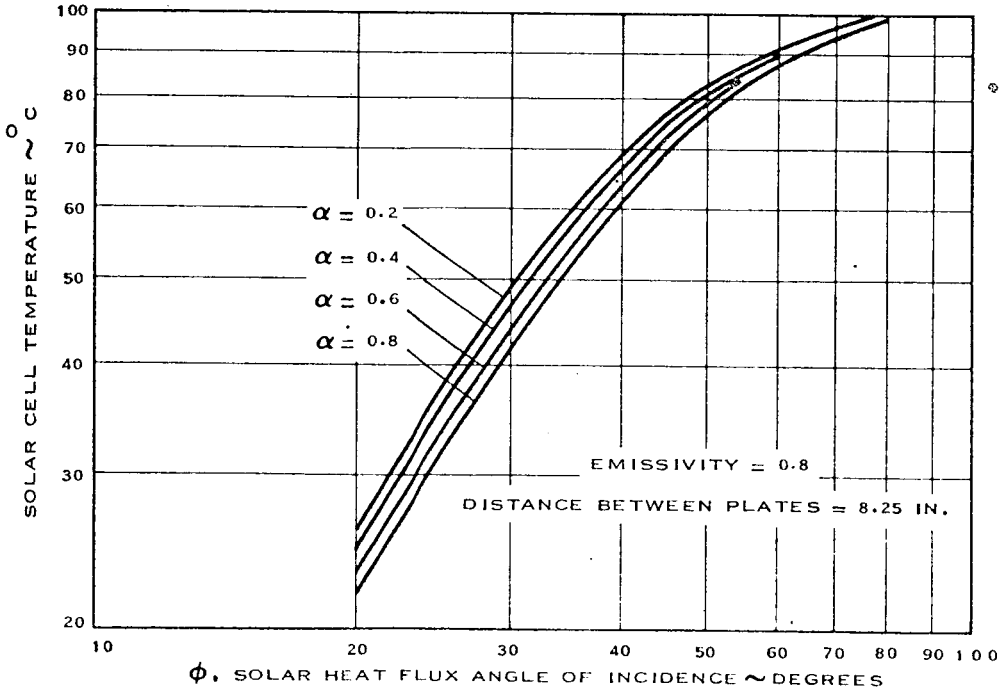

FIGURE 3.23 CELL TEMPERATURE, CROSS SECTION B

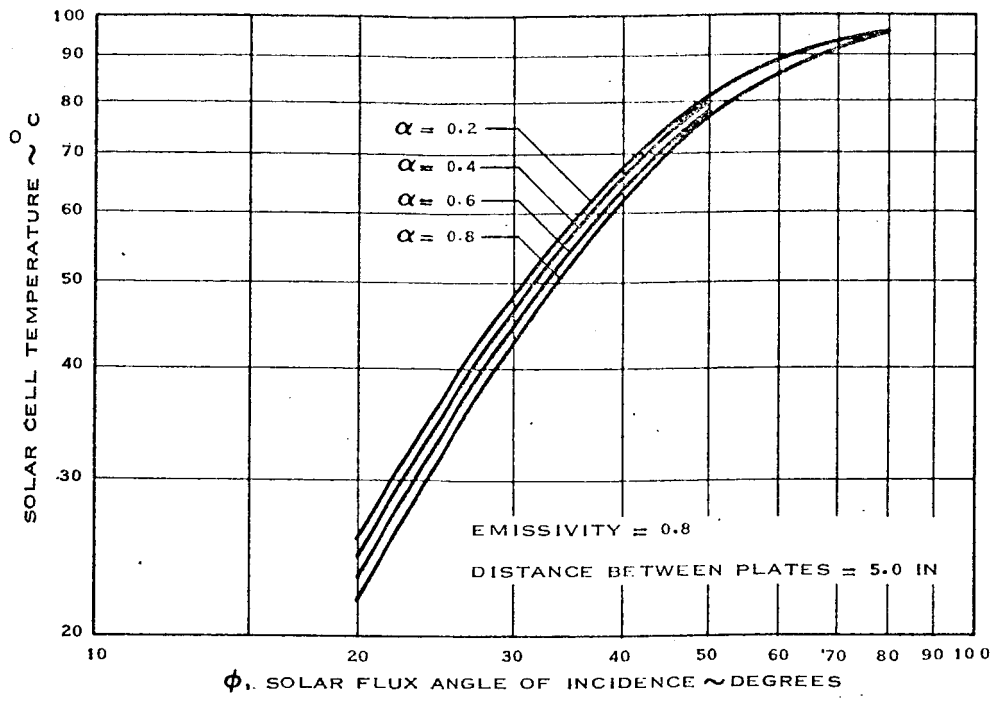

FIGURE 3.24 CELL TEMPERATURE, CROSS SECTION B

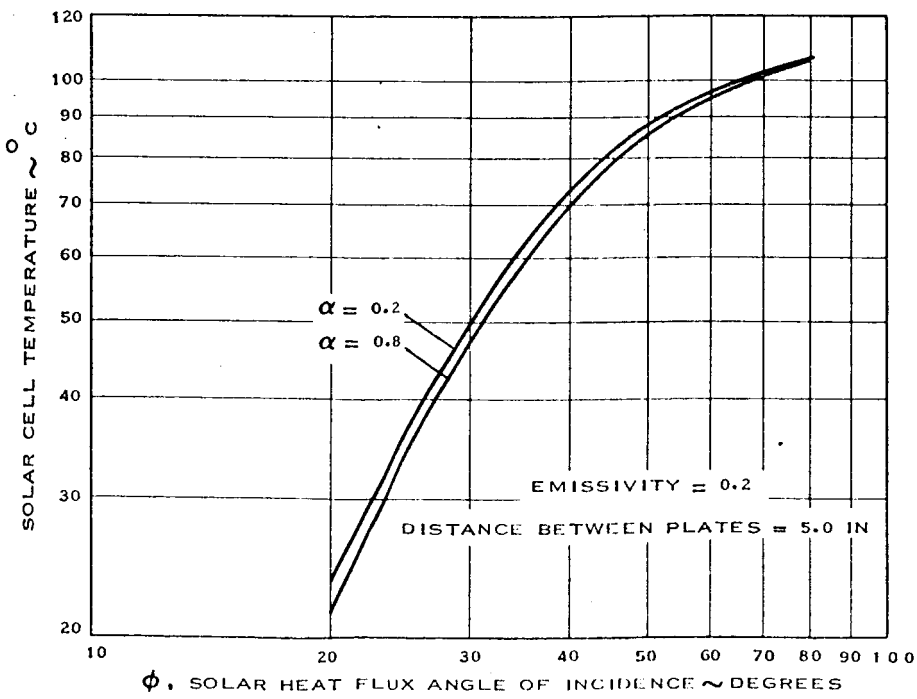

FIGURE 3.25 CELL TEMPERATURE, CROSS SECTION A

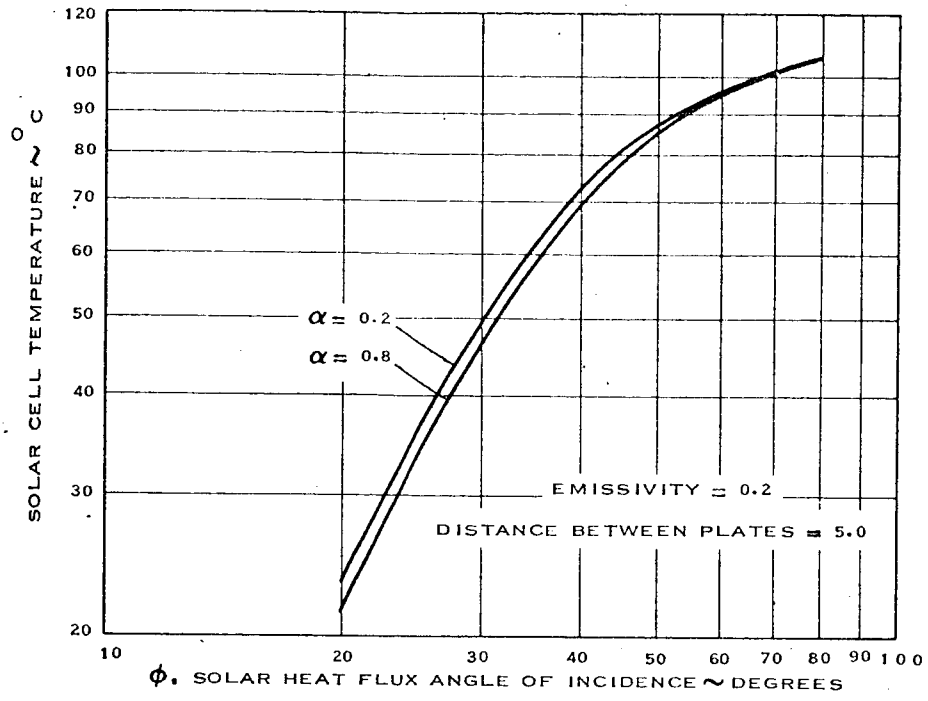

FIGURE 3.26 CELL TEMPERATURE, CROSS SECTION A

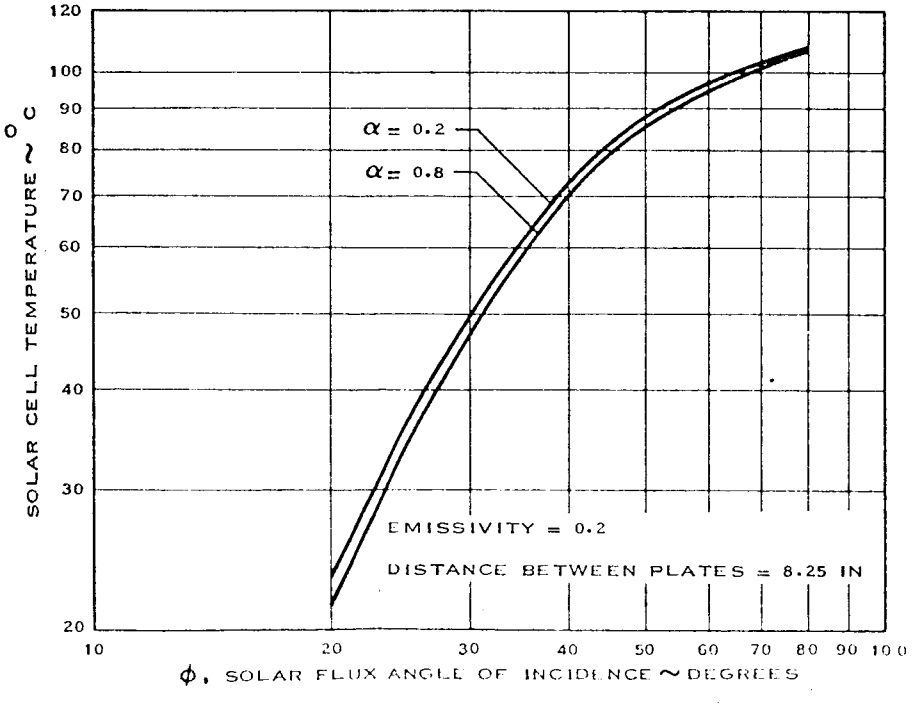

FIGURE 3.27 CELL TEMPERATURE, CROSS SECTION B

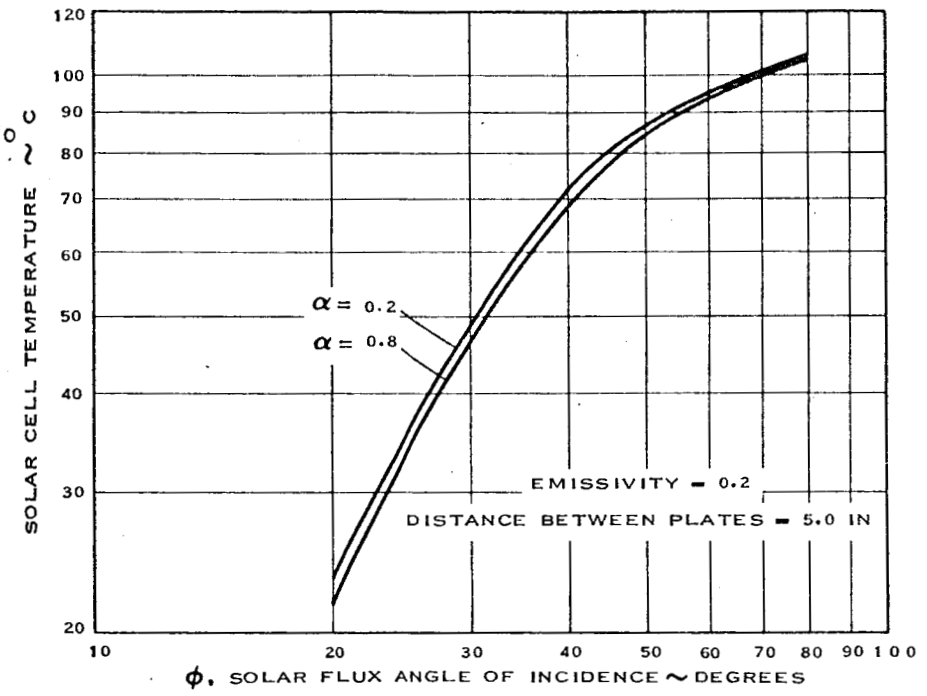

FIGURE 3.28 CELL TEMPERATURE, CROSS SECTION B

3.5 WEIGHT SUMMARY

Nomenclature	Quantity	Total Weight
Structure		
End Plate (Drive End)	1	.29
End Plate	1	.29
Housing	1	.32
Front Plate (Substrate Support)	1	.10
SUB TOTAL		1.00
Drive and Deployment Mechanisms		
Spring Motor	1	.25
Drum and Gear Assembly (Drive)	1	.15
Drum Assembly (Take Up)	1	.06
Gear Assembly (Idler)	2	.06
Gear (Pinion)	2	.02
Shaft (Drive Assy)	1	.04
Shaft (Take-up Assy)	1	.015
Shaft (Idler Assy)	2	.015
Ball Screws	4	.24
Ball Bearing Screw Assembly	2	.71
Bearing Block Assembly (Scr. Support)	2	.06
Pin (Scissors Links to B/B Nuts)	2	0
Box Links	8.5	1.79
Channel Links	8.5	.71

FIGURE 3.29 WEIGHT SUMMARY

Nomenclature	Quantity	Total Weight
Scissors Hinge Pins	25	.21
Washers	A/R	.25
Fitting - Support Plate Attach	1	.04
SUB TOTAL		4.62
Damper Mechanism		
Brake Drum	1	.16
Brake Shoe Assembly (Wt. & Friction Pad)	2	.20
Intermediate Gear	1	.05
Brake Lever and Gear	1	.05
Shaft Intermediate Gear	1	.07
Gear and Clutch Assembly	1	.07
SUB TOTAL		.60
Release System	1	.14
SUB TOTAL		.14
Array	2	
Membrane		.24
Stiffeners		.68
Adhesive		.50
Cells, Bond		4.58
Rollers		.87
SUB TOTAL		6.87
Miscellaneous		
Bearings		.18
Fasteners		.15
SUB TOTAL		.33
TOTAL		13.56

FIGURE 3.29 (CONT'D)

4.0 TEST

A series of development tests were run on the PROP model. These were designed to check out the system, verify the analytical analysis, and determine the integrity of the design.

The chronological order of the scheduled test was:

- Downward deployment
- Humidity
- Vibration
- Spin deployment

Due to scheduling problems the vibration test was performed partially before the spin deployment and the rest later.

In addition to the scheduled tests, an additional test was requested for the brake assembly to determine if it was the major contributor to the failure on the spin test.

4.1 DOWNWARD DEPLOYMENT TEST

This test was primarily for mechanical system checkout. A secondary task was to obtain data on the brake mechanism. A formal test plan was not issued since this was more an effort to "de-bug" the system than to obtain information.

The test setup is shown in figures 4.1 through 4.3. It was performed at the FHC facility using fixture 528-80006. During the test, weights of increasing size were added to the end plate bracket and the total deployment time for each run was measured.

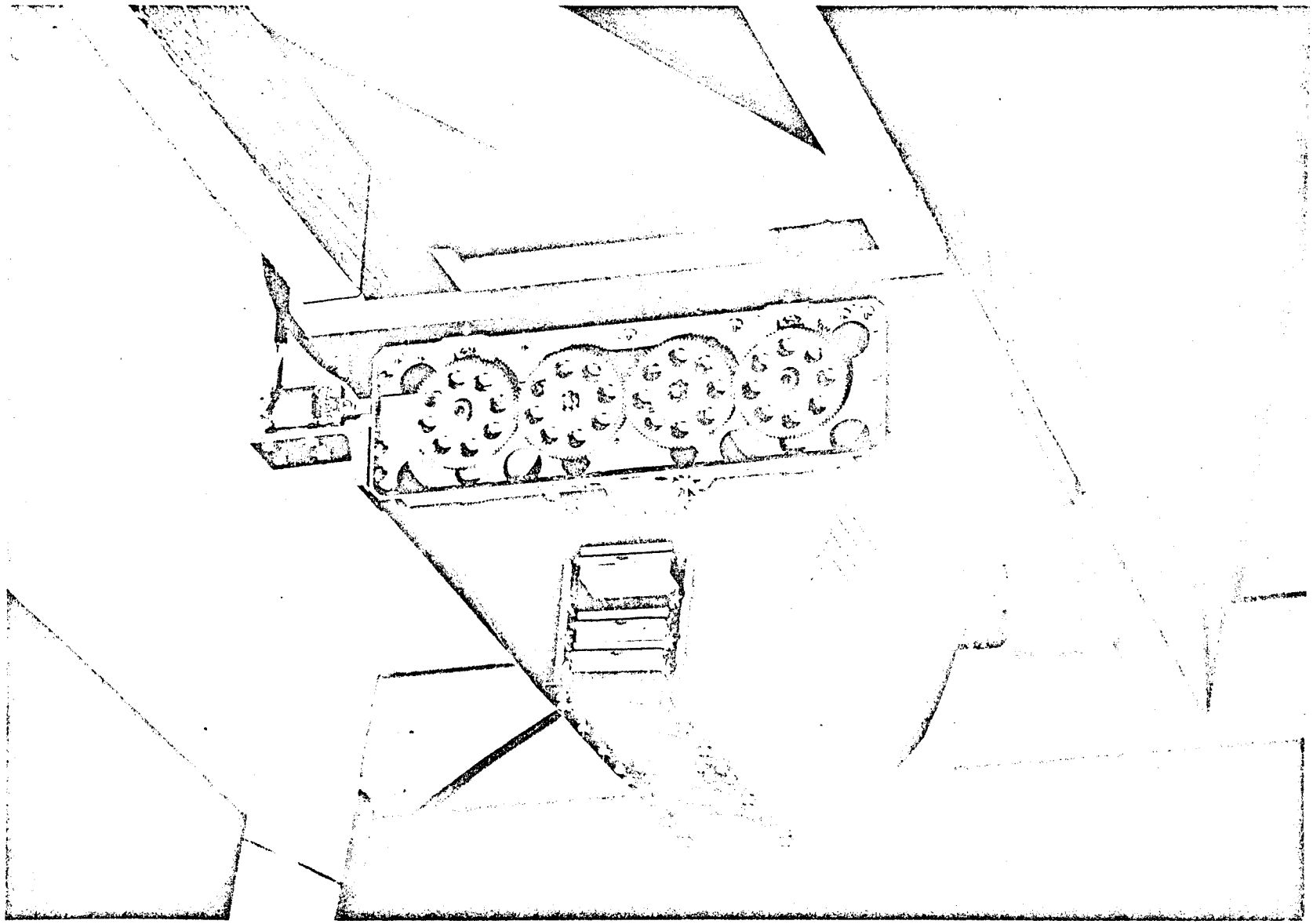

FIGURE 4.1 DOWNWARD DEPLOYMENT TEST

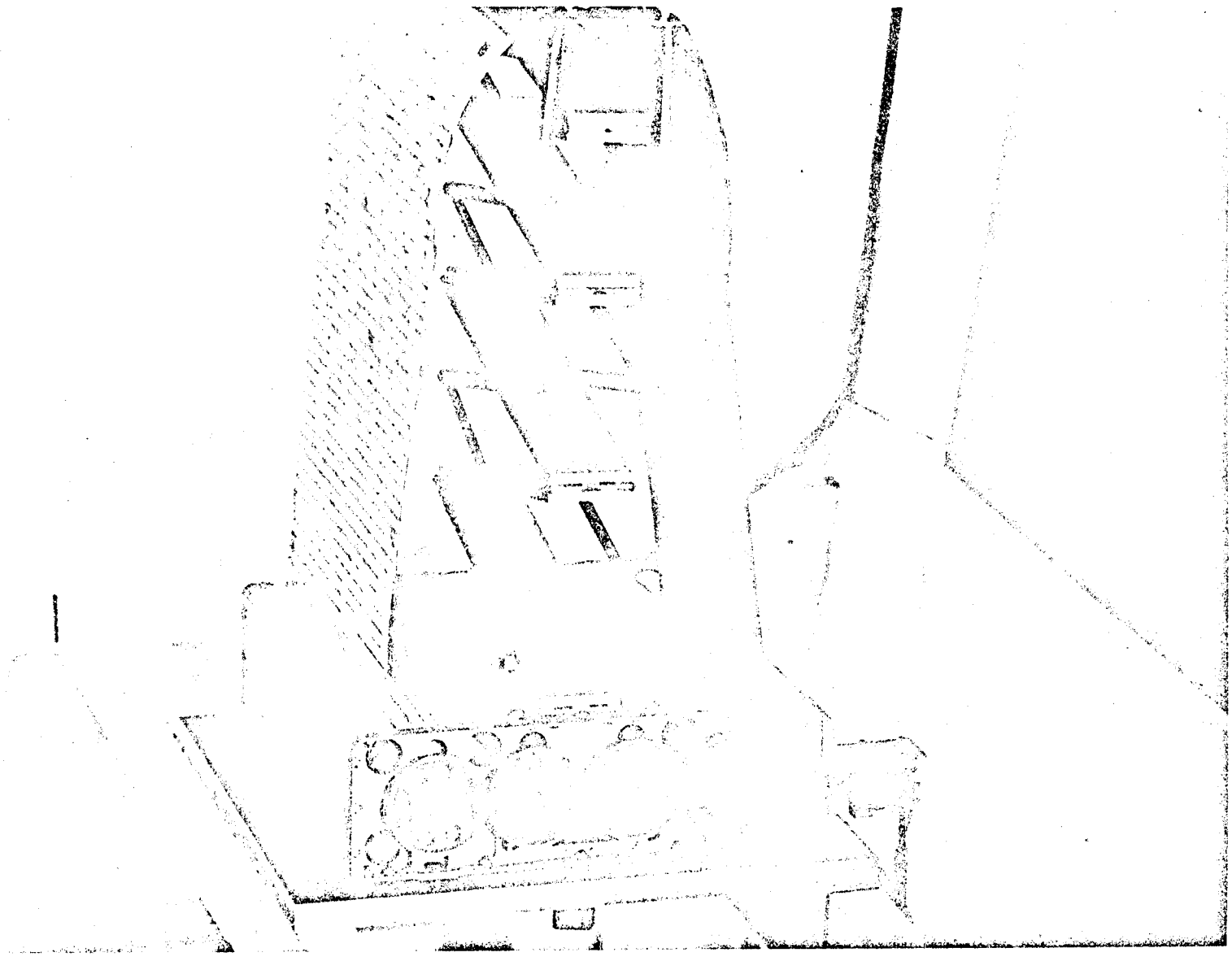

FIGURE 4.2 DOWNWARD DEPLOYMENT TEST

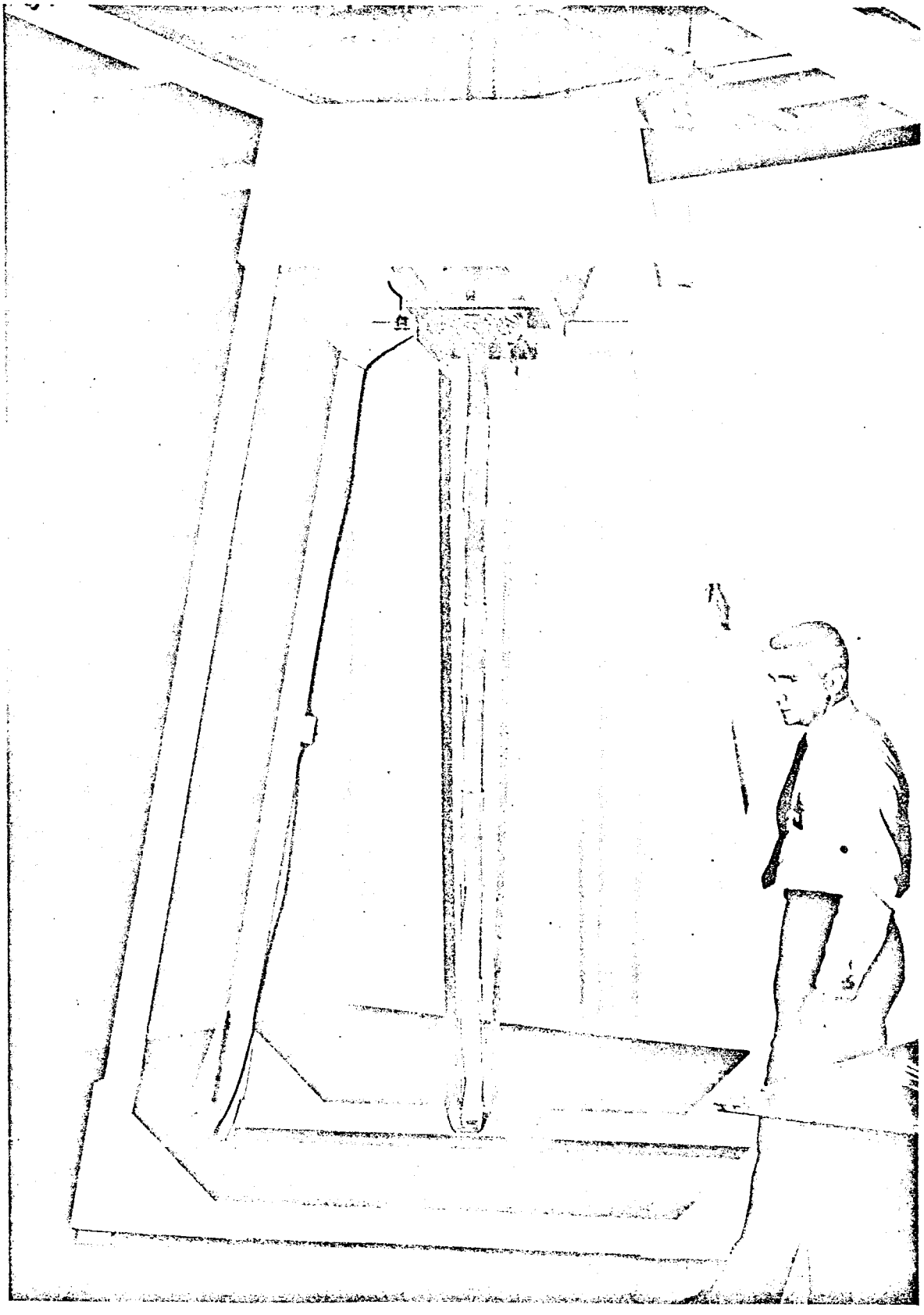

FIGURE 4.3 DOWNWARD DEPLOYMENT TEST

Data from the test is shown in figure 4.4. It generally describes a parabolic locus expected from a V^2 damper.

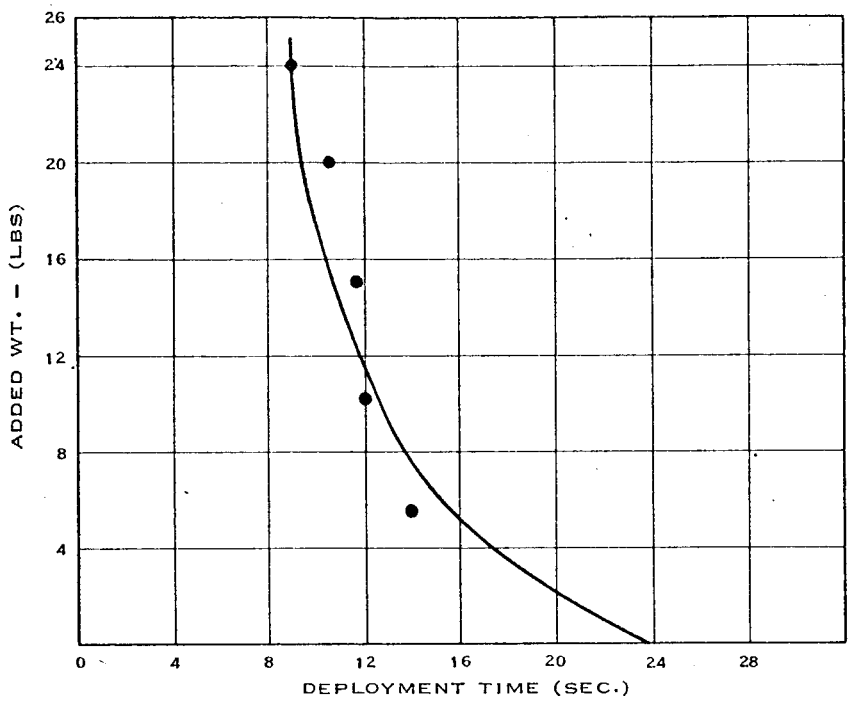

FIGURE 4.4 DOWNWARD DEPLOYMENT TEST ADDED WT. VS TIME

4.2 HUMIDITY TEST

The principle environmental effects being investigated were:

- Corrosion
- Swelling
- Deterioration

The test was conducted in FHC facilities using a Tenney Chamber. The test article was in the undeployed condition during test. Test conditions were 24 hours at $86^{\circ} \pm 2^{\circ}$F at a relative humidity of 45 ±5%. A post test visual examination disclosed no physical degradation. The test was initiated 11/11/65 and completed the following day. Figure 4.5 is a view of the test setup.

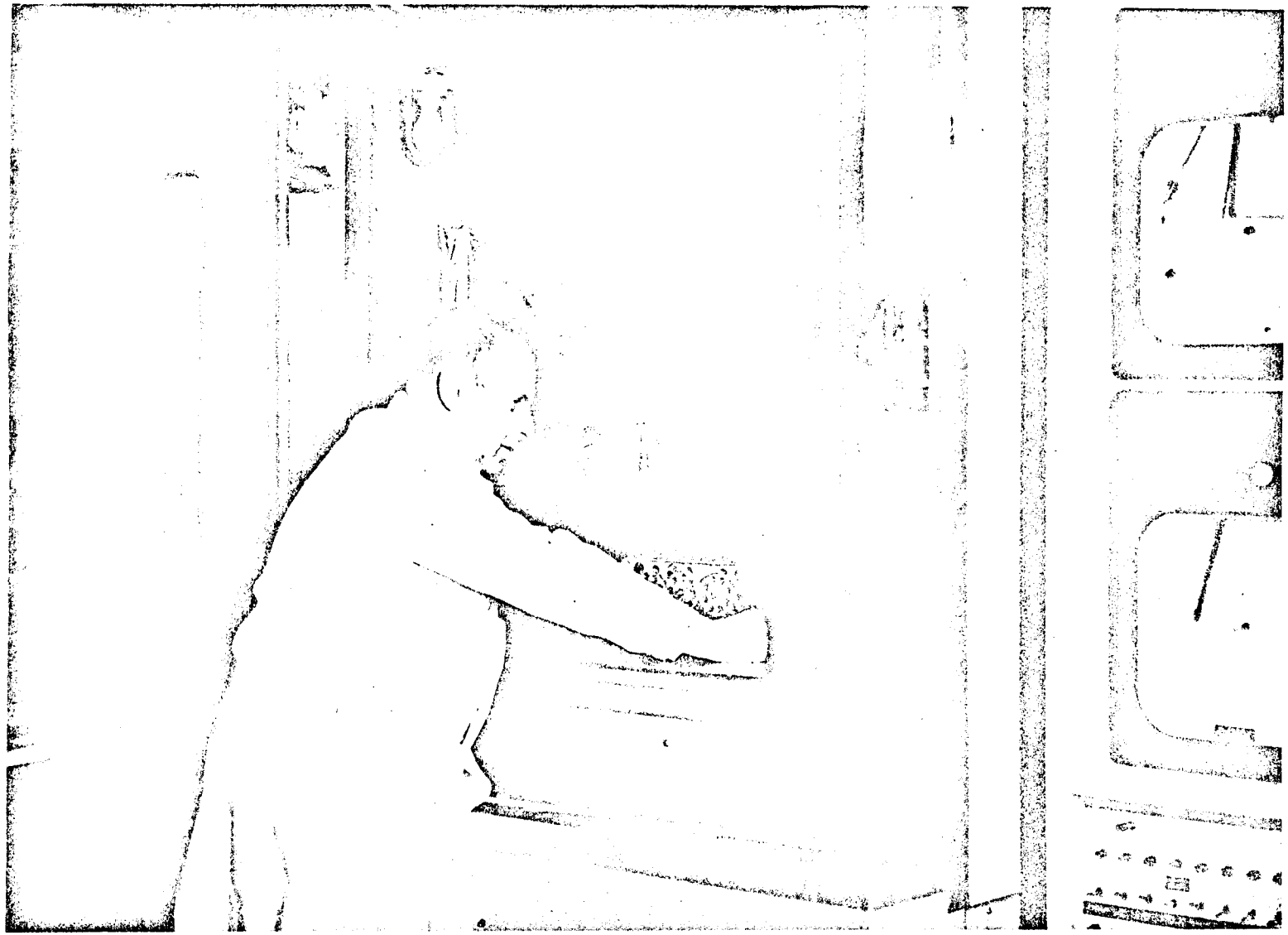

FIGURE 4.5 HUMIDITY TEST SET-UP

4.3 VIBRATION TEST

The vibration test included both sinusoidal and random shake. The specification encompassed a range that would be expected for components on a small scientific satellite. The specific levels are tabulated below:

Sinusoidal Vibration

Frequency (cps)	Thrust Axis (Z) (g's)	Transverse Axis (X & Y) (g's)
10-50	2.3	0.9
51-500	10.7	2.1
501-2000	21.0	4.2
2001-3000	54.0	17.0

Speed = One sweep up at a constant rate of two octaves.

Random Vibration

Frequency Range	PSD (g^2/cps)	Amplitude (g-rms)	Duration (min.)
20-2000	.07	11.78	4.0

The test was carried out at the FHC test facility using the Ling A300B shaker and fixture 528-80002 (see figure 4.6). Five CRL 606 accelerometers were attached to the structure as shown in Figure 4.7 . Responses of the instruments were recorded on a visicorder.

The only deviation to the input levels was in the Z axis direction for 2000-3000 cps. The capability of the shaker was limited to 21 g's vs. the required 54.

A post test deployment and inspection of the unit revealed no physical damage to either the structural and mechanical system or to the flexible array.

Amplification and resonant responses are indicated in Figures 4.8 thru 4.10.

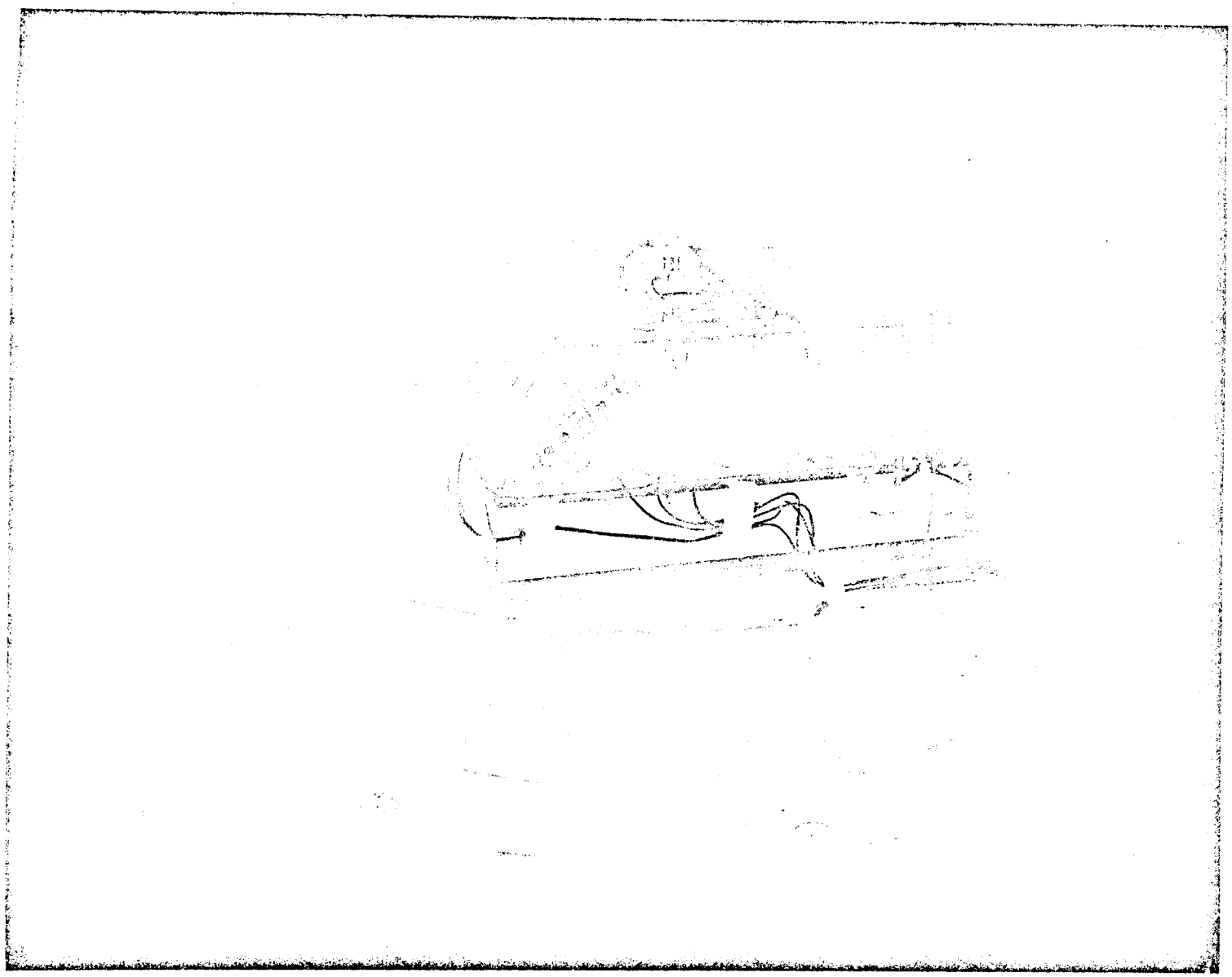

FIGURE 4.6 VIBRATION TEST

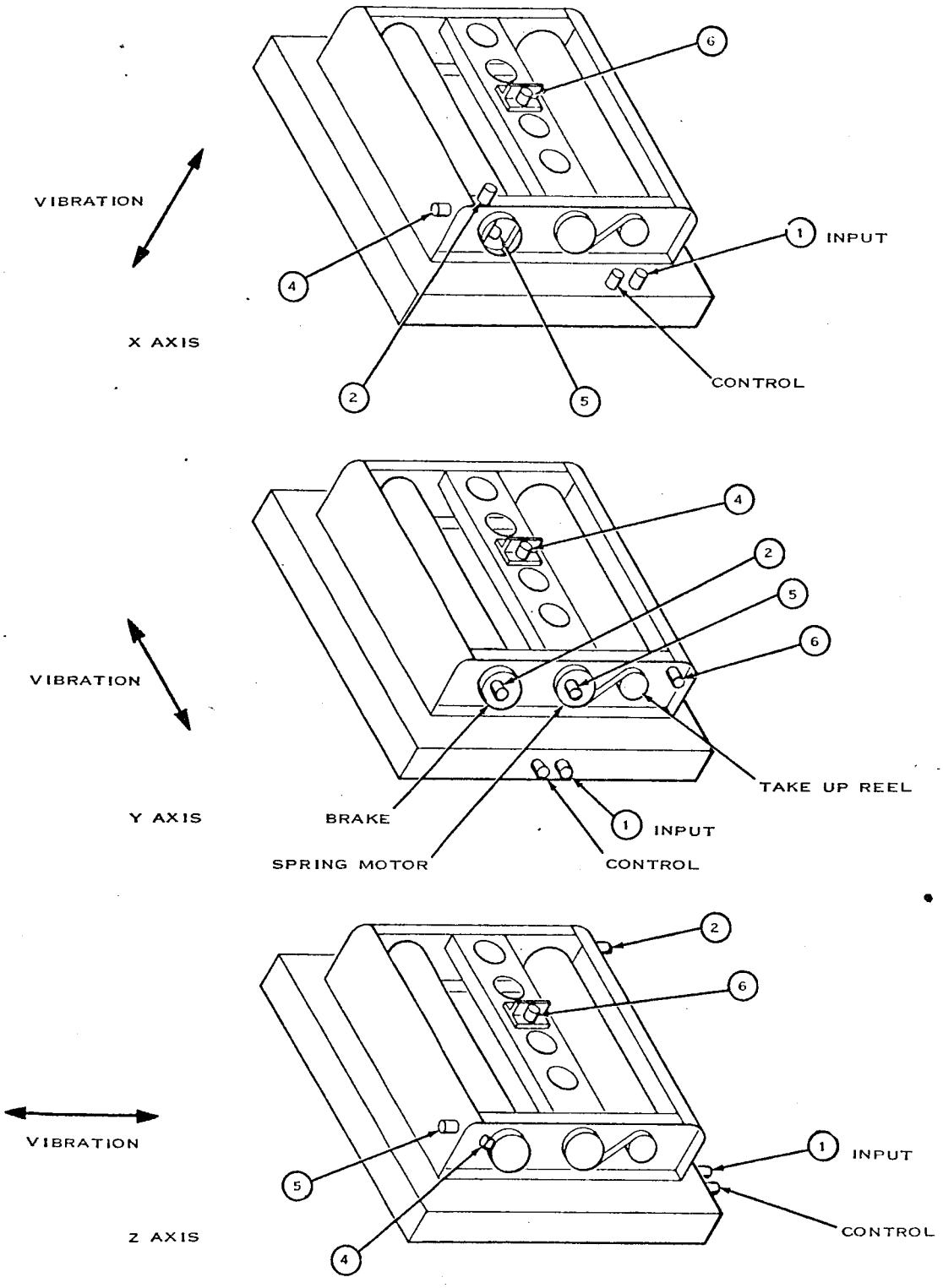

FIGURE 4.7 VIBRATION TEST INSTRUMENTATION

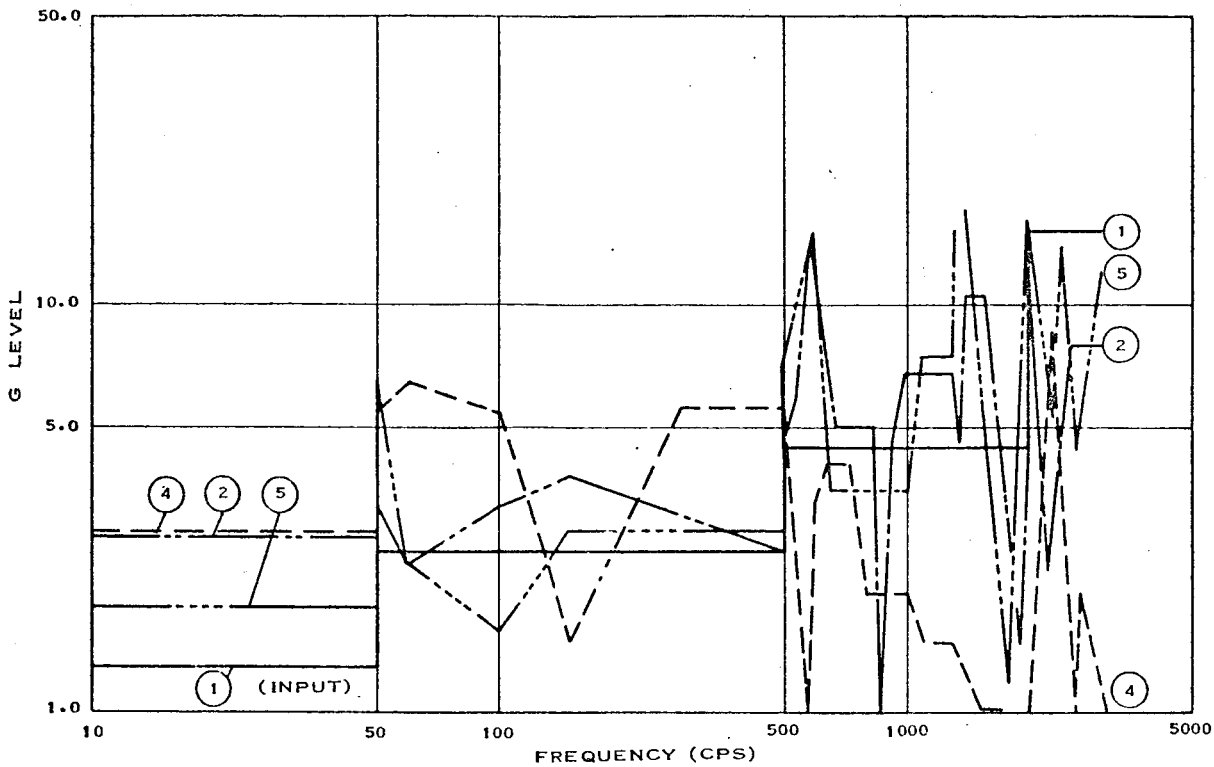

FIGURE 4.8 'G' LEVEL VS FREQUENCY — X AXIS

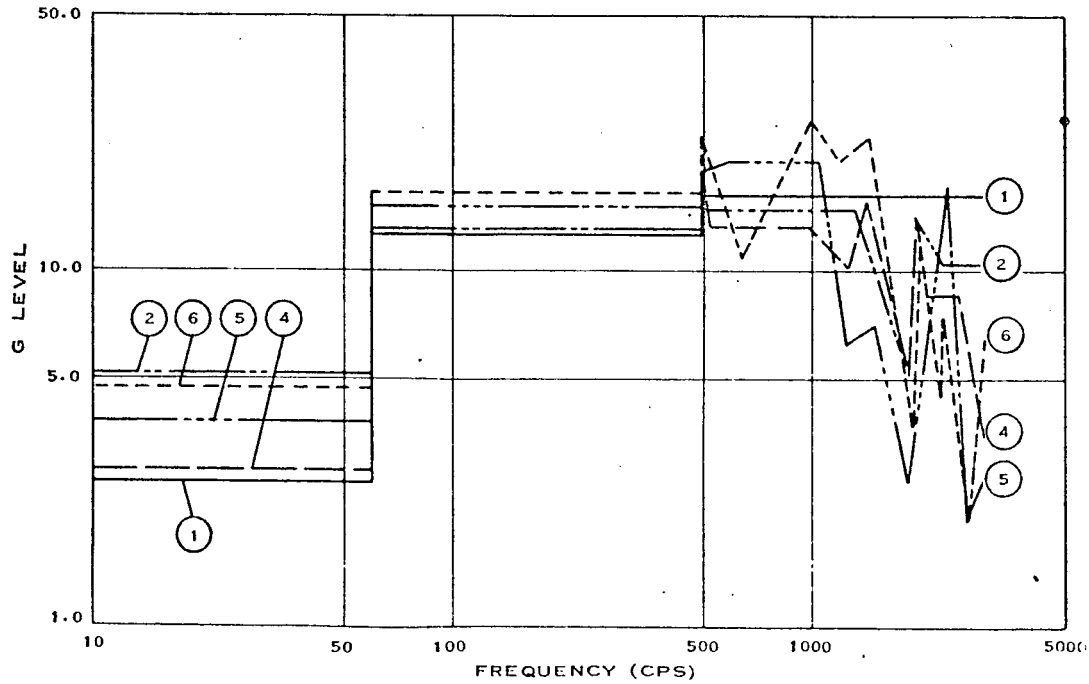

FIGURE 4.9 'G' LEVEL VS FREQUENCY — Z AXIS

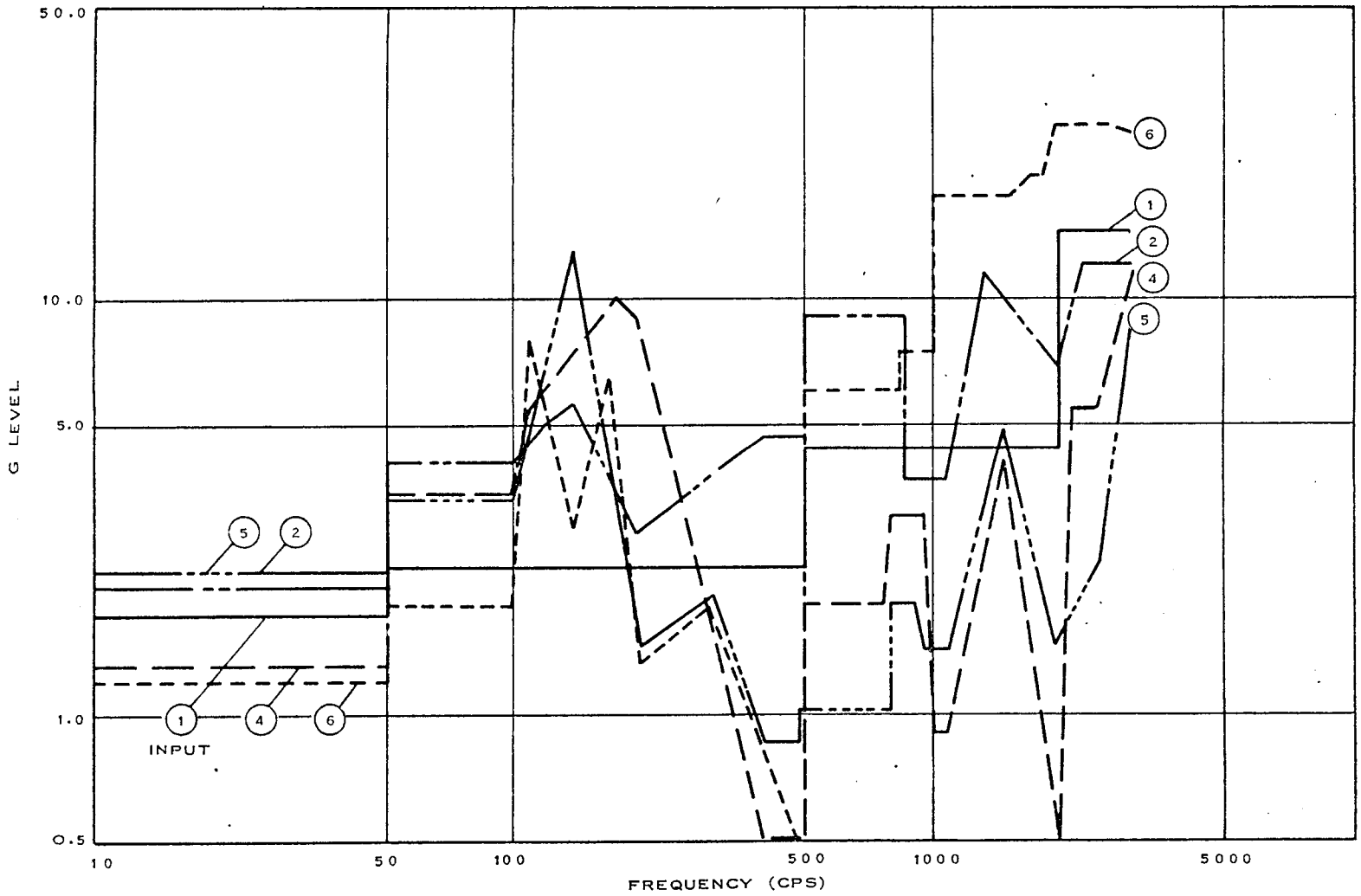

FIGURE 4.10 'G' LEVEL VS. FREQUENCY-Y AXIS

4.4 SPIN DEPLOYMENT TEST

This test was of most interest to the program. Its intent was to successfully demonstrate the feasibility of deploying a flexible array under conditions simulating those of a spinning vehicle in space.

Unfortunately these conditions can only be approximated by a ground test. The obvious problems are gravity and the atmosphere. Several schemes were proposed to solve these difficulties. The one selected was to spin deploy in a vacuum chamber. The Dynamic Test Chamber at GSFC - T&E was chosen. This chamber is 34 feet in diameter, can be evacuated to below 10^{-3} torr and has a 5 H.P. spin table available. This effectively simulated the spacecraft motion and at the same time eliminated air drag. Elimination of gravity forces was not possible, but their effect was minimized by the monorail device on the test fixture, 528-80000 shown in figures 4.11 and 4.12. The monorail was attached by a small slack cable to the bracket on the front plate of the Deployable Solar Array. This support was not intended to be operable during deployment since the combination of centrifugal force and mechanism stiffness makes the linkage self-supporting. The cable was needed when the angular velocity decayed to a point where the radial forces were too small to limit the deflections. As mentioned in a previous section, the linkage was designed to be self-supporting, but it was felt prudent not to test it until all other tests were completed.

The disadvantage of the monorail device is the increased mass moment of inertia of the test setup. This increased the deployment rate of the substrate and tended not to despin the fixture to the rate of an orbiting vehicle. The effect on the Deployable Solar Array was to increase the tension in the substrate and induce greater side loads into the linkage. This, incidentally, was the criteria for the Deployable Solar Array design.

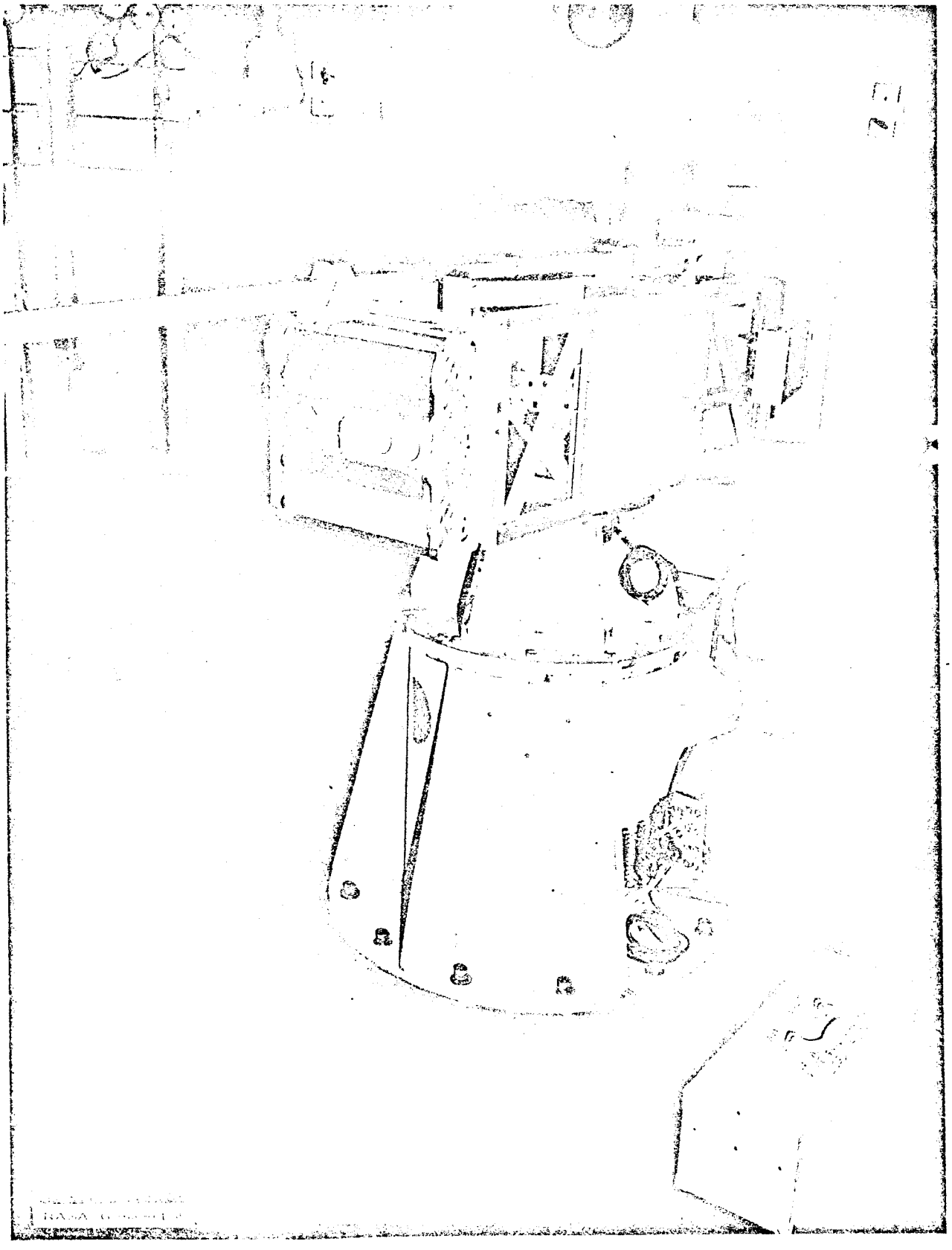

FIGURE 4.11 SPIN DEPLOYMENT TEST SET-UP — UNDEPLOYED

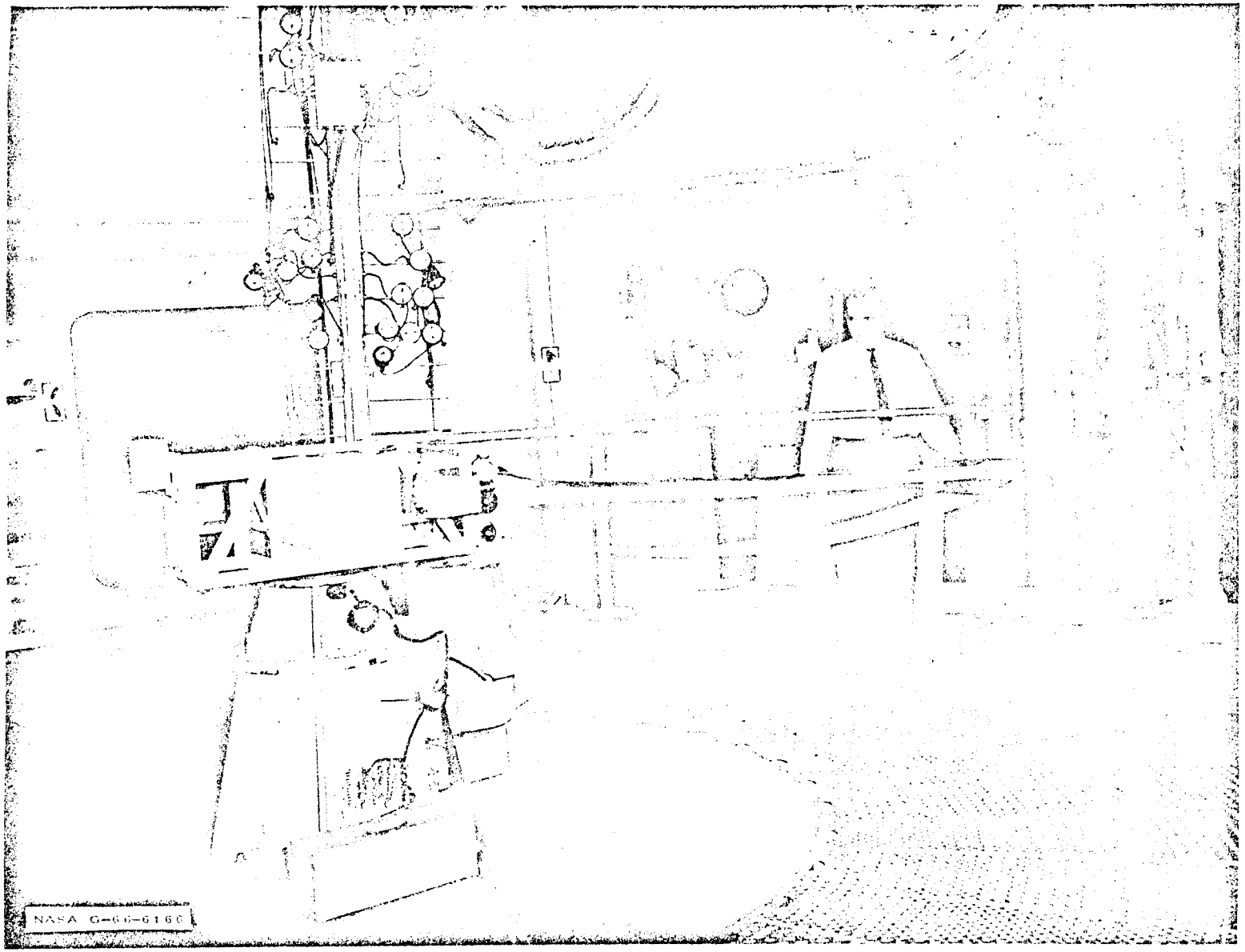

FIGURE 4.12 SPIN DEPLOYMENT TEST SET-UP — DEPLOYED

The test setup in the chamber is shown in figures 4.11 and 4.12. Test data included spin rate decay and two high speed movie cameras. One camera was mounted on the chamber ceiling; the other was attached to the test fixture, rotating with the test specimen.

The test plan specified two deployments. One at 80 rpm and the second at 160. The 80 rpm test was completed on 11/18/65 without incident. The chamber pressure was approximately $4.5 \times 10^{-}$ torr. The recorder data is shown in figure 4.13. A comparison of the data with that calculated for the test is shown in figure 4.14. It reflects reasonably good correlation. The film coverage was good, and did not reveal any unusual event.

The 160 rpm was started 11/19/65. The chamber was evacuated to 4×10^{-3} torr, the table spun up and the substrate released. Almost immediately the substrate was half deployed, separated and thrown against the chamber wall. One complete revolution later the linkage broke and it too was thrown off.

A post test examination disclosed that the rip in the substrate occured 50% of the way out. The tear appeared to be instigated by wedging the array in the corner formed by the end plate and the top plate. The film from the camera on the fixture shows an obviously large side load imposed on the deploying array and linkage and a very rapid initial deployment. The spin rate data is shown in figure 4.15. The sinusoidal shape of the curve after failure was due to vibration of the monorail support tube after the failure. The restraint wire from the end plate to the tube was the means of imparting the load to the tube. This wire is also the probable reason for the array jamming in the upper corner of the structure rather than the lower. Normally it would be expected that the array would catch in a lower corner because of gravity. The wire, however, must have rotated the end of the array about the tube axis thereby forcing the array upwards and catching in the upper corner.

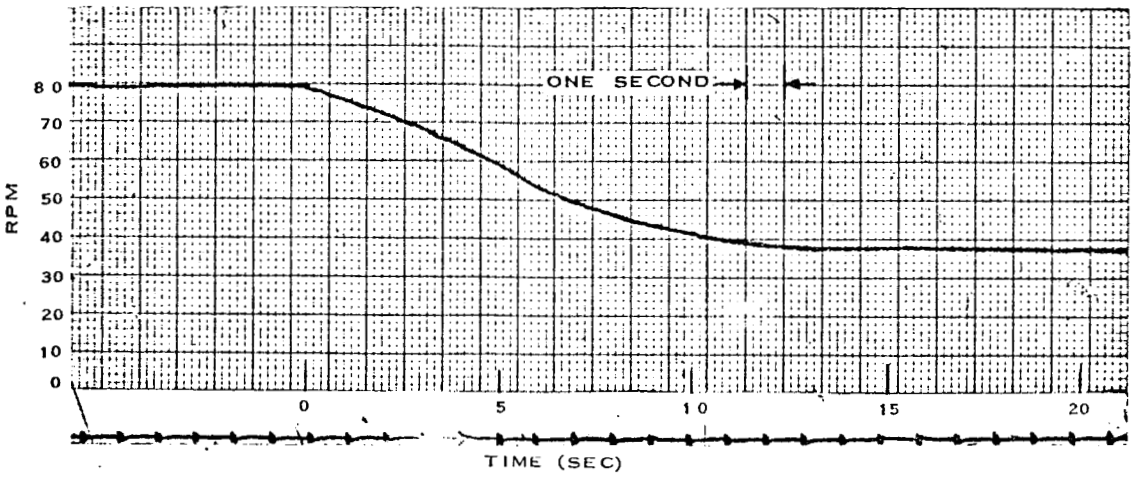

FIGURE 4.13 TEST DATA 80 RPM DEPLOYMENT

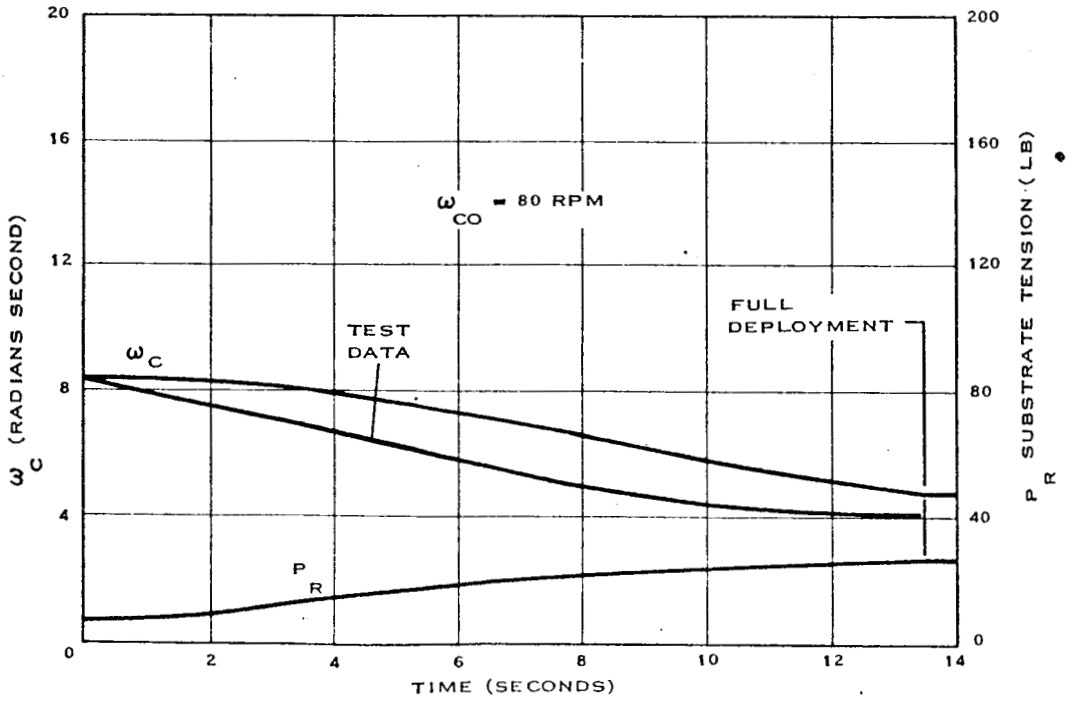

FIGURE 4.14 ANGULAR VELOCITY AND SUBSTRATE TENSION VS TIME
528—80000 TEST FIXTURE

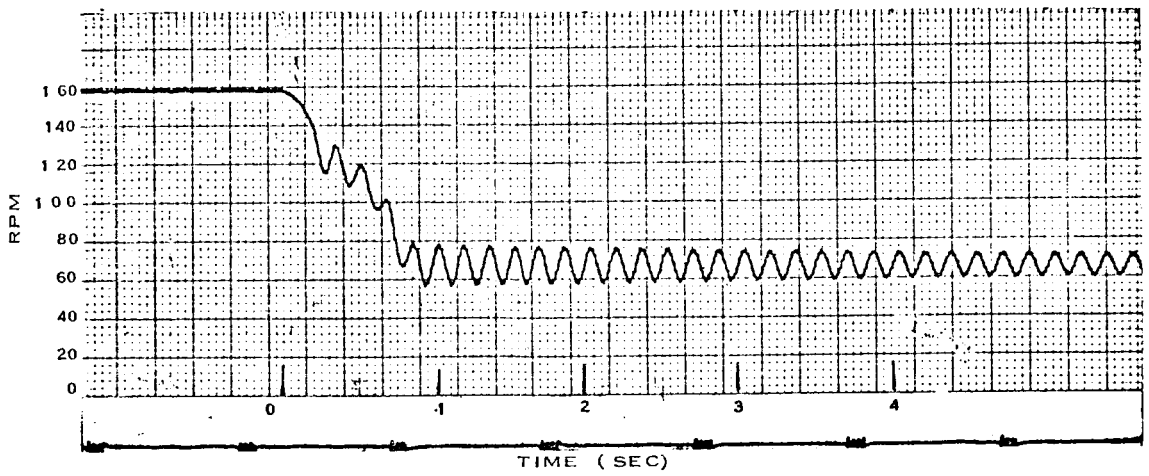

FIGURE 4.15 TEST DATA 160 RPM DEPLOYMENT

From the data and movie coverage it is evident the failure was caused by too high a radial velocity of links and array, thus causing excessive side loads due to corolis acceleration.

$$A_{corolis} = 2\omega_c \dot{X}$$

ω_c = angular velocity

$\dot{X}$ = radial velocity

Several causes were considered:

- Brake malfunction
- Broken shear pin in substrate roller
- Substrate separation from roller

Careful disassembly of the unit did not reveal the latter two, and it was concluded a brake failure had occurred.

Possible causes of brake failure are:

- Vacuum effects
- Centrifugal force effects
- Failure of brake components
- Error in analysis

The first item probably can safely be disregarded since the effect of vacuum is to cold weld or increase friction. Both would tend to retard rather than increase deployment rates.

Centrifugal force effects (F_a) caused by table rotation, especially those which produce a side load on the brake, are good possibilities. Centrifugal forces in the plane of the flyweights (F_r) caused by rotation about the spacecraft axis, tend to balance out or increase the brake effectiveness. See Figure 4.16.

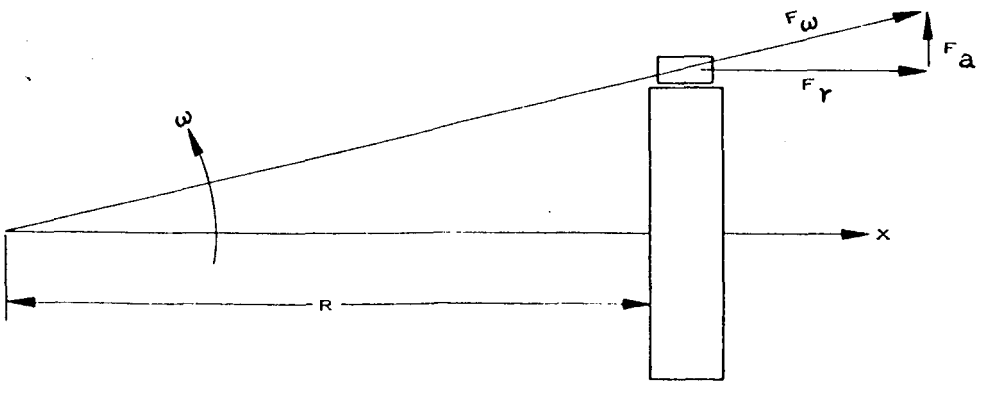

FIGURE 4.16 FORCE DIAGRAM

Disassembly of the brake disclosed no mechanical failure of brake components and was, therefore, disregarded as a possible cause.

Close correlation between analytical and test data on the 80 rpm run lends confidence that the analysis is accurate (see figure 4.14).

The indication then, is that the failure was in the brake and probably due to centrifugal forces. A new test was planned to verify this. A description of this test and the results are in Section 4.5.

4.5 BRAKE TEST

The need for this test was explained in the previous section. The FHC facility was used. The specific equipment was a Schaevitz type B-8-A Rotary Accelerator.

Test fixture 528-80007 was attached to the arm of the centrifuge as shown in figures 4.17 and 4.18. Parameters examined were:

- Angular velocity
- Friction shoe material

The results are shown in figure 4.19. An additional set of tests were also completed for the condition of no braking. This data is also shown in figure 4.19. Figure 4.20 presents the tare information or non-spinning results using various weights to obtain frictional and inertial data.

During this test, the failure of the brake was not duplicated. Several reasons are possibilities:

- The brake was not the cause of failure
- Subsequent handling and disassembly after the failure removed the cause of the failure
- Failure of the brake was caused by improper rewinding of the substrate after the 80 rmp test

It would be imprudent to flatly state that the first item is false. There is, however, some reason to believe that this is so. Review of the calculated and test data for the 160 rmp substrate deployment test indicates an actual rate four times that expected. The brake spin test for phenolic shoes also shows a deployment four times that of the brake off case. Again, this is not conclusive, but it is felt to be a little more than coincidence.

Greater forethought may have directed a closer scrutiny of the brake after the test, but this unfortunately was not done.

Subsequent effort on the brake system will be directed toward developing a more jamproof system and at the same time increasing the capacity of the brake.

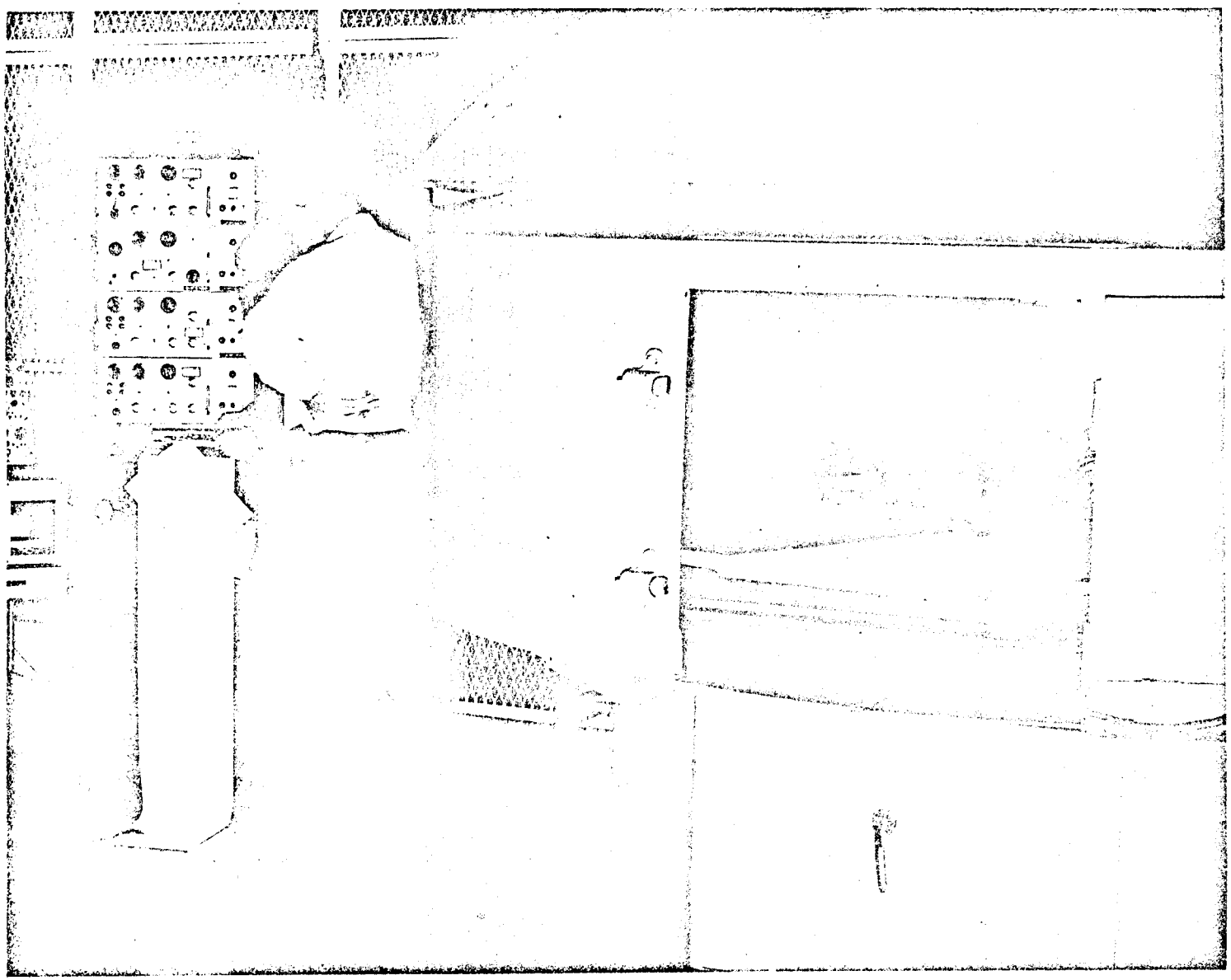

FIGURE 4.17 BRAKE TEST SET-UP

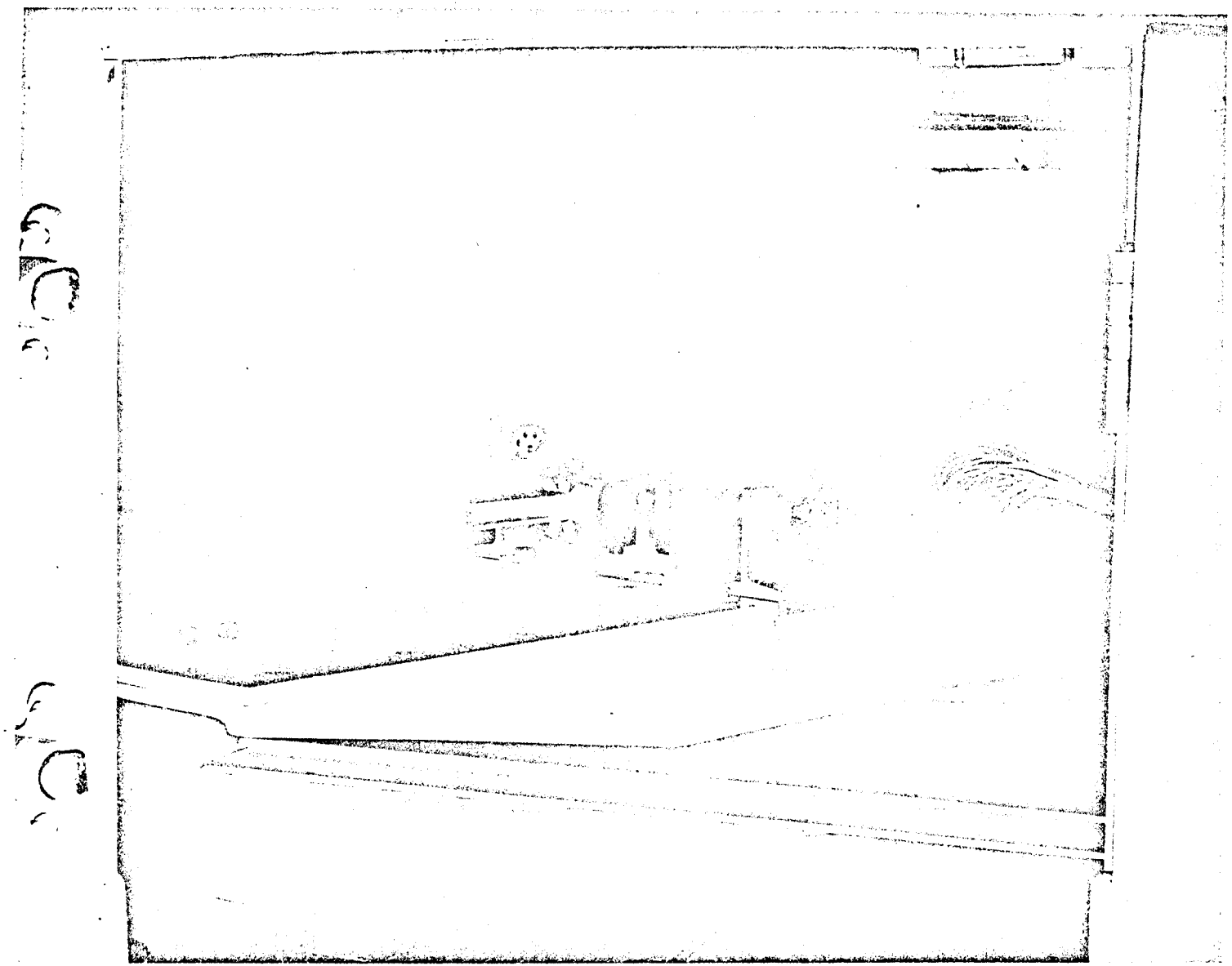

FIGURE 4.18 BRAKE TEST SET-UP

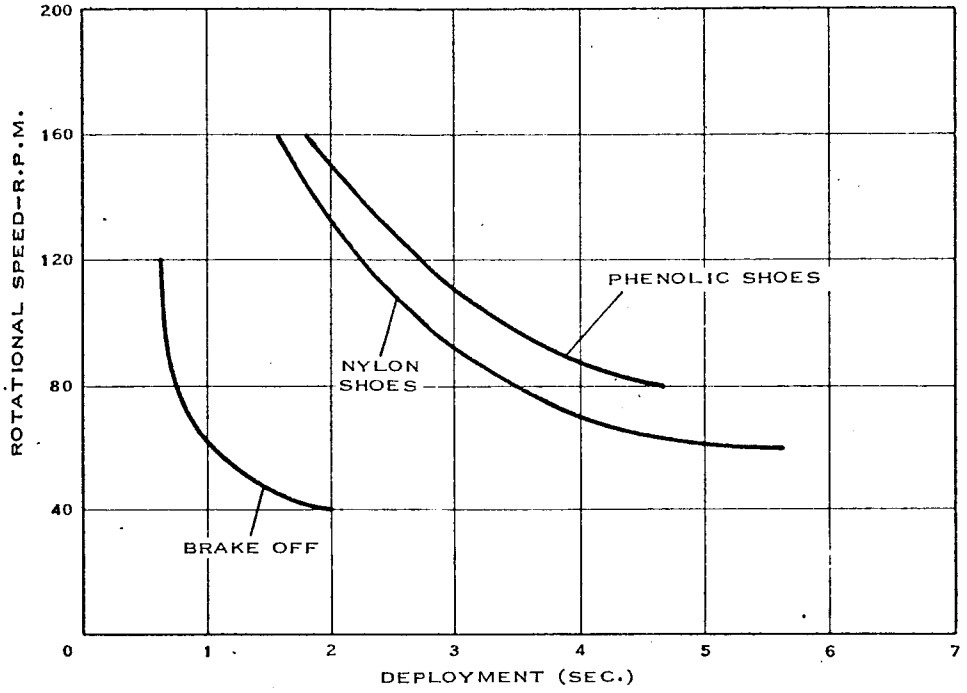

FIGURE 4.19 DSA DAMPER SPIN DEPLOYMENT TEST
SPIN RATE VS DEPLOYMENT TIME

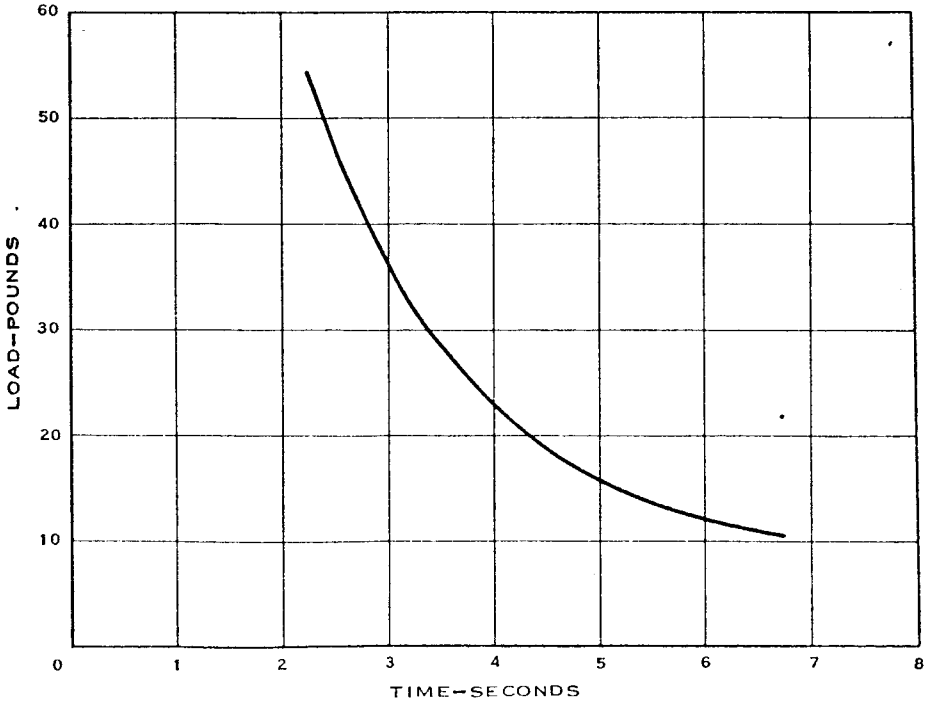

FIGURE 4.20 STATIC DEPLOYMENT TEST, DSA BRAKE

5.0 CONCLUSIONS AND RECOMMENDATIONS

It can be shown analytically that deployment at 80 rpm on the spin fixture is a more stringent test of the integrity of the mechanism than the specified deployment at 160 rpm on a spacecraft with four arrays. Therefore, all the objectives of Phase I were met even though a failure occurred during testing at 160 rpm. The results of the analysis are shown in figures 5.1 and 5.2. They indicate that, except for the first two feet, the shear and moment is always greater for the 80 rpm test than the deployment specifications. Note also that the maximum M for test is 50% higher than the maximum M for the flight article. It is also evident from this figure that the 160 rpm test was quite unrealistic since both maximum shear and maximum moment are much greater than necessary. It is interesting to note that the maximum moment occurs at approximately 4 feet of deployed length on the test calculations and also seems to be independent of rpm. Since this is also the failure condition on testing, it provides greater confidence in the deployment analysis. The tension on the substrates, shown in figure 5.2, also indicate that the 80 rpm test is valid test criteria to show successful deployment.

The development of the hardware also verifies the study results that, for this application, the Deployable Solar Array is a much more efficient packaging concept than rigid systems. It also provides slight gains in power-to-weight ratios over rigid concepts. The results of an investigation of the growth possibilities of this array are in figures 5.3 and 5.4. Data used for the study are actual weights and volumes derived from the Deployable Solar Array hardware. The asymptote for the arrays in figure 5.3 is probably around 2.5 sq.ft. per pound. This is the case where the weight of mechanism and structure becomes very small compared to the substrate. The substrate alone has an area/weight ratio of 2.67 $ft.^2$/lb. It could be improved using lighter cells and cover glass, but no effort was made in this direction.

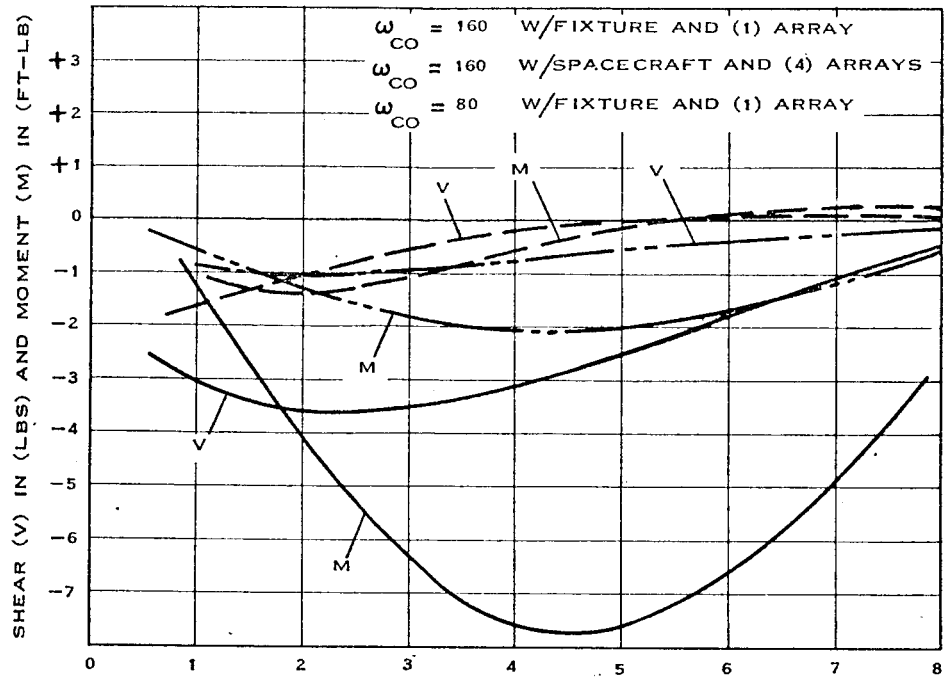

FIGURE 5.1 SHEAR AND MOMENT VS DEPLOYED LENGTH

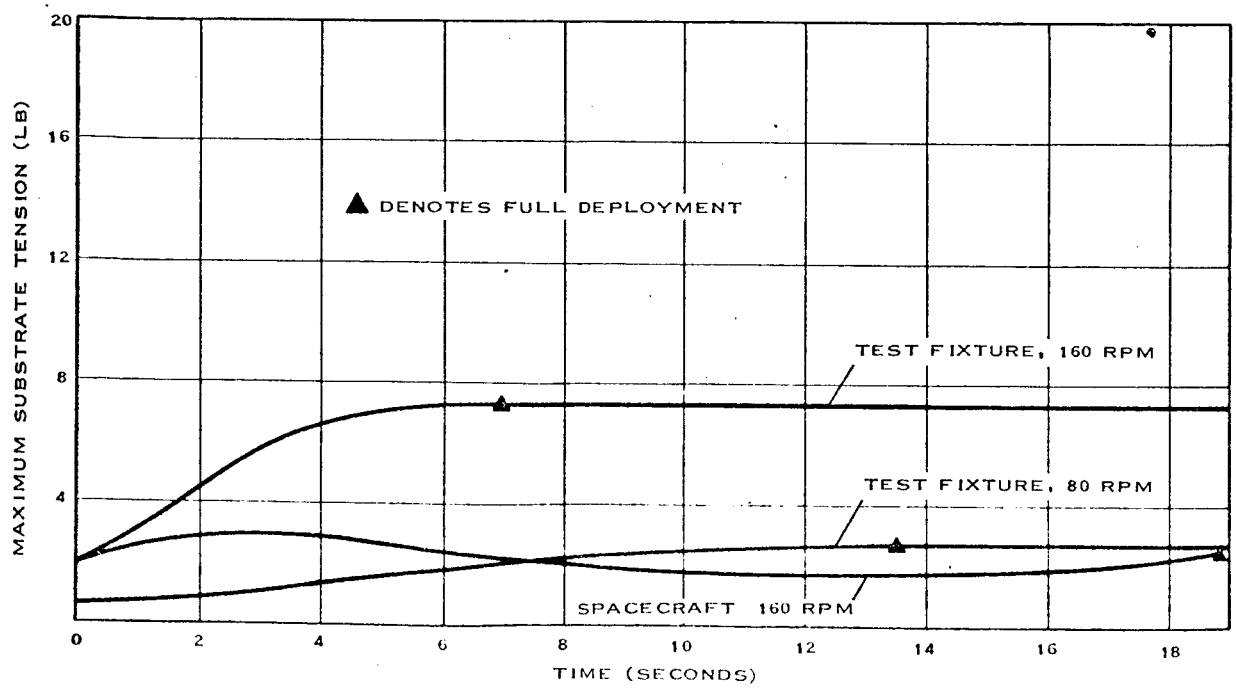

FIGURE 5.2 SUBSTRATE TENSION VS DEPLOYMENT TIME

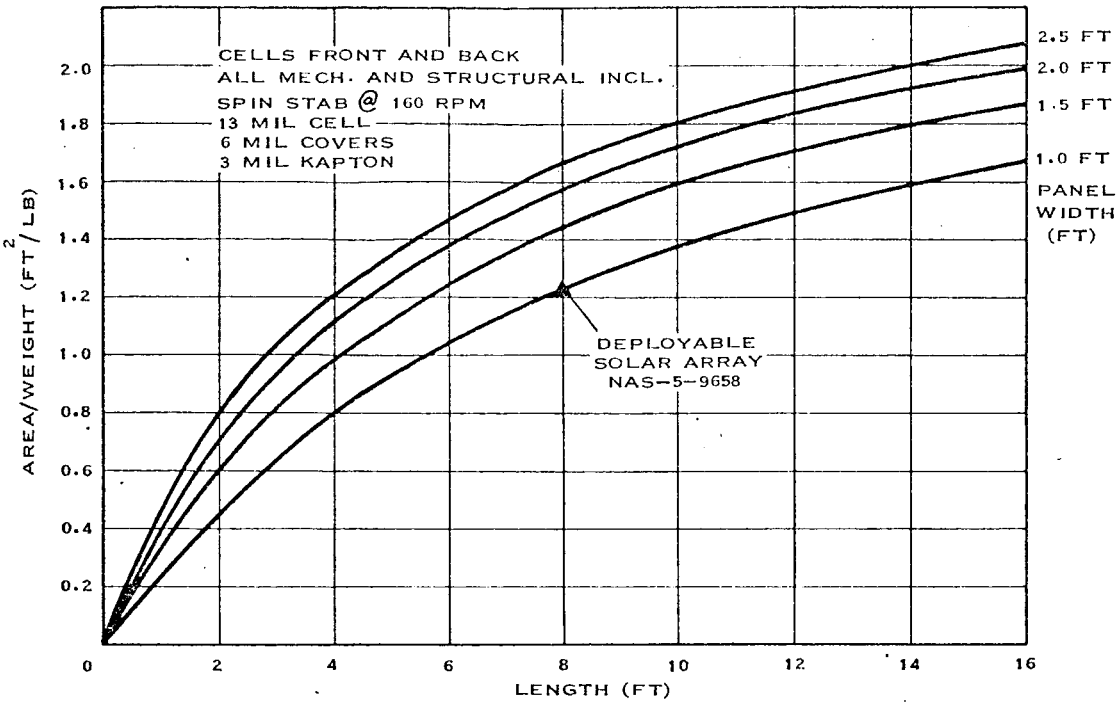

FIGURE 5.3 AREA/WT. RATIO VS LENGTH
FLEXIBLE SOLAR ARRAY

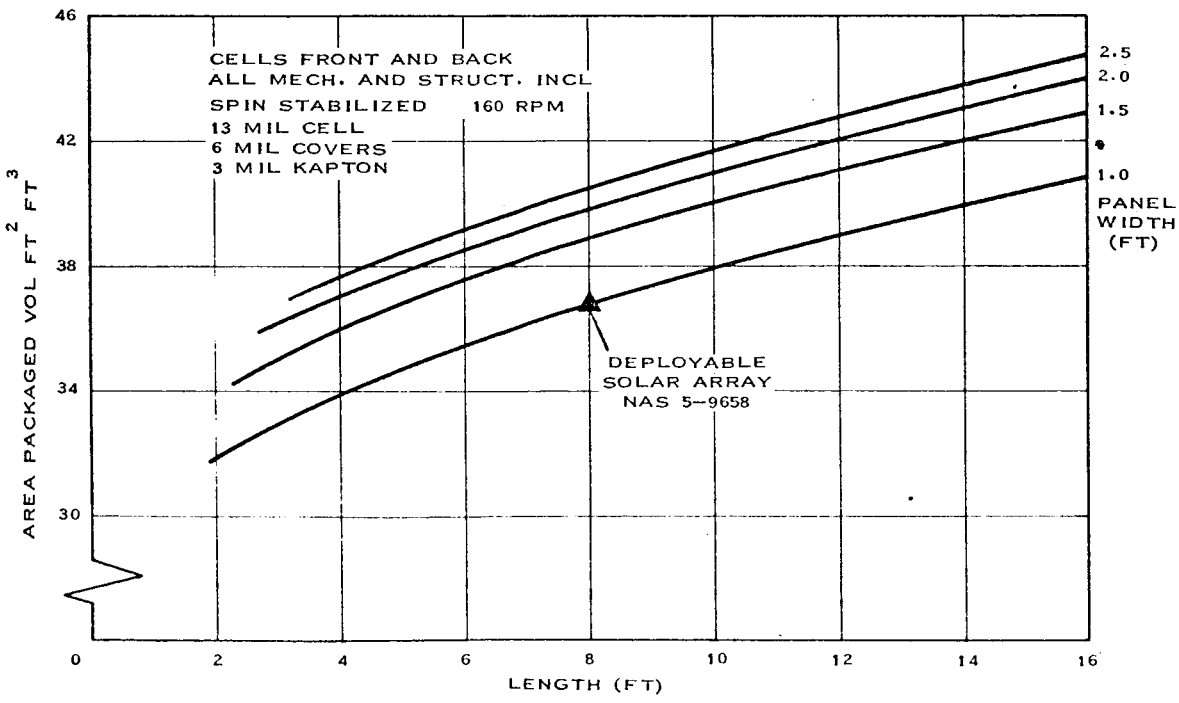

FIGURE 5.4 AREA/VOLUME RATIO VS LENGTH
FLEXIBLE SOLAR ARRAY

Figure 5.4 does not indicate a theoretical limit on the gain in Area/Volume ratio for this concept of solar array. The practical limit would probably be dictated by the linkage, etc. Figure 5.4 does point up, however, a considerable gain in packaging efficiency for a flexible array.

Several recommendations are evident from the results of Phase I. The most important is to develop a more reliable damping system. Several new designs are under consideration. They are all of the centrifugal type previously used, but with refinements. The reasons for using a brake of this type are still valid and are covered in the study report. In addition, a more exhaustive brake test program should be conducted prior to installation into the array to detect any malfunction.

Another area in which it became apparent that more work was needed is handling equipment for the deployed array. Automatic or semi-automatic rewind equipment would also be helpful. The latter should not be a permanent part of the design but would be removable A.G.E. items.

According to the present Phase II plan, more work will be done on the substrate. As part of this task it would be advisable to consider the repairability aspects of the design. It would also be appropriate to investigate production methods of array fabrication.

It would also be considered a more worthwhile endeavor to design and fabricate one new unit with twice the area of the present design rather than the two planned prototypes. In addition to providing more insight into the problems involved with larger arrays, it will provide another data point from which extrapolation can be made on the design of larger arrays.

As far as future work is concerned, it would be well to study the uses of a flexible array on other than a spinning vehicle. This study would be roughly the same as the forerunner of this program, but would also include re-design studies of existing spacecraft to determine what possible weight, volume or other advantages may be obtained.

6.0 NEW TECHNOLOGY

No new inventions have been disclosed as a result of this contract.